Titre: Title:	Microscale thermofluidic modeling of LCVD fiber growth
Auteur: Author:	Jun Yu
Date:	2007
Type:	Mémoire ou thèse / Dissertation or Thesis
Référence: Citation:	Yu, J. (2007). Microscale thermofluidic modeling of LCVD fiber growth [Thèse de doctorat, École Polytechnique de Montréal]. PolyPublie. https://publications.polymtl.ca/7926/

UNIVERSITÉ DE MONTRÉAL

MICROSCALE THERMOFLUIDIC MODELING OF LCVD FIBER GROWTH

JUN YU
DÉPARTEMENT DE GÉNIE MÉCANIQUE
ÉCOLE POLYTECHNIQUE DE MONTRÉAL

THÈSE PRÉSENTÉE EN VUE DE L'OBTENTION
DU DIPLÔME DE PHILOSOPHIÆ DOCTOR
(GÉNIE MÉCANIQUE)
AVRIL 2007

Your file Votre référence
ISBN: 978-0-494-29208-2
Our file Notre référence
ISBN: 978-0-494-29208-2

UNIVERSITÉ DE MONTRÉAL

ÉCOLE POLYTECHNIQUE DE MONTRÉAL

Cette thèse intitulée :

MICROSCALE THERMOFLUIDIC MODELING OF LCVD FIBER GROWTH

présentée par : YU Jun

en vue de l'obtention du diplôme de : Philosophiæ Doctor

a été dûment acceptée par le jury d'examen constitué de :

M. PELLETIER Dominique, Ph.D., président

M. CAMARERO Ricardo, Ph.D., membre et directeur de recherche

M. LUAN Ben, Ph.D., membre et examinateur externe

M. REGGIO Marcelo, Ph.D., membre

REMERCIEMENTS

Pr. Alain GLEIZES, du laboratoire LAPLACE du CNRS,
à L'Université Paul Sabatier de Toulouse, et

Pr. Gerard L. VIGNOLES, du laboratoire des Composites ThermoStructuraux (LCTS)
de l'Université Bordeaux

ont gracieusement expertisé cette thèse à titre d'évaluateurs externes.
Nous les remercions pour leur contribution.

ACKNOWLEDGEMENTS

This research project was initiated under the supervision of Dr. Ricardo Camarero and Dr. Joseph Pegna. I am grateful to them for giving me the opportunity to work on such an exciting project and for their guidance throughout the course of this project. Due to other commitments, Dr. Pegna was unable to continue in that capacity.

The financial support of NSERC is gratefully acknowledged.

Special thanks are given to my colleague, Ramkiran Goduguchinta who provided me with many useful LCVD papers and valuable experimental data.

Sincere thanks are given to my another colleague, Dominique Croteau for his valuable help in learning the commercial CFD software FLUENT.

Thanks are also given to the present members of Freeform Fabrication Laborary, Christian Fauteux and Remi Longtin, to the computer system administrator, Atmane Laras, and to all the staff of the Mechanical Engineering Departement. Their help and friendship made my stay here a very pleasant experience.

Finally, I would like to extend my appreciation to my husband, Xin Liu, my children, Yuwei and Annie, my parents, Zhongfang and Shansen, and my three sisters, Ying, Ling, and Han, for their love, understanding and encouragement.

RÉSUMÉ

Cette dissertation présente une recherche sur modélisation numérique de la croissance d'une fibre par la déposition pyrolytique en phase vapeur (LCVD) induite par laser.

Le but de ce travail est le développement et la mise en oeuvre d'un modèle numérique de réacteur, capable de simuler le comportement des divers phénomènes qui entrent en jeu lors du procédé LCVD de fabrication d'une fibre. Les bénéfices qui découlent d'un tel réacteur virtuel sont liés à la précision et la rapidité que permettent les calculateurs modernes. Ceci permettra de prédire le comportement du procédé avec une grande plage de paramètres clés qui caractérisent le fonctionnement du réacteur. En plus, cet outil peut fournir des données détaillées sur les variables telles les champs de vitesse, de pression, la distribution des diverses espèces issues de la réaction etc.. Présentement, celles-ci sont difficiles et coûteuses à obtenir par les méthodes expérimentales, sinon carrément impossible.

Dans un contexte d'ingénierie, la conception de tels appareils nécessite une compréhension appronfondie des phénomènes en présence, et leur développement doit s'appuyer sur des campagnes de mesures en laboratoire pour optimiser les caractéristiques d'un prototype. Un réacteur virtuel se veut un outil pour assister les concepteurs dans cette démarche en permettant des analyses paramétriques exhaustives réduisant le nombre d'essais et erreurs. Les coûts et le temps de développement en sont grandement réduits.

Avec succès, cette recherche préparera le terrain pour l'entrée du procédé LCVD dans l'arène commerciale, puisqu'il y a une grande demande de nouveaux matériaux composites où des fibres performantes leur fournissent la structure squelettique. On trouve des applications dans tous les secteurs industriels allant de l'aérospatiale à la biomécanique.

En conséquence, le projet de cette dissertation est de fournir une machine virtuelle pour

simuler numériquement le processus de LCVD et d'étudier en détail les processus d'échanges d'énergie et les mécanismes de dépôt de matière dans un réacteur en convection forcée et à haute pression qui sont les conditions les plus prometteuses sur le plan d'industrialisation du procédé.

Puisque le LCVD est un processus thermiquement activé, caractérisé par un écoulement fluide en corrélation avec une réaction chimique, la modélisation des divers phénomèmes d'échange d'énergie et de masse constitue la première étape de l'étude. Le processus de discrétisation des équations gouvernantes sur un support discret de volumes finis permettent, avec l'imposition de conditions frontières appropriées, la formulation d'un problème bien posé dans le sens mathématique. On propose l'utilisation d'un logiciel commercial, FLUENT, pour la mise en oeuvre numérique de la simulation et les analyses paramètriques.

L'étude de deux genres de réacteurs a été réalisée. En premier lieu, un réacteur opérant à des conditions de température ambiante et de pression atmosphérique, présentement à l'étude par le FFL, a servi de base pour valider les modélisation physique et numérique proposées. Le second type de réacteur, en régime de convection forcée, à haute pression et de basse température a été ensuite utilisé pour exploiter cette méthodologique dans le but d'identifier les paramètres géométriques et les conditions d'exploitation optimales. L'objectif étant d'analyser et d'évaluer le potentiel de tels réacteurs.

L'utilisation de ce modèle numérique peut être employée pour réduire le nombre de expériences requises pour obtenir un maximum d'informations dans le choix d'un ensemble approprié de paramètre du processus et pour guider le concepteur dans sa démarche d'optimisation d'un prototype de réacteur LCVD.

ABSTRACT

This dissertation presents an investigation of the modeling of pyrolytic laser-induced chemical vapor deposition (LCVD) fiber growth solved with Navier-Stokes equations.

Pyrolytic LCVD is a thermally driven process in which the energy of a laser beam is used to heat the surface of a substrate to the temperature required for chemical deposition. This process permits superb spacial resolution because the chemical reactions are restricted to the heated zone created by the focused laser spot. The deposition zone is determined by the laser beam and the thermal and optical properties of the substrate.

It appears that LCVD is capable of producing fibers of indefinite length as long as the tip of the growing fiber is maintained at the laser focus. However, one of the most important hurdles in making LCVD into a commercially viable technology for the production of fibers is achieving simultanously high growth rate and desired material properties. Demonstrating a prototype reactor capable of sustaining high growth rates and producing stable material characteristics is the goal in which this research is undertaken. Successfully, this research would pave the way for LCVD to enter into the commercial arena, since there is such a great demand of the new material in fiber form, which provides the skeletal structure to almost every composite in use today.

A literature survey revealed that the growth rate can be improved significantly by increasing the reactor pressure. In addition to the high pressure, another interesting experimental observation is that a natural convection current occurs along the fiber axis into the laser beam. It is therefore legitimate to infer that, if one is to use a forced precursor jet to increase the growth rate, it should be coaxial with the fiber and oriented in the direction of growth. Consequently, this led the Freeform Fabrication Laborary (FFL) of Ecole Polytechnique de Montréal. to propose a unique reactor design with a precursor flow directed

along the fiber growth axis.

A comprehensive research project is currently undertaken by FFL of Ecole Polytechnique de Montréal for producing, testing, and process control of continuous high performance fibers. It was found that some aspects of the physical process are difficult or impossible to study through experimental techniques. For example, LCVD is often used to produce three dimensional structures having characteristic radius of the order of μm. The physical phenomena associated with LCVD also occur on radius length scales of μm while axial length scale range from μm to mm depending on proximity to the reaction zone. For this reason, with the exception of the observation of bulk properties, detailed experimental observations of the fluid flow and heat transfer associated with the LCVD process are not available. Measuring spatial temperature profiles, precisely,i.e. on the order of fraction of a μm is extremely difficult.

Consequently, the project of this dissertation is to provide a virtual reactor for numerically simulating the LCVD process and to investigate the physical processes in depth and in detail. We aim at further insight into the LCVD process through numerical modeling and analysis on the effect of forced convection of precursor gas along the direction of LCVD fiber growth. It is an advanced computational model implemented into the FLUENT CFD package for studying mass, momentum and energy exchange, including species transport, as well as chemical kinetics within a forced flow LCVD environment.

Two kinds of reactors are simulated. One is the reactor for the conditions of room temperature and pressure which is currently undertaken by FFL, the other is the reactor for the conditions of low temperature and high pressure to be undertaken in the future.

Since LCVD is a thermally activated process characterized by the inter-related fluid flow, chemical reaction and mass and heat transfer phenomena, the outcomes of this numerical

simulation will allow us to analyze how these factors will effect the process. They can be used to evaluate the relative importance of the different process parameters, such as laser power, pressure, the best focus position of the laser, and different flow rates of the percursor and the surrounding gases, and the mixture situation of the two species to gain insight into the LCVD process.

LCVD experiments of FFL were carried out to verify the modeling. A validating simulation was firstly be done. Since we could measure the pulling rate of the fiber by experiments which should be equal to the growth rate in steady state, we could compare the calculated deposition rate with the measure growth rate to validate our modeling.

For the simulation results, we calculated the deposition rate and the temperature and species concentration. We further investigated the insights of the phenomena of the flow, flow plus heat transfer, and flow plus heat transfer plus chemical kinetics separately.

We investigated how the growth rate depending on the laser power (or tip temperaure), precursor flow rate, and the position of the laser beam focus. Next, we compared the outcomes of two forced convection which are along and against the fiber growth direction to prove the working hypothesis which is that forced convection of the precursor gas along the direction of fiber growth contributes to enhance cooling, increase growth rate and provides better mechanical support of the growing fiber.

Then, the situation at high pressure conditions were investigated through virtual experiments. The outcomes provided a basic understanding of the chemical kinetics and the deposition mechanisms in HP-LCVD reactor.

Lastly, benefits and contributions of this dissertation are discussed.

CONDENSÉ EN FRANÇAIS

Cette dissertation présente une recherche sur modélisation numérique de la croissance d'une fibre par la déposition pyrolytique en phase vapeur (LCVD) induite par laser résolue avec Navier-Charge des équations.

LCVD pyrolytique est un processus thermique dans lequel l'énergie d'un rayon laser est appliquée à la surface d'un substrat causant, après l'atteinte d'une température critique, le dépôt de matière résultant d'une réaction chimique dans un gaz précurseur. Ce processus permet une résolution spaciale précise parce que les réactions chimiques sont limitées à la zone de chauffage créée par la focalisation du laser. La zone du dépôt de matière est déterminée par le rayon laser et les propriétés thermiques et optiques du substrat. La technique LCVD a le potentiel de produire des fibres de longueur indéfinie tant que le bout de la fibre en croissance est maintenu au foyer du laser. Cependant, un des obstacles les plus importants qui empêche le passage de la fabrication LCVD vers une technologie commercialement viable pour la production des fibres est l'atteinte d'un taux de croissance élevé et l'obtention des propriétés désirées du matériau.

Le but de ce travail est le développement et la mise en oeuvre d'un modèle numérique d'un réacteur, capable de simuler le comportement des divers phénomènes qui entrent en jeu lors du procédé LCVD de fabrication d'une fibre. Les bénéfices qui découlent d'un tel réacteur virtuel sont liés à la précision et la rapidité que permettent les calculateurs modernes. Ceci permettrait de prédire le comportement du procédé avec une grande plage de paramètres clés qui caractérisent le fonctionnement du réacteur. En plus, cet outil peut fournir des données détaillées sur les variables telles les champs de vitesse, de pression, la distribution des diverses espèces issues de la réaction etc.. Présentement, celles-ci sont difficiles et coûteuses à obtenir par les méthodes expérimentales, sinon carrément impossible.

Dans un contexte d'ingénierie, la conception de tels appareils nécessite une compréhension appronfondie des phénomènes en présence, et leur développement doit s'appuyer sur des campagnes de mesures en laboratoire pour optimiser les caractéristiques d'un prototype. Un réacteur virtuel se veut un outil pour assister les concepteurs dans cette démarche en permettant des analyses paramétriques exhaustives réduisant le nombre d'essais et erreurs. Les coûts et le temps de développement en sont grandement réduits.

Avec succès, cette recherche préparera le terrain pour l'entrée du procédé LCVD dans l'arène commerciale, puisqu'il y a une grande demande de nouveaux matériaux composites où des fibres performantes leur fournissent la structure squelettique. On trouve des applications dans tous les secteurs industriels allant de l'aérospatiale à la biomécanique.

Une recherche bibliographique indique que le taux de croissance d'une fibre par ce procédé peut être amélioré de manière significative en augmentant la pression du réacteur. En plus de la haute pression, une autre observation expérimentale intéressante est que le taux de déposition sur le substrat est grandement facilité par une configuration des jets des gaz précurseur et ambiant. En effet, dans les premiers réacteurs de recherche, le jet est généralement orienté dans une direction perpendiculaire au faisceau laser. En orientant le jet dans la direction axiale au faisceau laser, non seulement on augmente la croissance, mais on peut obtenir une production en mode continu. Ceci donne lieu à des configurations qui se prêtent facilement à une industrialisation.

Il est donc légitime d'en déduire, que pour augmenter le taux de croissance, on doit employer un jet du gaz précurseur à fort débit, orienté dans la direction coaxiale avec la fibre et dirigé dans le sens de la croissance de la fibre. Ceci a mené le Laboratoire de fabrication en forme libre (FFL) de l'Ecole Polytechnique de Montréal à proposer une conception unique de réacteur avec un écoulement de précurseur dirigé le long de l'axe de croissance de la fibre.

Ce travail s'insère dans un projet de recherches entrepris par le FFL de l'École Polytechnique de Montréal pour la production, l'essai, et le contrôle du processus de production en continu de fibres. Ce qui est visé est la qualité des fibres ainsi que la fiabilité et le rendement du procédé.

À l'origine, et la motivation première de cette thèse, est le constat qu'il est difficile voire impossible d'étudier la totalité des différents aspects de la physique du processus par des techniques expérimentales. Par exemple, le LCVD est souvent employé dans la production de structures tridimensionnelles ayant une taille caractéristique de l'ordre du μm. Les phénomènes physiques associés au procédé de fabrication de fibres se produisent à l'échelle de la taille de celle-ci, également de cette dimension. Avec par surcroît, que l'essentiel des phénomènes d'échanges d'énergie se trouvent localisés dans une région dans la proximité du bout de la fibre dont l'étendue est de l'ordre quelques μm. Il en résulte une grande disparité dans les échelles des divers mécanismes d'échanges, situation qui rend l'observation ou la mesure très difficile. En fait, de telles données expérimentales sont presqu'inexistantes.

Pour cette raison, avec exception de l'observation des propriétés en bloc à un niveau macroscopique et global, le détail expérimental des flux de fluide et du transfert thermique etc associés au LCVD n'est pas disponible, et constitue une grande lacune pour la réalisation de telles machines. Il en va de même pour la mesure de la distribution spatiale de température, c-à-d de l'ordre de la fraction d'un μm est extrêmement difficile. Ce type de précision est pourtant nécessaire pour prédire le procédé dans son ensemble et le détail de la qualité au niveau crystallographique de la fibre.

En conséquence, le projet de cette dissertation est de fournir une machine virtuelle pour simuler numériquement le processus de LCVD et d'étudier en détail les processus d'échanges

d'énergie et les mécanismes de dépôt de matière dans un réacteur en convection forcée et à haute pression qui sont les conditions les plus prometteuses sur le plan d'industrialisation du procédé.

Puisque le LCVD est un processus thermiquement activé, caractérisé par un écoulement fluide en corrélation avec une réaction chimique, la modélisation des divers phénomèmes d'échange d'énergie et de masse constitue la première étape de l'étude. Le processus de discrétisation des équations gouvernantes sur un support discret de volumes finis permettent, avec l'imposition de conditions frontières appropriées, la formulation d'un problème bien posé dans le sens mathématique. On propose l'utilisation un logiciel commercial, FLUENT, pour la mise en oeuvre numérique de la simulation et les analyses paramètriques. L'étude de deux genres de réacteurs a été réalisée. En premier lieu, un réacteur opérant à des conditions de température ambiante et de pression atmosphérique, présentement à l'étude par le FFL, a servi de base pour valider les modélisation physique et numérique proposées. Le second type de réacteur, en régime de convection forcée, à haute pression et de basse température a été ensuite utilisé pour exploiter cette méthodologique dans le but d'identifier les paramètres géométriques et les conditions d'exploitation optimales. L'objectif étant d'analyser et d'évaluer le potentiel de tels réacteurs.

Les résultats de cette simulation numérique ont permis l'analyse de l'impact des divers facteurs sur le rendement du processus: évaluer l'importance relative des différents paramètres du processus, tels la puissance du laser, le diamètre du faisceau laser, la meilleure position du foyer du laser et pression du gaz à l'intérieur de la chambre de dépôt, et les débits des différents gaz précurseur et gaz ambiant. Il en résulte un compréhension fine de la situation de mélange des deux gaz et des conditions qui affectent les mécanismes de dépôt de matière. Les résultats du modèle établissent le rapport entre la température, la pression, la concentration , le débit du gaz précurseur, et les paramètres du rayon laser.

L'utilisation de ce modèle numérique peut être employée pour réduire le nombre de expériences requises pour obtenir un maximum d'informations dans le choix d'un ensemble approprié de paramètre du processus et pour guider le concepteur dans sa démarche d'optimisation d'un prototype de réacteur LCVD.

TABLE OF CONTENTS

LIST OF FIGURES

LIST OF TABLES

NOTATIONS AND SYMBOLS

ρ - Density

∇ - Differential Operator

$\mathbf{V}$ – Velocity vector

S_m - Mass source term

x - Axial coordinate

r - Radial coordinate

v_x - Axial velocity

v_r - Radial velocity

k_{eff} - Effective thermal conductivity ($= k + k_t$ where k_t is the thermal conductivity in the turbulent regime)

$\vec{J}_j$ - Diffusion of flux for specy j

S_h - Thermal source term

J - mass flux

J_i - the rate of diffusion for the ith species ($molcm^{-2}s^{-1}$)

k - reaction rate

k_c - thermal conductivity coefficient

$D_{T,i}$ - Thermal (Soret) diffusion coefficient

C - reagent concentration

C_i - concentration of ith species

C^0 - concentration of the reagent in the gas stream

C^s - concentration of the reagent at the substrate

C_p - specific heat ratio at constant pressure

n - the order of reaction

n_i - number density of species $i(cm^{-3})$

N - Total number density (cm^{-3})

δ - the boundary layer thickness

k_0 - pre-exponential constant

q'' - heat flux

Q - activation energy of the reaction

R - ideal gas constant n

Re - Reynolds number

T - the reaction temperature

D - diffusion coefficient

D_{ij} - binary mass diffusion coefficient of ij system

D_0 - a constant depending on the gases involved

U - internal energy

$X_i =$ mole fraction of i

$\bigtriangledown X_i$ - gradient in mole fraction of i

Y_i - mass fraction of i

E_r - the energy produced in the fluid (i.e.chemical reaction)

CHAPTER 1

INTRODUCTION

1.1 Motivation

A composite material has two main constituents, the first is the matrix material and the second are the fibers that provide reinforcement to the matrix. There is a great demand for fibers that can be used as reinforcements in high performance composite materials such as ceramic matrix composites that find a wide usage in industry. Applications in the areas of structures, power generation and aerospace require fibers with high strength, toughness and oxidation resistance at elevated temperatures, as well as chemical stability, low density, and good creep resistance. Fibers possessing some or all of these properties are commonly referred to as high performance fibers.

The two major hurdles in the rapid and economical development of new high performance fibers are:

1. the high costs involved in the development of new fibers using existing technologies.
2. and the absence of a suitable methodology to rapidly prototype small volumes of fibers of interest.

There is a variety of fiber production techniques in industry today, such as chemical vapor deposition, spinning, drawing from melts, sol gel synthesis, etc. Most of the conventional fiber production technologies are tailored to suit the material being produced. This customization leads to an increase in the investment in the form of specialized equipment for precursor processing, fiber handling and heat treatment. On the other hand, equipment

designed for laser-induced chemical vapor deposition (LCVD) operations can produce a variety of fibers by merely changing the precursor gas. Gaseous LCVD precursors require no further processing and can be used directly for fiber production. These advantages translate into considerable saving in investment. Furthermore, some high-end applications might require fibers only in small volumes. LCVD has proven itself to be a more efficient tool than other conventional fiber production technologies at rapid prototyping short fibers and 3-D micro-objects. One can therefore utilize LCVD to produce small batches of fibers for evaluation before continuing to produce them on a large scale.

Fibers produced by laser-induced chemical vapor deposition are of high quality where the deposited material usually possesses high purity, low porosity, and a high degree of homogeneity. Depending on the process parameters, the deposit may be crystalline, polycrystalline, or amorphous. In addition, this process has the potential for the high speed production of a wide variety of fibers with high deposition rate, high resolution, and high deposit strength.

The flexibility of the process and its adaptability to a wide range of materials is an incentive to investigate further the physics of this phenomenon.

LCVD has three main advantages over other material synthesis techniques. First, LCVD shares conventional chemical vapor deposition's ability to synthesize and carefully control the composition of a wide variety of materials. Second, LCVD deposits material only in areas where the laser spot interacts with the substrate. This localized deposition makes it possible to create dots, lines, and coatings by focusing and scanning a laser beam over the area where material deposition is desired. Finally, the rapid growth rates observed in LCVD make it possible to deposit material at a much faster rate than any other vapor deposition technique (Shaarawi (2001)). Some of the other important features and advantages of the LCVD process are summarized as follows:

1. LCVD is a containerless process and the deposits thus obtained have high optical

and chemical purity. This is in contrast to the traditional processes such as molding and chemical vapor deposition wherein the mold and the reactor contribute to the impurities in the deposit.

2. The microstructure of the material that is deposited by the LCVD process can be tailored on a molecular scale by adjusting the process parameters such as precursor pressure and temperature.

3. The LCVD process offers high spatial resolution (that is crucial in the case of direct writing processes), as the chemical reaction that produces the deposit is restricted to the heated zone created by the laser focus spot.

4. It has the ability to produce arbitrarily shaped three-dimensional microstructures and structures with very high aspect ratios (Dean & Nordine (1999), Wanke & Lehmann (1997), Williams (2000)).

5. Some materials such as silicon carbide, titanium carbide, boron fibers, and sensor fibers such as germanium and zinc zelenide (Wallenberger (2000)) are impossible to produce by other technologies .

LCVD processes are generally divided into two main categories, photolytic and pyrolytic, depending upon the mechanism that initiates the chemical reactions.

Photolytic LCVD uses photons from a laser beam to break chemical bonds within the reactive gases. The molecules either recombine or decompose to form a powder or solid deposit on the surface of the substrate. A successful deposit requires that the reactive gases are able to absorb the wavelength of light in the laser beam. Therefore, the gases and laser must be "tuned" to react with each other, restricting the flexibility of photolytic processes.

Pyrolytic LCVD is a thermally driven process in which the energy of a laser beam is used to heat the surface of a substrate to the temperature required for chemical deposition. The

high temperature produced at the focus point on the substrate causes the precursor gas to dissociate thereby producing a deposit. This process permits unmatched spatial resolution because the chemical reactions are restricted to the heated zone created by the focused laser spot. The deposition zone is determined by the laser beam and the thermal and optical properties of the substrate.

1.2 Context

The schematic of fiber formation by LCVD is shown in Fig. 1.1. With a reaction chamber filled with a gaseous specie, the focused laser beam is projected onto the substrate and local heating enables chemical reactions to occur and the fiber to deposit. By moving either the substrate or the focal plane of the laser beam, the deposition reaction proceeds on top of the previous deposit still in the focus of the laser beam. The focal point of the laser beam is continually adjusted to coincide with the tip of the growing fiber with the laser beam direction, resulting in fiber growth.

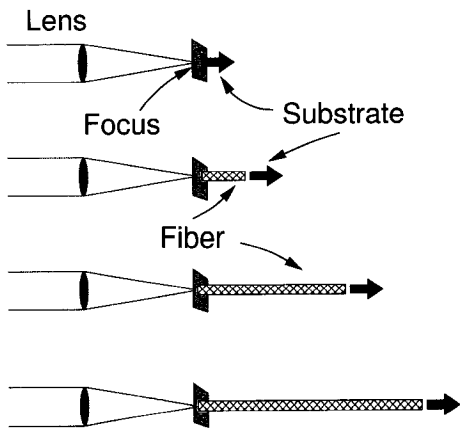

Figure 1.1 LCVD fiber growth

Thus, LCVD appears to be capable of producing fibers of indefinite length as long as the tip of the growing fiber is maintained at the laser focus. However, one of the most important hurdles in making LCVD into a commercially viable technology for the production of

fibers is achieving simultanously high growth rate and desired material properties. Demonstrating a prototype reactor capable of sustaining high growth rates and producing stable material characteristics is the context in which this research is undertaken. Successfully, this research would pave the way for LCVD to enter into the commercial arena, since there is such a great demand of the new material in fiber form, which provides the skeletal structure to almost every composite in use today.

A literature survey revealed that the growth rate can be improved significantly by increasing the reactor pressure. Frischknecht (1995) found that increasing the reactor pressure for a given beam power is likely to produce several effects simultaneously:

1. The fiber tip should experience a slight decrease in temperature due to an increase in the convective heat transfer coefficient.

2. The temperature gradient at the interface between the surface of the fiber tip and the gaseous phase should become steeper.

3. Although the volume of the hot zone in the gas phase (where synthesis occurs) should decrease, there is likely to be a range of pressures where the number of (effective) species within the (effective) hot zone is increased.

4. The local transport at the fiber tip may be modified due to changes in the natural convection flow characteristics which are the dominant energy exchange processes on this scale.

It is reported by Longtin (2003) that fibers produced by LCVD at atmospheric and sub-atmospheric pressures have low hardness and elastic modulus. The low pressure (LP) LCVD fibers have poor mechanical properties when compared to high pressure (HP) LCVD produced fibers in which the reactor pressure is above atmospheric.

Maxwell & Pegna (2004) reported a pressure range between 3 and 10 bars where linear

growth rate of carbon from ethylene increased exponentially with pressure. Williams & Maxwell (1999) increased reactor pressures up to 11 bar and grew carbon rods using ethylene as a precursor gas resulting in growth rates as high as 13 cm/s. This led us to induce that further increases in reactor pressures should yield higher fiber growth rates.

In addition to the high pressure, Maxwell & Pegna (1998) suggested the use of a forced precursor jet to improve the process. Injecting a stream through a nozzle situated at an angle towards the fiber growth region, could enhance the convection of precursor gas around the reaction zone and thus increase the growth rate. In this configuration, shown in Fig. 1.2, the precursor gas from the nozzle flows in a direction opposite to the direction of fiber growth. However, Duty & Johnson (2003) found out later that this could actually impede the growth rate of the fiber. This was attributed to the increased convection cooling.

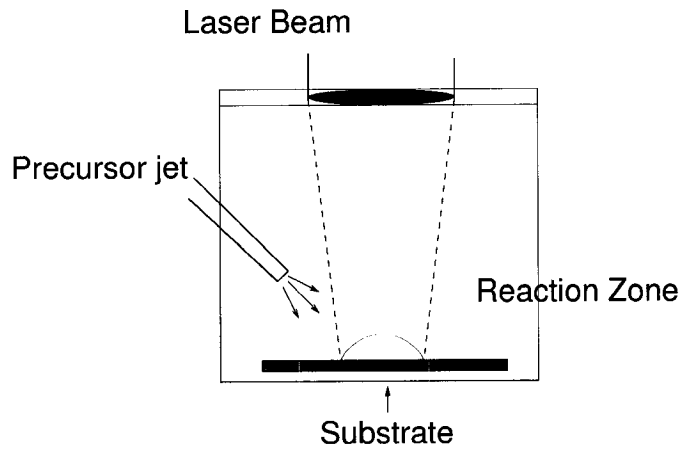

Figure 1.2 Forced precursor flow

Another interesting experimental observation is that a natural convection current occurs along the fiber axis into the laser beam. It is therefore legitimate to infer that, if one is to use a forced precursor jet to increase the growth rate, it should be coaxial with the fiber and oriented in the direction of growth. Consequently, this led Pegna and Goduguchinta (2004) to propose a unique reactor design with a precursor flow directed along the fiber growth axis shown in Fig. 1.3.

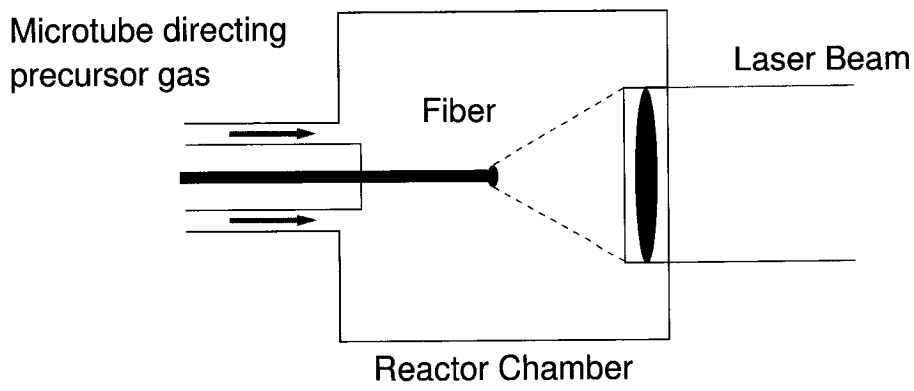

Figure 1.3 Aligned precursor gas flow

Experimental evidence (Goduguchinta (2004)) points to the thermal decomposition of the precursor at the tip of the fiber producing a concentrated jet, which by momentum transfer produces a strong convection current forcing the surrounding precursor gas to move in the growth direction of the fiber, parallel to its axis. The effect of this convection current is two-fold:

1. It enhances the cooling rate of the fiber at the reaction zone, leading to smaller diameter fibers.
2. It brings in fresh precursor to the reaction zone thereby increasing the growth rate.

It appears that the conventional model for LCVD growth (Hill (1995)) is inappropriate to describe the transport of precursor and its by-products. Also, it can be inferred that a forced precursor jet in any direction other than the axial growth direction of the fiber would actually impede the growth rate by:

1. obstructing the self-sustained supply of reagent gas,
2. lowering tip temperature as was shown by Duty & Johnson (2003)

In the present work, we provide a working hypothesis which is that forced convection of the

precursor gas along the direction of fiber growth contributes to enhance cooling, to increase growth rate and to provide better mechanical support of the growing fiber.

1.3 Problem Definition

The present work is part of a comprehensive research projet currently undertaken by the Freeform Fabrication laboratory (FFL) of Ecole Polytechnique de Montréal for producing, testing, and process control of continuous high performance fibers. At the origin, and as the motivation for undertaking this study is the fact that some aspects of the physical process are difficult or impossible to study solely through experimental techniques. For example, LCVD is often used to produce three dimensional structures having characteristic radius of the order of μm. The physical phenomena associated with LCVD also occur on radius length scales of μm while axial length scale range from μm to mm depending on proximity to the reaction zone. For this reason, with the exception of the observation of bulk properties, detailed experimental observations of the fluid flow and heat transfer associated with the LCVD process are not available. Measuring spatial temperature profiles precisely, i.e. on the order of fraction of a μm is extremely difficult.

Consequently, we aim at gaining further insight into the LCVD process through numerical modeling and analysis. Computer simulations will be used to investigate the physical processes in depth and in detail as a complement to experiments. Accordingly, the goal of the present project is to establish the basis for a methodology of the numerical study of LCVD fiber growth with an analysis on the effect of forced convection of precursor gas along the direction of LCVD fiber growth.

As mentioned earlier, fibers form an integral part of today's composites. In order for LCVD to be a viable commercial tool, it should be able to produce continuous fibers at a sufficiently high rate. Specifically, it appears clearly from the review of previous studies that

this is achievable by developing a reactor that can be used at high precursor pressure with forced convection of the precursor gas.

The objective of this dissertation is to devise a virtual machine for numerically simulating the LCVD process and to investigate in detail the complex physics involved.

Two types of reactors, and the phenomena involved, will be modelled and investigated in this work. The first reactor will be for operating conditions at ambient temperature and pressure. The purpose is to establish and validate the modelling and numerical methodology. The second reactor will be for the conditions of low temperature and high pressure for the purpose of investigationg the process at such conditions.

The reactor chamber for both types is composed of two main parts:

1. The quartz tube which bounds the reactor and injects the carrier gas;
2. The microtube made of steel which injects and guides the precursor gas into the reactor.

The precursor gas acts as the reaction source, and physically supports the fiber inside the reactor. The precursor gas flows into the interior of the microtube and takes an annular form until the fiber is presented in the reactor (in the mode of continuous deposition). Alkenes (i.e., C_xH_{2x}) and methane are usually used as precursors because they are easy to obtain and their costs are low. Also, reference experimental data from similar research is readily available for these materials.

In addition to the reactant gas, the process requires an inert gas as the carrier gas whose function is:

1. to cool the precursor gas. This allows the reduction of soot formation and provides adherence to the substrate at high pressure and low temperature;

2. to produce smaller diameter fibers, as the result of cooling which confines the heat transfer. Helium is used as it takes away more heat from the reaction zone due to its higher heat capacity compared to argon and nitrogen.

3. to flush the soot away from the reaction zone in the reactor.

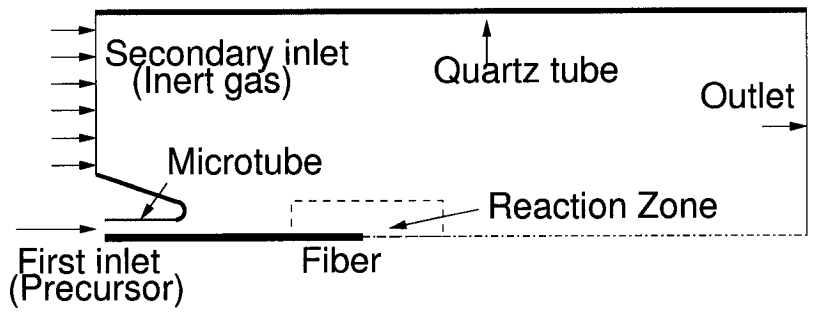

(a) Reactor

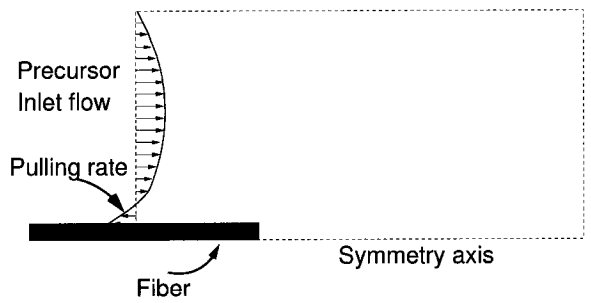

(b) Reaction zone

Figure 1.4 Model for the HP-LCVD reactor

The chemical reaction for the fiber growth is in the tiny area around the fiber tip which is our main concern for the current project. Figure 1.4 shows the computational domain for the fiber tip.

Since pyrolytic LCVD is a localized process that involves a chemical reaction at or near the surface of the fiber tip where gaseous reagents react to produce a solid deposit and gaseous by-products, this requires the adjustement of the flow rates of the precursor gas and the

inert gas to insure that the precursor gas will reach sufficient concentration in this area. An analysis of this process involves the modelling of several coupled energy exchange phenomena:

1. advection-diffusion of reagent gases and by-products;
2. chemical kinetics of the reaction;
3. radiative heat transfer and heat conduction in the fiber.

1.4 Goals and Objectives

The successful operation of a LCVD system demands that the fundamentals of the process be well understood. The purpose of this LCVD modeling research is to gain a quantitative understanding of the process. The fundamental insights thus obtained will guide experimental investigation and to be applied to establish reactor design and process control guidelines.

The HP-LCVD process modelling proposed in this work will serve as a demonstration model of the prototype fabrication tool for the production of a variety of fibers at high speed. Such prototypes can then be tested for their feasibility in terms of cost-effectiveness and efficiency. This approach based on physical modelling and numerical simulation can significantly reduce the high cost and long cycle time necessary for the development of separate systems for individual fibers.

The goal of the project is to put together the software components of such a virtual facility and to test numerically the working hypotheses concerning the operation of a LCVD reactor.

Since LCVD is a thermally activated process characterized by the inter-related fluid flow,

chemical reaction and mass and heat transfer phenomena, the outcomes of this numerical simulation will allow us to analyze how these factors will effect the process. They can be used to evaluate the relative importance of the different process parameters, such as the laser power, the best focus position of the laser and the gas pressure inside the deposition chamber, and different flow rates of the precursor and the carrier gases, and the mixture situation of the two gases.

While the ultimate criteria is the growth rate of the fiber, several specific objectives will lead towards this goal:

1. effect of reactor geometry and laser beam focus position;
2. effect of flow rates of the precursor and carrier gases;
3. effect of laser power or the fiber tip temperature;
4. investigating the mass transport of reagent gases and the prediction of deposition rate.

Therefore, the outcomes of the model will establish the relationship of how the deposition rate and the concentration distributions of the gas depend on the precursor gas flow rate in low pressure and high pressure reactors. The outcomes also will provide a basic understanding of the chemical kinetics and the deposition mechanisms.

This numerical model can be used to minimize the number of experiments required to obtain the maximum amount of information, to select a proper set of the process parameters for experiments, and to design an optimized LCVD system.

1.5 Thesis Organisation

As an introduction to this work, we attempt to demonstrate that there is a significant need for a method that can produce high performance fibers. Chapter 1 presents LCVD fiber

development technology along with a statement of the problem and the objectives of the work. It is argued that LCVD proves itself to have more advantages than other conventional fiber development technologies. The most important hurdles in making LCVD into a commercial technology are discussed and identified. Namely, the growth rate can be improved significantly by increasing the reactor pressure and using of a forced precursor jet, as well as the direction of the precursor jet as a key feature in the reactor design. This leads to the formulation of the objectives of the work which are to provide a virtual machine for the numerical simulation of the LCVD process and to use it to investigate the physical phenomena involved in order to guide the design development of a high growth rate reactor.

The contribution of the present thesis is presented with respect to previous studies on LCVD and LCVD modelling reviewed in Chapter 2. These are critically analysed according to the types of assumptions made, the calculation method, and the resulting modelling capabilities. From this literature survey, it was found that there was a lack of modelling for the continuous fiber growth process. It is shown in this chapter how the current research can contribute to fill this gap in modelling methodology. A critical assessment of previous research and the expected benefits of the current undertaking are presented.

To complement the traditional experimental approach to the design of LCVD reactor, this thesis proposes a virtual prototyping development based on analytical and computational tools. Chapter 3 describes the methodology used for the models, including the physical process and their mathematical modeling. These are then applied to the modeling of LCVD fiber growth process and related phenomena, selecting the appropriate governing equations, and material properties.

Chapter 4 describes the numerical simulation methods including the rationale for the selected CFD environment. Specific numerical developments undertaken to address the particularities of the reactor phenomena and their implementation are presented. The validation methodology is described in Chapter 5 together with the experimental data used for

that purpose.

Together, these provide the basis for the virtual LCVD facility which is used to simulate and investigate the effects of various design configurations and operating conditions on the growth rate characteristics of the fiber production. The methodology and results are presented in Chapters 6 and 7 including the effect of the precursor flow and carrier gas flow, the fiber tip temperatures, the laser focus positions, and the chemical kinetics. These simulation results for two generic reactors, an open air LCVD reactor and the HP-LCVD reactor are compared. Some of the modelling results are compared with and validated by the experiment data.

Lastly, conclusions and discussions of the contributions are presented in Chapter 8.

CHAPTER 2

LITERATURE REVIEW

The field of LCVD is very wide and its evolution has been so rapid and extensive that complete coverage is not possible. In this chapter, a brief review of LCVD developments is presented where the main emphasis is given to the aspects of LCVD numerical modeling, with the objectives to:

- establish the state of the art of LCVD modelling;
- carry out a critical assessment of previous research;
- position the present study with respect to the above and identify potential contributions and expected benefits.

2.1 The LCVD Process

Pyrolytic LCVD research formally began in 1972 when Nelson & Richardson (1972) produced short carbon rods from methane and ethane precursors with CO_2 laser. The 200 μm diameter fibers were grown by focusing on the growing fiber tip. The rods were weak and brittle because of considerable structural non-uniformity. Since, LCVD technology has progressed considerably. Numerous materials have been successfully deposited with pyrolytic LCVD technologies including carbon, tungsten, tungsten carbide, boron, titanium carbide, titanium nitride, silicon, silicon carbide, silicon nitride, gold and aluminum. However, most of the research work so far has concentrated on low pressure LCVD processes conducted below one atmosphere. The disadvantage of using a low pressure is the low growth rate achieved, in the order of 1 to 100 μm/s.

In the mid-80's Wallenberger (1997) reported that smaller (< 20 μm) diameter carbon, boron and silicon fibers were obtained with Ar^+ laser, but the use of low reaction pressure (< 1 bar) continued to result in low growth rates. Fiber growth rates could be increased in the low pressure regime when the reaction chamber pressure was increased.

High pressure LCVD (HP-LCVD) (> 1 bar) is a generic fiber process. It facilitates the formation of advanced inorganic fibers and microstructures directly from the vapour phase. This process is capable of affording chemically pure, structurally uniform, small diameter fibers of almost any substrate that can be produced by the methods of the conventional CVD.

Wallenberger & Nordine (1994) experimented with pressures starting from one bar to 10 bar. Using a Nd:YAG laser, they obtained boron, silicon, silicon nitride and silicon carbide fibers with small diameters (< 20 μm) and high growth rates (0.3 to 1.1mm/s). The growth rates were 30-200 times higher than those obtained on the same substrate at low pressures. Maxwell & Boman (2006) investigated the growth of long carbon fiber using hyperbaric-pressure laser chemical vapor deposition (HP-LCVD). Precursors included the unbranched alkenes with linear structure C_xH_{2x} (where x= 2,4,5,6,7,8), the unbranched alkynes, and benzene. Rate constants, reaction orders, and apparent activation energies were derived for each precursor over a range of experimental conditions. These parameters are used to validate the current modelling work described in detail in Chapter 5.

With these encouraging results, further work is required to find out the effect of even higher reactor pressure (P > 10 atm) on the growth rate as well as on the microstructure of the deposit formed.

2.2 LCVD Numerical Simulation

Several attempts to simulate the LCVD process have been undertaken. Each differs according to the types of assumptions made, the calculation method, and, most importantly, by the resulting modelling capabilities. Two comprehensive tables are presented to summarize these. Table 2.1 enumerates those with respect to the physical modelling, while Table 2.2 identifies those studies in the numerical modelling, giving such details as the geometry, grids, properties, and numerical methods.

Table 2.1 Previous LCVD physical models

	Conduc.	**Reaction**	**Natural Conv.**	**Forced Conv.**	**Radiation**
Hill (1995)	Yes	Yes			Yes
Maxwell (1996)	Yes	Yes	Yes		Yes
Yu & Duncan (1998)	Yes		Yes		Yes
Shaarawi (2001)	Yes	Yes	Yes		
Chen (2002)	Yes	Yes			
Nassar & Dai (2002)	Yes	Yes			
Zhang (2003)	Yes	Yes	Yes		
Zhang (2004)	Yes	Yes	Yes		Yes
Koutlas & Vlachos (2003)	Yes	Yes		Yes	
Duty & Johnson (2003)	Yes	Yes	Yes	Yes	Yes
Zheng (2003)	Yes				
Johnson (2005)	Yes	Yes	Yes	Yes	
Lan (2005)	Yes	Yes			
Croteau (2005)	Yes			Yes	

The majority of the reviewed models assume a Gaussian distributed laser beam, and focus on conduction as the primary heat transfer mode. Conduction is heavily stressed because the temperature distribution is typically calculated for an infinite or semi-infinite substrate. In this case, the pathways available for conduction are relatively large compared to the surface area that is available to convection and radiation losses. As expected in such situations, conduction dominates the local heat transfer behavior. When more complicated geometries are considered, such as during fiber growth, conduction of heat away from the tip of the

Table 2.2 Previous LCVD numerical methods

	Geometry	Grids	Properties	Numerics
Hill (1995)	Cylinder	n/a	f(tem)	F.E.
Maxwell (1996)	fiber	n/a	f(tem)	F.E.
Yu & Duncan (1998)	rectangular	9965	f(tem)	F.E.
Shaarawi (2001)	fiber	80x80	f(tem)	F.D.
Chen (2002)	cylinder	n/a	f(tem)	F.D.
Nassar & Dai (2002)	semi-infinite	40x40x40	constant	F.D.
Zhang (2003)	semi-infinite	82x42x82	f(tem)	F.D.
Zhang (2004)	finite slab	42x82	f(tem)	F.D.
Koutlas & Vlachos (2003)	thin layer	120x60	f(tem)	F.V.
Duty & Johnson (2003)	cylinder	16000	f(tem)	F.V.
Zheng (2003)	cylinder	200x100	f(tem)	F.D.
Johnson (2005)	cylinder	32000	f(tem)	F.V.
Lan (2005)	cylinder	20000	constant	F.D.
Croteau (2005)	fiber	197826	f(tem)	F.V.

fiber is restricted by the small fiber diameter.

Hill (1995) proposed two numerical models (transient and steady-state) to simulate and investigate the deposition of a cylindrical carbon rod during the initial stages of growth, and afterwards when the rod has reached a constant diameter. The transient simulations showed that the growth of carbon rods must involve evaporation of the deposition material and this played a significant role in the heat transfer and reaction kinetics of the LCVD process. The steady-state simulations included radiative and conductive heat transfer. He also found the geometry of the base of the rod to have no significant effect on the steady-state phase of the growth.

The other common mechanism of energy transfer found in previous models is natural convection. This mode prevailed in the LCVD process modelling because the majority of reactors operated in a static atmosphere. It has been shown that in the absence of flowing gases, heat losses due to natural convection can play a significant role in the LCVD process, especially when growing fibers horizontally. In particular, in his model Maxwell

(1996) suggests that natural convection is the dominant mode of heat transfer when growing extremely small diameter fibers.

A three-dimensional mathematical and numerical model for the natural convection induced by an incident laser beam around a fiber was developed by Yu & Duncan (1998). This effort does not account for the effects of the chemical reactions associated with the LCVD process. The laser irradiance characteristics and the absorption by the fiber material is incorporated into the energy equation. The velocity and temperature profiles in the boundary layer demonstrated the existence of a small area in which large temperature gradients prevail.

Zhang (2004) investigated numerically the effect of natural convection on LCVD of titanium nitride on a finite slab under irradiation by a stationary laser beam. The effects of temperature and concentration differences in the gas mixture were modeled and implemented into the thermal model. The results showed that the effect of natural convection on the shape of deposited films was insignificant for all cases studied.

Very few models consider the thermal contribution of chemical reactions in the LCVD process. This is based on the general assumption that the ratio of heat supplied by the exothermic reactions to that of laser irradiation is extremely small and can be ignored. The relative contribution of the heat of reaction appears to increase with pressure as pointed out by Maxwell & Pegna (2004). Indeed, Maxwell even speculated about the possibity of sustained reaction at high pressure.

Lan (2005) developed a mathematical model considering both kinetically limited and mass transport limited growth for simulating the process of fabricating a rod using LCVD. The model describes heat transport in the substrate and deposit as well as the gas-phase mass transport and temperature in the reaction zone in order to determine the growth rate. A finite difference method is developed for solving the governing equations and an iterative algorithm is presented for simulating the process. The applicability of the model is demon-

strated by growing a rod from silicon deposited on a graphite substrate.

Only a couple of models were found to simulate numerically the process of the forced convection of LCVD. Duty & Johnson (2003) extended the modelling efforts by incorporating the effects of forced convection from a directed stream of high velocity reagent gases. In an attempt to model the gas-jet LCVD process, an analysis of the temperature distribution on the substrate surface demonstrated that the shape of the heated zone was unaffected by a high velocity directional flow. The temperature distribution in the gas phase, however, was significantly affected by increases in flow rate, causing the thermal boundary layer to shrink. Thus showing the effects of forced convection cooling to be significant. They also developed a mass transfer model for understanding the role of a gas jet in the LCVD process. They found that across all deposition regimes, the gas jet was an effective tool for increasing the concentration of reagent gases at the surface of the substrate. If the deposition process was kinetically limited or in the transition phase, the forced convection cooling effects of the gas jet dominated and the deposition rate decreased with increasing flow rates for a fixed laser power. However, if the deposition process was severely limited by diffusion, the gas jet was shown to have a signficant positive impact on both the deposition rate and the deposit resolution. These findings could logically be extended to a system in which the laser power is automatically adjusted to maintain a constant temperature.

At a more complex level, a coupling between the exchange mechanisms in the gaseous and solid phases was proposed by Koutlas & Vlachos (2003). A numerical model based on the Navier-Stokes equations governing the flow, heat transfer, and chemical reactions was developed for the gases, while the temperature distribution in the substrate was determined by solving the corresponding heat conduction equation. This model includes the solid phase and gas phase and the substrate are assumed to be temperature dependent. In this LCVD process, a laser beam irradiates the substrate at a specific position where a thin layer can be deposited. The precursor flow jet direction is parallel to the substrate. The model provided an opportunity to assess the important parameters concerning the LCVD process,

such as the gas flow field, temperature distribution, concentration of reactants/products, and deposition height.

Johnson (2005) provided a model for the fabrication of the first high aspect ratio multi-layered LCVD wall structures. The kinetics studies enabled the formulation of an advanced computational model in the FLUENT CFD package for studying energy transport, mass and momentum transport, and species transport within a forced flow LCVD environment. But this CFD deposition rate model does not explicitly account for the dynamics of the growth process through the creation of new solid material; therefore, the deposition rate profiles only serve as indicator of the deposit shape during the initial growth periods. Some insight into the changing thermal conditions within a growthing LCVD carbon fiber is gained through another model which is not simulating with Navier-Stokes equation.

Croteau (2005) investigated the concentration distributions of the precursor (methane) and the carrier gas (argon) and the temperature distribution on the carbon fiber in the forced convection situation in a HP-LCVD reactor. This study can be thought to be the first attempt at modelling continuous fiber growth even though it involved only the coupling of flow and energy exchange mechanisms. It used a very fine grid size which was the major weakness of the other LCVD models.

Another interesting feature found in previous research is the inverse problems. That is development of models able to predict required boundary conditions from specified global operating characteristics.

Nassar & Dai (2002) developed an axisymmetric model for predicting the laser power required as a function of time, for the growth of a cylindrical rod by laser-induced chemical vapor deposition. They first specified the geometry of the rod and the expected growth, computed the required temperature from the growth rate equation, obtained the temperature profile based on the solution of the heat conduction equation, and then optimized the laser intensity for a given beam width by using the least squares method. This problem is an

inverse problem because it is from the temperature field required for the pre-determined growth that one can determine the laser power.

Chen (2002) advanced a numerical model for simulating axisymmetric rod growth at a stationary laser focal spot in an LCVD process. Using an inverse approach, the model could predict the laser power for growing a rod with a pre-specified shape at steady state. This model could predict the laser power for growing a rod with a pre-specified shape with the assumption that the temperature distribution of the rod under the laser focus was at unsteady state. The optimum laser power calculated from this model was compared with the power calculated from the model of Chen's under steady state.

In a summary, several kinds of LCVD models have been developed which include the following energy transfer mechanisms:

- Conduction between the solid deposition and the substrate;
- Natural convection;
- Forced convection;
- Inverse heat conduction.

2.3 Critical Assessment of Previous Work

From the review of LCVD modelling, it is apparent that there is a lack of modelling for the continuous fiber growth process. This is because modelling research always follows the steps of experiments. Initially, only short fibers were produced and consequently, the modelling work was generally directed at simulating the initial stages of the fiber growth and the heat transfer between the fiber and the substrate. Recently, the production of longer fibers, and more specifically, continuous fibers for industrial applications have been attempted.

In such situations, the initial stages of the fiber growth and the heat transfer between the fiber and the substrate are no longer the main concerns. The requirements for this type of modelling are more demanding and require:

- a detailed analysis around the fiber tip;
- an assessment of the effects of high pressure;
- the ability to estimate the effect of precursor and carrier gas flow rates;
- the evaluation of a forced flow jet along the direction of fiber growth;
- the incorporation of fiber motion for continuous fiber production.

Nassar & Dai (2002), Chen (2002), and Zheng (2003) studied the inverse heat conduction problems which could have a bearing on optimal design. This is not yet a crucial issue at this stage of the development of the field.

Yu & Duncan (1998) and Zhang (2004) studied natural convection problems which is not a dominant mechanism in the present study, as Duty & Johnson (2003) found that natural convection is negligeable compared to forced convection if the both modes of energy transfer co-exist.

Shaarawi (2001) did not consider the effect of varied reaction orders. The current study found that the reaction order was a very important kinetics parameter.

Maxwell (1996) and Lan (2005) developed a novel integrated mathematical model to describe the heat transport in the deposited material and substrate, as well as to simulate the gas-phase in the heated reaction zone and its effect on growth rate. The models do not solve the Navier-Stokes equations. The modeling results could be useful references to compare with the results from the current modeling which is used with another methodology (Navier-Stokes equations).

One of the main characteristics of the proposed model is based on the forced convection of the process. From Table 2.1, there is only a few papers which deal with this flow mechanism.

The model of Koutlas & Vlachos (2003) provided some understanding of the LCVD process. He studied the temperature profile of the substrate and produced thin layer. However, as mentioned in Section 1.1, we believe that the substrate structure will not play a key role for the substantially long continuous fiber. Therefore, this work is not directly relevant to the current problem.

Duty & Johnson (2003) developed two models, and focused on some insights for the entire reactor. One is the thermal and fluidic modelling and the other is the mass transfer including chemical reactions. However, he did not combine these two models. He suggested in his Ph.D. thesis that in future studies, the combined flow, heat transfer and mass transfer should be coupled.

Johnson (2005) continued the work undertakened in the model of Duty (2001) and developed an advanced computational model in the FLUENT CFD package for coupling energy transport, mass and momentum transport, and species transport within a forced flow LCVD environment. Both CFD deposition rate models of Duty & Johnson (2003) and Johnson (2005) did not explicitly account for the dynamics of the growth process through the creation of new solid material; there were no coupling between the fiber and the fluid mixture. Neither of these studies are directly relevant to the current problem.

The research of Croteau (2005) could be considered as the first stage of the current work and has provided useful data about the material properties, the geometry of the HP-LCVD reactor, and the boundary condition profiles of the precursor and carrier gas inlets for the current reactor configuration. Some results were revised by the present work. For example, the figure shown the concentration distribution of the methane and argon in Croteau (2005) showed a "waving" boundary line between the two gases. This is troubling and can be

traced to inadequate numerical techniques used in this first attempt at coupling the various energy exchange mechanisms. Indeed, Croteau (2005) used First Order Upwind discretization techniques as well as uniform grids. This problem is improved in the present work. Further, Croteau (2005) did not simulate the reaction kinetics in the HP-LCVD which play a crucial role in real LCVD modelling. The current work will include theses mechanisms.

As shown in Table 2.2, some authors (Hill (1995), Maxwell (1996), Chen (2002), Lan & Nassar (2003)) did not provide a complete numerical modelling information such as the meshing sizes, convergence, and accuracy. It is difficult to judge whether their modelling was adequate from the numerical point of view. Some of them used too few grids points for adequate numerical modelling. Nassar & Dai (2002) used only 40x40x40 for the geometry of semi-infinite. Zhang (2004) used only 42x82 for the geometry of finite slab. An appropriate grid size is a very important aspect for a reliable and accurate numerical simulation. The accuracy of the computation is dubious due to the lack of grid size information and in some cases, these are clearly too coarse.

Another main weakness for the previous models is the lack of sufficient information of modeling validations.

2.4 Contributions of Current Work

From this review, it has been found that a state of the art numerical model of continuous LCVD fiber growth has not been carried out previously. Specifically, LCVD modelling is lacking in three respects:

- rigourous and validated numerical modelling for the continuous fiber growth process;
- physical modelling for the complex coupling of the phenomena specific to HP-LCVD.
- detailed microscale process analysis in LCVD.

The research presented in this thesis anticipates to uncover fundamental relationship between process parameters (flow, pressure, temperature, laser power, laser focus position) and product characteristics (fiber growth rate, specie concentration distributions, flow velocity vector field). In addition, since the chemical kinetics of the deposition is modelled, we also anticipate to provide a representative description of the physics occuring at the fiber tip (by-product, jet directions, temperature).

On a more applied level, this work also aims at finding which factors affect the fiber growth rate. The numerical simulation methodology is used to assess separately the various phenomena which occur in a simplified reactor; namely the flow field, energy exchange mechanisms and the chemical kinetics. Investigation of the contribution of each of these can help to gain insight into the LCVD process. Specifically, how the growth rate (deposition rate) depends on such parameters as the laser power (or tip temperature), precursor flow rate and the position of the laser beam focus have been studied. Similarly, an attempt to investigate how the detailed flow properties and species concentration affect the deposition rate is undertaken.

This research is to gain a quantitative understanding on the process of continuous fiber growth. All anticipated insights derived from these simulations can hopefully support experimental observations that have not been confirmed for lack of existing measurement tools with the required spatial resolution and the chemical kinetics parameters for HP-LCVD operating conditions. The quantitative informations derived from numerical simulations can be used as guidelines for reactor design and process control.

A reliable and credible modelling methodology covering all the above requirements is clearly lacking and this work will attempt to fill this gap.

CHAPTER 3

PHYSICAL MODELLING

3.1 Introduction

The modelling of a LCVD reactor is a difficult task as it involves a classical fluid mechanics problem (mass and momentum transfer with temperature effects) and a chemical kinetics problem with mass production occurring at a very small scale and high energy level. The latter is imbedded within the former and both interact through very complex transport phenomena. The general conservation laws constitute the basis of the model which is built progressively in order of increasing complexity through three stages (Bird & Stewart (2002)):

1. modelling of the fluid mixture at constant temperature, with emphasis on viscous and convective momentum transport;
2. introducing temperature variations and heat addition, with emphasis on conduction and convection energy transport;
3. inclusion of the variation of species concentration, with emphasis on reaction kinetics and mass transport.

The governing equations (Patankar (1980)) for a general transport phenomenon are given by the following system of differential equations:

$$\frac{\partial(\rho\phi)}{\partial t} + \nabla \cdot (\rho \mathbf{V}\phi) = \nabla \cdot (\Gamma grad\phi) + S \tag{3.1}$$

where Γ is the diffusion coefficient, $\mathbf{V}$ is the velocity field and S is the source term. The four terms in the general differential equation represent the contributions to the transport of the variable ϕ due to the unsteadiness, the convection, the diffusion, and the sources. The dependent variable ϕ represents the transported quantity and can stand for a variety of different variables, such as the mass or mass fraction of a chemical species, a velocity component, the enthalpy or the temperature. Accordingly, for each of these variables, an appropriate meaning is given to the diffusion coefficient Γ and the source term S.

Convective transport : Convective transport describes the motion of fluid quantities in space through the interpenetration of fluid particles. Convective effects are represented in the equations by fluxes of conserved quantities through control volumes; for example, $\nabla \cdot \mathbf{V}\phi$ where ϕ can represent $\rho, n_i, E, \rho\mathbf{V}$, or P. Convection is a continuum concept, which assumes that quantities such as density, velocity, and energy are smoothly varying functions of position.

Diffusive transport : Diffusive transport expresses the transfer of mass, momentum, and energy due to the presence of gradients in concentration, velocity, and temperature. The transport coefficients and the gradients with which they are associated are given in Table 3.1. Molecular diffusion represents a diffusive transfer of mass and energy due to a species concentration gradient. Viscosity represents diffusive transfer of momentum due to a velocity gradient. Thermal conduction or thermal diffusion represent transfers of energy due to a temperature gradient (Oran & Boris (2001)).

Table 3.1 Transport coefficients and associated gradients

Diffusion Coefficient	**Symbol**	**Associated Gradients**
Molecular diffusion	D_{ij}	$\nabla(n_i/N), \nabla T, \nabla P$
Viscosity	μ	$\nabla \mathbf{V}$
Thermal conduction	k_c	$\nabla T, \nabla P$
Thermal diffusion	$D_{T,i}$	∇T

Reaction kinetics : Chemical reactions among constituent species are represented by the production and loss terms (source terms). They are called local phenomena because they do not depend on spatial gradients. The macroscopic form used in the continuum equations arises from processes that average over microscopic effects. They are only truly local in the continuum limit.

The reaction kinetics which occur in the LCVD process are described by the unimolecular reactions among the interacting species,

$$C_2H_{4(g)} \longrightarrow 2C_{(s)} \downarrow +2H_{2(g)} \uparrow \tag{3.2}$$

$$CH_{4(g)} \longrightarrow C_{(s)} \downarrow +2H_{2(g)} \uparrow \tag{3.3}$$

The reaction rate constants may be complicated function of temperature and sometimes pressure. The expression for the rates are usually written in an Arrhenius or modified Arrhenius form which will be described in detail in the next section.

3.2 LCVD Fiber Growth Modelling

The process of pyrolytic LCVD, illustrated in Figure 3.1, is constituted of the following seven mechanism steps (Boman (2001)):

1. macroscopic transport of reagent gases to the reaction zone;
2. diffusion of gases through the boundary layer and to the fiber surface;
3. adsorption of precursor gases onto the fiber;
4. surface chemical reaction;
5. desorption of by-products off the fiber surface;

6. diffusion of by-products;

7. macroscopic transport of by-products away from the reaction zone.

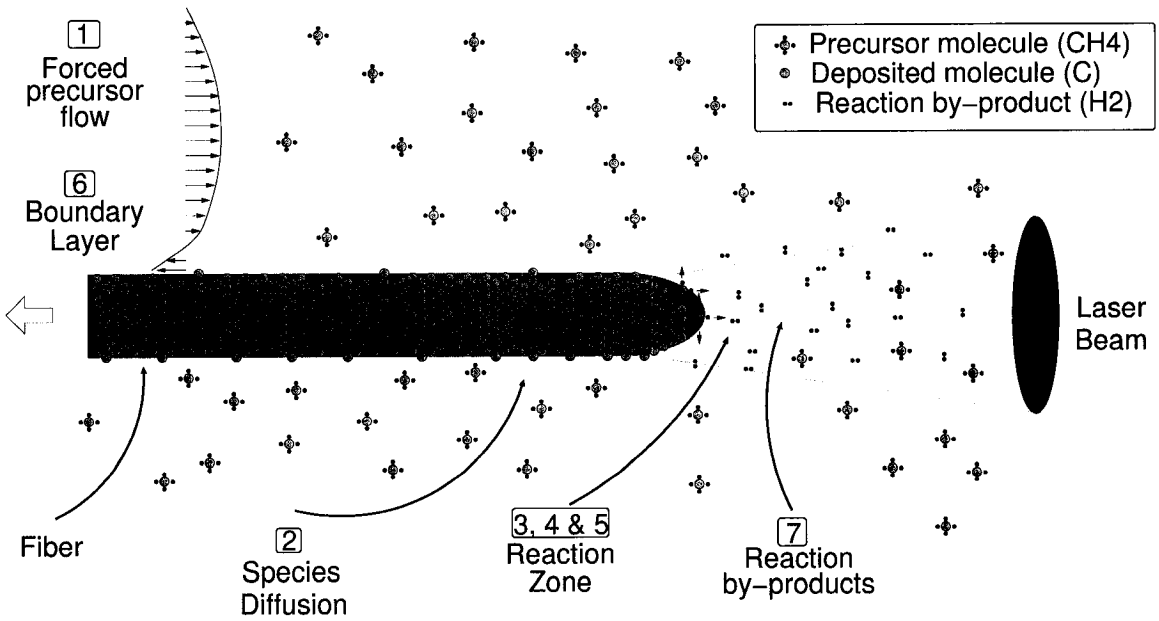

Figure 3.1 The LCVD fiber growth process

According to the description given in Duty & Johnson (2003), these seven steps are divided into three distinct categories: mass transport, diffusion, and chemical kinetics. The slowest step in this sequence is said to be the rate limiting step. If Steps 3,4 and 5 are rate-limiting, then the overall process is said to be in the Kinetic Regime. If Steps 2 and 6 are rate-limiting, then the process is diffusion limited and is said to be in the Mass Transport Regime. Steps 1 and 7 are macroscopic momentum transport. The overall deposition rate will be dictated by the limiting or slowest of these steps.

The diffusion of reactive gases to the substrate is described by Fick's first law of diffusion.

$$J_i = -D_i \frac{\Delta C_i}{\Delta X_i} = \frac{D_i}{\delta_i}(C_i^0 - C_i^s) \tag{3.4}$$

where for the ith gas specie, J_i is the rate of diffusion; D_i is the diffusion coefficient; the ratio $\Delta C/\Delta X$ is the concentration gradient; δ is the boundary layer thickness; C^0 and C^s are the concentrations of the reagent in the gas stream and at the substrate, respectively. Often, the deposition rate can be assumed to be proportional to some power of reagent concentration at the surface of the substrate, and this is expressed by:

$$J = k(C^s)^n \tag{3.5}$$

where J is the deposition rate, k is the reaction rate, C^s is the concentration of the reagent at the substrate surface, and n is the order of the reaction.

At steady state, the rate of diffusion is equal to the deposition rate. After applying the ideal gas law and assuming that the order of the reaction is 1 for the simplest case, there is the relationship:

$$C^s = J/k \tag{3.6}$$

Putting C^s from Eq. 3.6 into Eq. 3.4, the relationship becomes:

$$J = \frac{D_i}{\delta_i} C_i^0 - \frac{D_i}{\delta_i}\frac{J}{k} \tag{3.7}$$

then, there is the relationship:

$$J = \frac{C_i^0}{[(\delta_i/D_i) + k^{-1}]} \tag{3.8}$$

This equation relates the known concentration in the gas stream to the deposition rate. The diffusion resistance is δ_i/D_i, and the kinetic resistance is k^{-1}. The reaction can be generally classified as (1) kinetically limited (low temperatures), (2) mixed regime, (3) and diffusion limited (high temperatures). If the reaction is kinetically limited, then the diffu-

sion resistance is much less than the kinetic resistance and the reaction rate equation then simplifies to:

$$J = kC_i^0 \tag{3.9}$$

The rate constant k increases with temperature according to the Arrhenius relationship, as follows:

$$k = k_0 e^{(-E_a/RT)} \tag{3.10}$$

Hence, the deposition rate follows the Arrhenius relationship at lower temperatures (Figure 3.2).

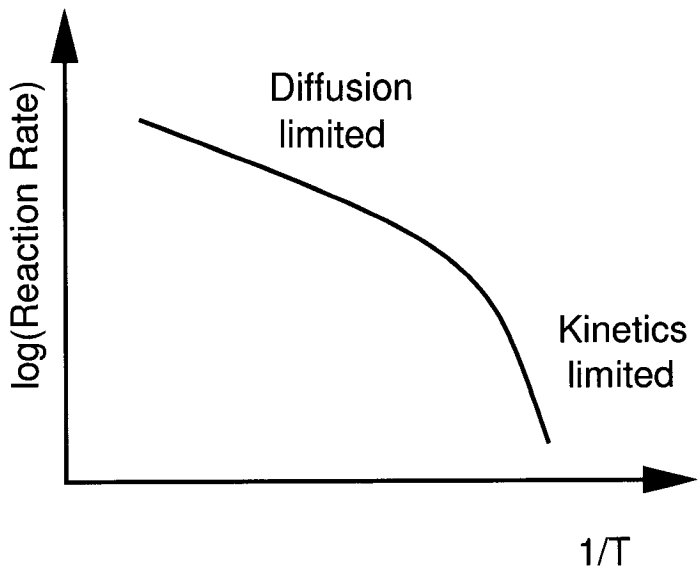

Figure 3.2 Reaction rate versus temperature Duty & Johnson (2003)

At lower temperatures, the kinetic resistance is greater than the diffusion resistance, and so the reaction is kinetically limited. As the temperature is increased and the activation energy is more readily overcome, the reaction rate increases. With further increases in temperature, the reaction becomes diffusion limited since new reagents cannot diffuse to the reaction zone fast enough to feed the reaction.

The diffusion coefficient D also increases with temperature, although not as rapidly as the rate constant, according to:

$$D = (\frac{D_0}{C})\sqrt{T} \tag{3.11}$$

The LCVD process is more complex than simply characterised as diffusion limited or kinetically limited. Since there is a large temperature gradient over the heated zone, different regimes may co-exist simultaneously. Concentration gradients will appear along the surface as well as in the normal direction.

At even higher temperatures, the deposition rate will decrease. This can be explained through several different phenomena. If the LCVD reaction is exothermic, then the presence of a large amount of thermal energy at high temperatures will force the reaction to slow down or possibly reverse, thereby causing etching of the deposit. The high surface temperatures may also cause the precursor gases to be sufficiently heated for the LCVD reaction to occur in the gas phase, producing solid particles (Maxwell (1996)). Extremely high temperatures may also cause the substrate or the underlying deposit to sublimate (Duty & Jean (2001)).

Equation 3.10 can be linearized in the following way:

$$lnk = lnk_0 - \frac{E_a}{R}\frac{1}{T} \tag{3.12}$$

The apparent activation energy of the process can be calculated from several growth rate-temperature data pairs. Besides the activation energy, the growth rate dependence as a function of the partial pressure of a reactant can also be established. This is determined experimentally by measuring the growth rate while keeping all parameters constant, except the partial pressure of the reactant of interest. By plotting the logarithm of the growth rate as a function of the logarithm of the varied partial pressure, the reaction order is obtained from the slope of the plot. The reaction rate dependence on the partial pressure of the

reactants is usually given as:

$$J = kP_A{}^a P_B{}^b \tag{3.13}$$

where a and b are the reaction orders for species A and B, respectively (Kajsa (2001)). Sometimes, it is difficult to obtain the partial pressure of the reagent gases. The reagent concentration will replace the partial pressure. If there is only one reagent specie for the reaction, this equation is substituted into Equation 3.5.

3.3 Assumptions

Based on the global characteristics of the problem, specific operating parameters of the process and the calculation of the relevant dimensionless numbers, the following assumptions can be made:

- The geometry of the fiber tip is assumed to be constant.
- The chemical reaction is only happened in fiber surface. The existence of soots is ignored.
- The reaction is such that pressure gradients can be ignored (isobaric conditions).
- The contribution of the Dufour effect (transport of energy originating from a concentration gradient) to the thermal flux is omitted.
- The generation of heat due to viscous effects of the flow is ignored.
- The effect of buoyancy forces is neglected. This can be established from the Grashoff number which is proportional to the ratio (buoyancy forces)/(viscous forces). Because the characteristic length in the LCVD process is very small, the value of the Grashof number is very small.

- Strictly speaking the process of the fiber growth is a transient problem. In the present work, the simulation of two distinct configurations were undertaken:

  Ambient reactor : with the laser beam focus fixed and without pulling the fiber.

  The fiber growth first increases from the initial stage, and after reaching the maximum rate, it finally decreases. This results because of the motion of the fiber tip away from the laser focus. However, the experiments show that the maximum growth rate is around 40 μm/s. With such a low growth rate, the movement of the fiber tip surface cannot make a significant contribution to the flow field. Hence the problem can be treated as quasi-steady where the fiber is a stationary surface, Chapter 6.

  High pressure reactor : with the laser beam focus fixed and pulling the fiber.

  The growth rate can be much higher so that the fiber tip surface cannot be treated as stationary but has a constant velocity. For a uniform pulling rate, it can be assumed to be equal to the growth rate. Therefore, the problem in high pressure still can be treated as a steady state problem by a change of reference frame and the appropriate modifications of the wall boundary conditions, details in Section 4.3.4.

3.4 Governing Equations

The mathematical modelling of flows is based on the theory of continuum mechanics. The governing equations consist of conservation equations and constitutive equations. The former are derived from the principle of conservation of mass, the principle of balance of linear momentum, and the principle of conservation of energy. Constitutive equations relate the stresses in the fluid to the deformation history. These are rather classical and can be found in a number of textbooks of Bird & Stewart (2002), Kohler & Wiegand (2002), Baehr & Stephan (2006), Saatdjian (2000) and are presented here for completeness.

3.4.1 Continuity equation

The principle of conservation of mass is expressed by:

$$\frac{\partial \rho}{\partial t} + \nabla \cdot (\rho \mathbf{V}) = 0 \tag{3.14}$$

For 2D axisymmetric flows, this equation becomes:

$$\frac{\partial \rho}{\partial t} + \frac{\partial}{\partial x}(\rho v_x) + \frac{\partial}{\partial r}(\rho v_r) + \frac{\rho v_r}{r} = 0 \tag{3.15}$$

3.4.2 Momentum equations

The momentum equation is derived from Newton's law in a continuum medium:

$$\rho \frac{D\mathbf{V}}{Dt} = \nabla \cdot \sigma + f \tag{3.16}$$

in which f is the resultant of volumetric forces, and σ is the Cauchy stress tensor. For the case of 2D axisymmetric, this equation becomes:

Axial direction:

$$\frac{\partial}{\partial t}(\rho v_x) + \frac{1}{r}\frac{\partial}{\partial x}(r\rho v_x v_x) + \frac{1}{r}\frac{\partial}{\partial r}(r\rho v_r v_x) = -\frac{\partial p}{\partial x} \tag{3.17}$$
$$+\frac{1}{r}\frac{\partial}{\partial x}\left[r\mu\left(2\frac{\partial v_x}{\partial x} - \frac{2}{3}(\nabla \cdot \mathbf{V})\right)\right] + \frac{1}{r}\frac{\partial}{\partial r}\left[r\mu\left(\frac{\partial v_x}{\partial r} + \frac{\partial v_x}{\partial x}\right)\right] + F_x$$

Radial direction:

$$\frac{\partial}{\partial t}(\rho v_r) + \frac{1}{r}\frac{\partial}{\partial x}(r\rho v_x v_r) + \frac{1}{r}\frac{\partial}{\partial r}(r\rho v_r v_r) = -\frac{\partial p}{\partial r} \tag{3.18}$$
$$+\frac{1}{r}\frac{\partial}{\partial x}\left[r\mu\left(\frac{\partial v_r}{\partial x} + \frac{\partial v_x}{\partial r}\right)\right] + \frac{1}{r}\frac{\partial}{\partial r}\left[r\mu\left(2\frac{\partial v_r}{\partial r} - \frac{2}{3}(\nabla \cdot \mathbf{V})\right)\right] \tag{3.19}$$

$$-2\mu\frac{v_r}{r^2}+\frac{2}{3}\frac{\mu}{r}(\nabla\cdot\mathbf{V})+\rho\frac{v_z^2}{r}+F_r$$

where,

$$\nabla\cdot\mathbf{V}=\frac{\partial v_x}{\partial x}+\frac{\partial v_r}{\partial r}+\frac{v_r}{r} \tag{3.20}$$

3.4.3 Energy equation

The energy equation balances the internal energy of the fluid, the viscous dissipation, the energy produced in the fluid (for example by a chemical reaction), and the energy transported by conduction and convection:

$$\rho\frac{DU}{Dt}=\sigma:\nabla\mathbf{V}+E_r-\nabla\cdot q \tag{3.21}$$

If we consider the thermal energy (i.e. the energy corresponding to the temperature of the fluid), the energy of motion and assuming that the conduction satisfies the Fourier law $q=-k\nabla T$, Eq. 3.21 becomes:

$$\rho C_p\frac{DT}{Dt}=\sigma:\nabla\mathbf{V}+E_r+\nabla\cdot(k_c\nabla T) \tag{3.22}$$

3.4.4 Species conservation and the chemical reaction

For the current problem, the mass transport is driven by the consumption of reagent gases across the laser spot. The rate at which the reagent gases are consumed equals the rate of the deposition reaction, which is described by chemical kinetics as Eq. 3.5. The reaction rate of the LCVD process is assumed to follow an Arrhenius relationship that is exponential with respect to temperature:

$$\frac{DC_i}{Dt}=D_i\nabla^2C_i+J \tag{3.23}$$

The rate of the reaction J is related to the mass of material reacted per unit area. If only one reagent specie is present in the reaction, with the reagent concentration replacing the partial pressure, Equation 3.13 becomes:

$$J = k(C_i)^n = k_0 e^{-E_a/RT}(C_i)^n \tag{3.24}$$

The variables k_0, E_a, and n are typically determined from a kinetic analysis of experimental data.

To account for the Soret effect, additional are required to describe the thermodiffusion phenomena, Kohler & Wiegand (2002). Equation 3.23 then becomes as

$$\frac{DC_i}{Dt} = D_i \nabla^2 C_i + D_{T,i} \bigtriangledown [C_i(1 - C_i) \bigtriangledown T] + J \tag{3.25}$$

The Soret effect is relevant when a temperature gradient is present, i.e. a Gaussian temperature profile on the fiber tip. Most of the configurations and results computed in this study were without considering such temperature variations. Therefore the inclusion of this parameter has no effect, and the results shown do not include the Soret modelling.

3.5 Boundary Conditions

For a well-posed problem, the flow properties are obtained by solving Eqs. 3.15,3.17, 3.18 and 3.22, subject to boundary conditions which reflect the operating conditions of the process. Boundary condition types are either Dirichlet boundary conditions (which specify the value of a variable) or Neumann boundary conditions (which specify the normal derivative of a variable).

Several kinds of boundary conditions are encountered in the present problem: axial sym-

metry, wall boundaries, mass flowrate, pressure outlet. In addition, we have introduced fictitious boundaries in the flow domain as part of the domain decomposition procedure, details in Chapter 7. At these internal boundaries data of the entire reactor's calculated flow are transferred from the reactor domain to the inner tip region, i.e. velocity, pressure, thermal and specie concentration fields. These are illustrated in Fig. 3.3.

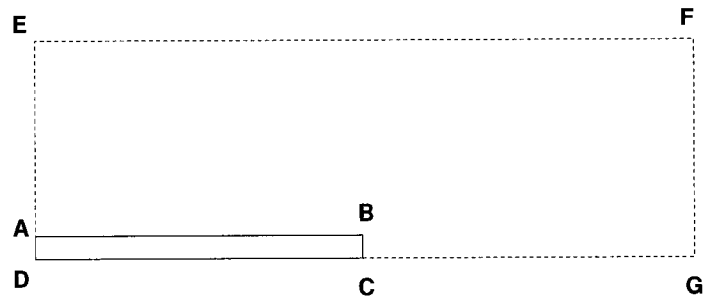

Figure 3.3 Boundary conditions in reaction zone

Boundary AE : velocity-inlet profile condition or mass flowrate;

Boundary EF : interface boundary where data is transferred from the entire reactor solution or solid no-slip condition;

Boundary FG : pressure outlet condition or an interface profile boundary;

Boundary DC and CG : symmetry conditions;

Boundary AB : moving solid condition with the same speed of the pulling rate. A conjugate heat transfer approach is used where the fluid and solid regions are coupled.

Boundary BC : moving solid conditions with temperature and mass deposition from the chemical reaction.

3.6 Material Properties

The material properties determine how physically accurate the model is and how realistically it will reproduce the behaviour of the reactor.

3.6.1 Precursor gas and carrier gas

The properties of precursor gas and carrier gas are given in Table 3.2 as obtained from the database of the Computational Fluid Dynamics commercial software used in this work, FLUENT. Under the conditions of the open air cases, the temperature and the pressure assume ambient values.

Properties may be temperature and/or composition dependent, with temperature dependence based on a polynomial, piecewise-linear, or piecewise-polynomial function and individual component properties either defined by the modeler or computed via kinetic theory.

Table 3.2 Material properties of ethylene, argon, and nitrogen under standard conditions

Property	**Ethylene**	**Argon**	**Nitrogen**
Density (kg/m^3)	1.137	1.6228	1.138
Viscosity (kg/m/s)	1.03×10^{-5}	2.125×10^{-5}	1.663×10^{-5}
C_p (J/kg/K)	2233	520.64	1040.67
Thermal conductivity (w/m/K)	0.0214	0.0158	0.0242
Stand.State Enthalpy (J/kgmol)	5.24554×10^{7}	-3117.71	0
Stand.State Entropy (J/kgmol-k)	219148.6	154719.3	191494.8
Reference temperature (K)	298.15	298.15	298.15

3.6.2 Full multicomponent diffusion

The theory describing diffusion in binary gas mixtures at low to moderate pressures has been well developed by Reid (1977). For an ideal gas,

$$D_{AB} = \frac{(1.858 \times 10^{-3})T^{3/2}[(M_A + M_B)/M_A M_B]^{1/2}}{P\sigma_{AB}{}^2\Omega_D} \tag{3.26}$$

where

D_{AB} = diffusion coefficient, cm^2/s

T = temperature, K

P = pressure, atm

σ = characteristic length, A

Ω_D = diffusion collision integral, dimensionless

To use Eq. 3.26, some rule for obtaining binary value σ_{AB} from σ_A and σ_B must be chosen. Also, it can be shown that Ω_D is a function only of kT/ϵ_{AB} (k is Boltzmann constant), where again some rule must be selected to relate ϵ_{AB} to ϵ_A and ϵ_B. The simple rules shown below are often employed:

$$\epsilon_{AB} = (\epsilon_A \epsilon_B)^{1/2} \tag{3.27}$$

$$\sigma_{AB} = \frac{\sigma_A + \sigma_B}{2} \tag{3.28}$$

Following several references, e.g. Reid (1977), Ω_D is tabulated as a function of kT/ϵ.

$$\Omega_D = \frac{A}{T^{*B}} + \frac{C}{e^{DT^*}} + \frac{E}{e^{FT^*}} + \frac{G}{e^{HT^*}} \tag{3.29}$$

where $T^* = kT/\epsilon_{AB}$, and $A = 1.06036$, $B = 0.15610$, $C = 0.19300$,$D = 0.47635$, $E = 1.03587$, $F = 1.52996$, $G = 1.76474$, $H = 3.89411$

Below is some related data from Reid (1977):

Substance	σ **(A)**	ϵ/k **(K)**
Argon (Ar)	3.542	93.3
Helium (He)	2.551	10.22
Methane (CH_4)	3.758	148.6
Ethylene (C_2H_4)	4.1463	224.7
Hydrogen (H_2)	2.827	59.7
Nitrogen (N_2)	3.798	71.4

Using Eq. 3.26, the mass diffusion coefficients can be expressed as functions of temperature. Under the conditions of room temperature and atmospheric pressure, the binary mass difffusion coefficients for several binary mixtures are given as:

Substance	**Mass diffusion coefficient**
C_2H_4 - N_2	1.51645×10^5 m^2/s
C_2H_4 - H_2	6.51246×10^5 m^2/s
N_2 - H_2	8.46062×10^5 m^2/s
C_2H_4-Ar	1.48136×10^5 m^2/s
CH_4-Ar	1.52797×10^4 m^2/s

Multicomponent diffusion in gas mixtures is described by the Stefan-Maxwell equation from Reid (1977).

$$\sum_{i=1,j\neq i}^{N} \frac{X_i X_j}{D_{ij}}\left(\frac{\vec{J}_j}{\rho_j} - \frac{\vec{J}_i}{\rho_i}\right) = \nabla X_i - \frac{\nabla T}{T}\sum_{i=1,j\neq i}^{N} \frac{X_i X_j}{D_{ij}}\left(\frac{D_{T,j}}{\rho_j} - \frac{D_{T,i}}{\rho_i}\right) \tag{3.30}$$

After some mathematical manipulations, the diffusive mass flux vector, $\vec{J}_i$, is obtained from

$$\vec{J}_j = -\sum_{j=1}^{N-1} \rho D_{ij} \bigtriangledown Y_j - D_{T,i}\frac{\bigtriangledown T}{T} \tag{3.31}$$

where

D_{ij} = binary mass diffusion coefficient of ij system

X_i= mole fraction of i

Y_j= mass fraction of j

$\vec{J}_i, \vec{J}_j$ = diffusive mass flux vector of i, j

$\bigtriangledown X_i$ = gradient in mole fraction of i

$D_{T,i}$ is the thermal (Soret) diffusion coefficient

The thermodiffusion coefficient is using the following empirically-based composition dependent expression from Fluent (2003):

$$D_{T,i} = -2.59 \times 10^{-7} T^{0.659} \left[\frac{{M_{w,i}}^{0.511} X_i}{\sum_{i=1}^{N} {M_{w,i}}^{0.511} X_i} - Y_i\right] \cdot \left[\frac{\sum_{i=1}^{N} {M_{w,i}}^{0.511} X_i}{\sum_{i=1}^{N} {M_{w,i}}^{0.489} X_i}\right] \tag{3.32}$$

This form of the Soret diffusion coefficient will cause heavy molecules to diffuse less rapidly, and light molecules to diffuse more rapidly, towards heated surfaces.

3.6.3 Properties under high pressure

Under conditions of high pressure, 50 bar, and temperature 193.15 K, the properties of methane and argon are given in Table 3.3.

Table 3.3 Properties of methane and argon at 50 bar and 193.15 K

Material Properties	Methane	Argon
Density (kg/m^3)	124.51	149.92
Viscosity (kg/m/s)	1.2633×10^{-5}	1.7929×10^{-5}
C_p (J/kg/K)	0.028	8.0553×10^{-4}
Thermal Conductivity (w/m/K)	0.066961	0.0160219

There are two sources for methods to compute property data in HP-LCVD reactor simulation. Figs 3.4 and 3.5 show the dependence of density, viscosity, and conductivity with temperature according to the data from the NIST ChemBook website, for methane.

Equation 3.26 cannot be used to calculate the binary mass diffusion coefficient under the conditions of high pressure and low temperature.

For predicting the diffusivity of binary gas mixtures at high pressures, the method of Takahashi (Chap.2 p.371 of Perry & Green (1997)), Equation 3.33, applies.

$$D_{12} = 1.013 \times 10^5 \frac{D_{12}'}{P}(D_{12}P)_R(1 - AT_r^{-B})(1 - CT_r^{-E}) \tag{3.33}$$

where D_{12}' is the low pressure diffusivity at the temperature of interest. $(D_{12}P)_R$ is a reduced diffusivity pressure product at infinite reduced temperature (T_r); P is the pressure given in Pa; and A, B, C, and E are constants.

All are tabulated in Table 2-401 of Perry & Green (1997). Component 1 is the diffusing specie, while component 2 is the concentrated specie.

The mass diffusion coefficient of argon and methane calculated by Croteau (2005) with the same method was D_{CH_4-Ar} = 1.8078×10^7 (m^2/s). Comparing to the data under ambient conditions (1.52797×10^4 m^2/s), it is about 1000 times less than that of ambient conditions, confirming the significant differences for gas properties under conditions of low and high

pressure.

Because the ideal gas law is applicable, the following properties are defined using kinetic theory:

- viscosity
- thermal conductivity (for fluids)
- specific heat capacity
- mass diffusion coeficients (for multi-species mixtures)

In the instance of a fluid's viscosity, the required parameters are the Lennard-Jones(L-J) characteristic Length, the L-J energy parameter and the number of degrees of Freedom (only required for specific heat).

The characteristic length is defined in units of Angstroms, the energy parameter, in units of absolute temperature and the degrees of freedom is a dimensionless input. If the kinetic theory is used for a fluid's viscosity, L-J characteristic length and L-J energy parameter are required input. For a fluid's thermal conductivity and specific heat, no inputs are required. Finally, the mixture material's mass diffusivity requires the L-J characteristic length and the L-J energy parameter for each chemical species.

The numerous simulation results carried out show that there is no significant difference by using the two methods of calculating the gas properties. Consequently, the kinetic theory will be used for the HP-LCVD simulation because of the complete data available in the adopted commercial software.

3.6.4 Material properties of carbon

There are five carbon properties needed to accurately model the LCVD fiber deposition process: reflectivity, density, emissivity, specific heat capacity and thermal conductivity. The carbon material property data used by earlier modelling efforts, i.e. Hill (1995), have shown that the first three properties do not vary significantly with temperature, and may be considered constant without adversely affecting simulation results. Table 3.4 shows these material properties and associated values for pyrolytic carbon. Based on Croteau (2005),

Table 3.4 Material properties of pyrolytic carbon

Material Properties	Pyrolytic Carbon
Normal reflectivity	0.152
Density	1470 kg/m^3
Emissivity	0.78

the specific heat varies with temperature as given by the polynomial equation:

$$C_p = 12.9 + 2.9T - 0.0014T^2 + 3.1 \times 10^{-7}T^3 - 2.4 \times 10^{-11}T^4 \qquad (3.34)$$

The thermal conductivity is the most important property to define accurately, since it is present in both the transient and the steady-state heat transfer equations. Earlier research work has shown that use of a temperature dependent thermal conductivity can have significant effects in the temperature profiles , Watt & Perov (1985). For the simulation of fiber growth, it is a critical information due to the role that the deposited material plays in the process.

Carbon deposited by CVD and LCVD is usually termed pyrolytic graphite or pyrolytic carbon. Pyrolytic carbon typically forms in layers, with a regular hexagonal crystalline structure in each layer. As a result of this structure, the thermal conductivity is strongly anisotropic. Kelly (1969) compiled data on the high-temperature thermal conductivity of

Table 3.5 Carbon thermal conductivity varying with temperatures

Temperature (K)	**Conductivity** (w/m-K)	**Temperature** (K)	**Conductivity** (w/m-K)
193.15	4	960.65	10.25
303.15	6.3	1054.4	10.5
335.65	7	1148.15	10.75
382.525	7.5	1273.15	11
523.15	8.5	1398.15	11.25
616.9	9	1585.15	11.5
679.4	9.25	1835.15	11.75
741.9	9.5	2148.15	12
804.4	9.75	2773.15	12.25
866.9	10		

polycrystalline graphite as shown in Fig. 3.6 which is the current model used for the deposited material.

According to Watt & Perov (1985), heat conductivity and heat capacity of carbon fibers depend on heat treatment temperature (HTT). Heat conductivity sharply increases at HTT 600°C; heat stability at first decreases but then depends only slightly on HTT.

Carbon has several material forms which are polymorphs. The properties vary with the physical structure. For carbon fiber, the section shows there is a core of vitreous carbon surrounding amorphous carbon. For simplifying the modelling, we use the properties of vitreous carbon for the simulation.

The thermal conductivity varies as a piecewise-linear polynomial as a function of temperature as shown in Table 3.5 from Croteau (2005).

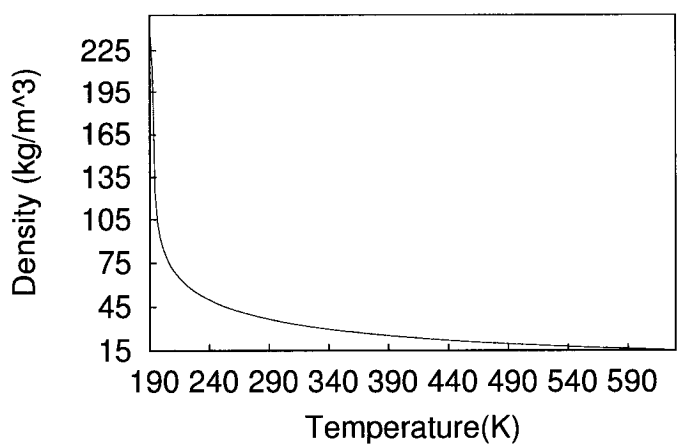

(a) Density vs. temperature - 50 bars

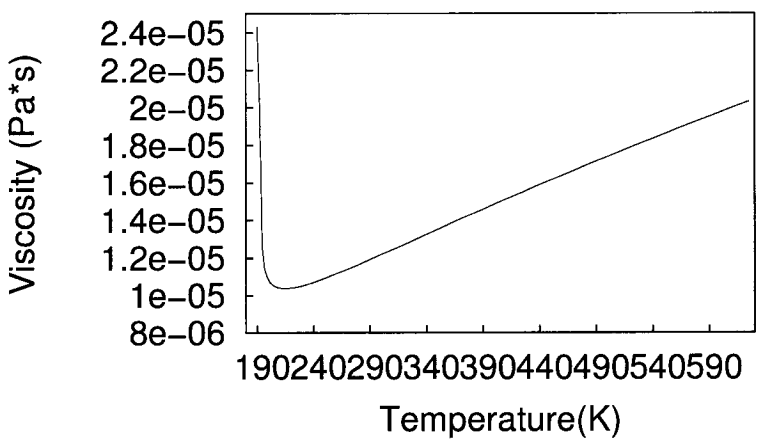

(b) Viscosity vs. temperature - 50 bars

Figure 3.4 Density and viscosity versus temperature for methane (NIST ChemBook web-site)

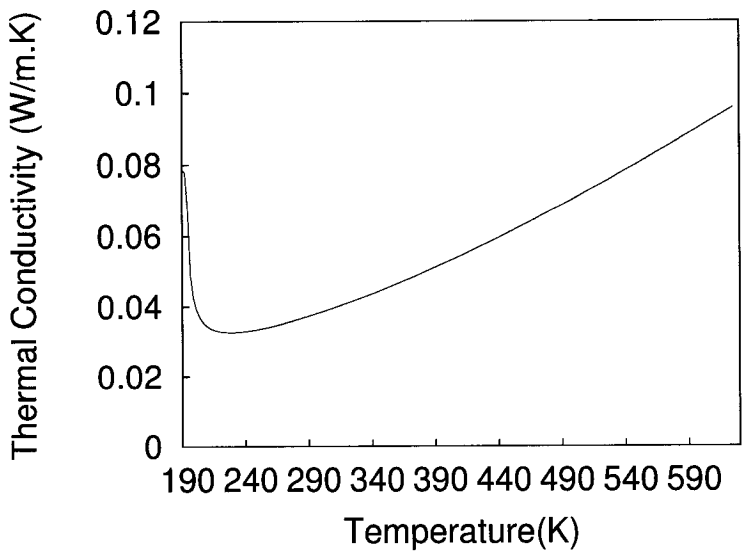

Figure 3.5 Thermal conductivity versus temperature at 50 bar

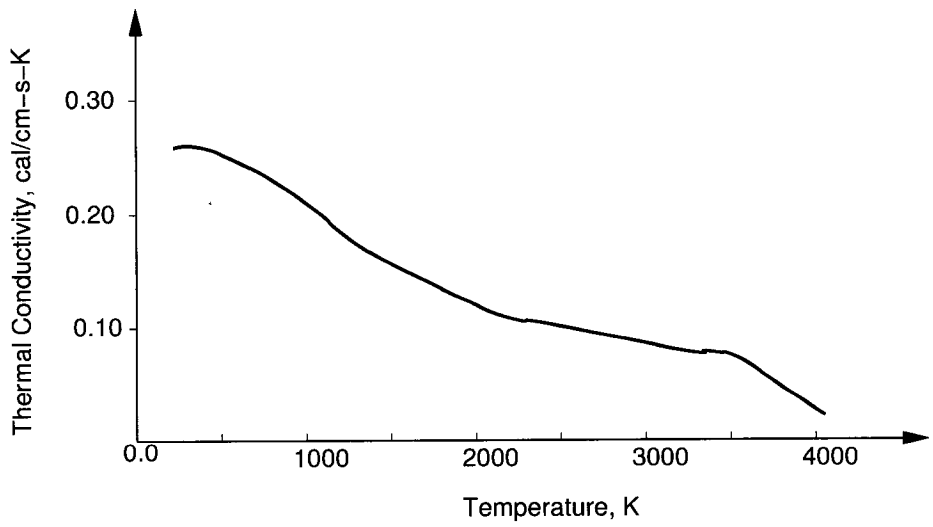

Figure 3.6 High temperature thermal conductivity of graphite Hill (1995)

CHAPTER 4

NUMERICAL SIMULATIONS

Historically, the dominant approaches in engineering design and analysis have been based on experimental and empirical techniques, complemented by analytical methods. From 1980s, these traditional tools have been complemented by computer-aided technologies which integrate classical scientific disciplines with discrete mathematics and computer science. For the purpose of analysis and design in engineering applications, this approach is becoming attractive because it can exceed the range of experimental test facilities, and is not limited by hypotheses of analytical models or empirical relations.

In the present work, numerical modelling will be used to guide the design of an experimental LCVD facility. This will be carried out by creating a virtual or numerical reactor based on Computational Fluid Dynamics (CFD) technology. This will benefit the design developpement in several ways:

- It can provide more detailed information for decreasing the repeat times of experiments. For example, we can use modeling work to obtain the results under different operating conditions, i.e. variation of flow rate of percursor gas and carrier gas.
- It can discriminate the effects between several parameters whose individual impact are very difficult to separate in a global experiments. For example, we can investigate separately the effects of the flow rates, the heat transfer, and the chemical kinetics.
- It can provide data which are impossible to measure. For example, the concentration field and the temperature field.

The outcomes of the numerical simulation will allow to analyze how some factors will

affect the process. This can be used to evaluate the relative importance of the different process parameters, such as the laser power, the best focus position of the laser and the gas pressure inside the deposition chamber, and different flow rates of the precursor and the carrier gases, and the mixture situation of the two gases. As a consequence, the use of such a numerical model can be used to minimize the number of experiments required to obtain the maximum amount of information, to select a proper set of the process parameters for experiments, and to design an optimized LCVD system.

The numerical aspects of the simulation will be established to insure that the solutions are accurate and reliable. The convergence and accuracy of the solutions are evaluated and compared with experimental and published results when available. The resulting digital experiments will be geared toward a comparative analysis against other published works and experiments when available.

4.1 Computational Fluid Dynamics

Computational Fluid Dynamics is a generic technology aimed at the numerical simulation of fluid flow based applications by modeling of mass and energy exchange phenomena such as conduction, forced convection, and in addition, in the present application, chemical kinetics. The resulting equations together with appropriate boundary conditions are solved through the development of specialized techniques for:

- geometric modelling and meshing algorithms
- discretisation techniques of governing equations
- equation solvers
- visualisation and analysis

To complete the engineering design and analysis, sophisticated software environnements are available for problem description, and solution visualisation and analysis.

In the present study, this methodology will be used for the simulation of the complex interactions of the various energy exchanges which occur in a LCVD reactor. More specifically, it will be applied in the context of a production facility illustrated in Fig. 5.1 to investigate the production of fibers as described in Section 1.3. The proposed numerical approach is based on a well established methodology used for the simulation of complex physical problems:

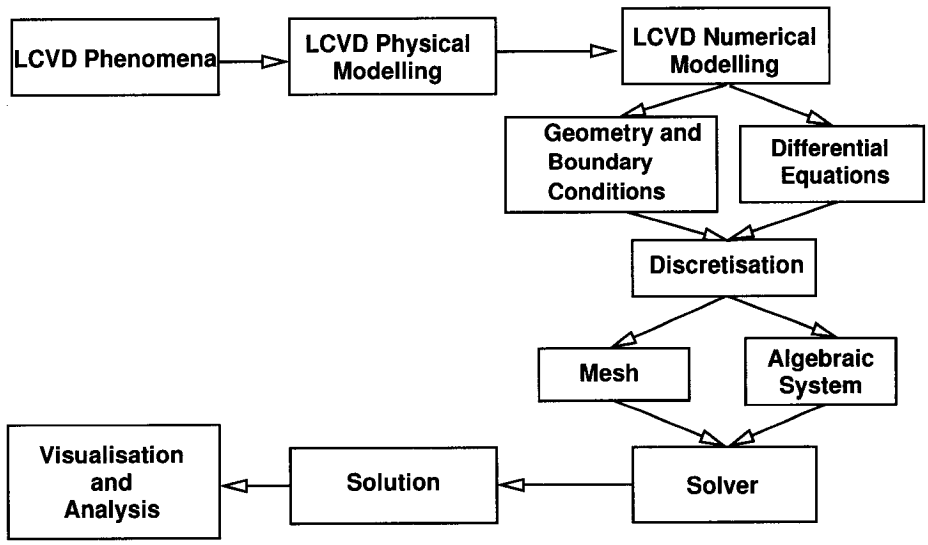

Figure 4.1 Computational methodology

This approach is appropriate because of the diversity of the physics and the wide range of parameters encountered in this problem. Furthermore, CFD is particularly well suited to obtain accurate and valid solutions for full scale simulations of such industrial problems where complex geometries and coupled phenomena drive the process.

4.2 Choosing a CFD Environment

Over the last two decades, a dynamic scientific community and commercial sector have developed innovative numerical techniques into reliable tools and brought them within the reach of the research engineer. The two CFD environments and their features are listed as below:

1. Commercial Packages:
    - turnkey architecture with fully integrated modules
    - diverse functionality relative to the physics and the simulation techniques
    - no programming is required.
2. In-House or research codes:
    - integration not provided,
    - very flexible,
    - programming is required,
    - ideal for prototyping by expert users.

It can be seen that each CFD environment has its own advantages and disadvantages. For the current project, a commercial software package is chosen because CFD techniques have matured and reached a high level of functionality and reliability. The commercial packages can provide powerful pre- and post-processors, accurate numerical discretization techniques and equation formation algorithms which are time consuming for coding and debugging. Such a choice allows the user to concentrate on the physical modelling and to gain insight into the phenomena at hand which in turn leads to the formulation of design solutions.

Specifically, the commercial CFD software FLUENT has been selected for the numerical simulation, because it is a powerful CFD software and its products address the particularities of the LCVD phenomena: fluid flow, heat and mass transfer, and a host of related phenomena involving chemical reactions and multiphase flows.

The general modeling capabilities of FLUENT match the methodology described in Figure 4.1 as follows:

Geometric model and problem description The geometric model is constructed using a program called Gambit. This environment is also used to generate the mesh within the model. The size function of Gambit allows control of the size of mesh-element edge for geometric edge entities and for faces or volumes that are meshed using triangular or tetrahedral elements, respectively. Integrated problem set-up and post-processing allows the specification of continuum types, and to set boundary conditions.

The geometry and mesh file from Gambit is then imported to FLUENT.

Physical modelling Heat transfer including forced, natural, and mixed convection, conjugate heat transfer, as well as several radiation models are available in FLUENT. The governing equations for the modelling are the Navier-Stokes equations for mass, momentum and energy conservation. These equations are embbeded within the software.

Boundary conditions are specified in greater detail and parameters are defined for solving the equations governing conservation of momentum, energy, and mass.

FLUENT uses its own terminology for the boundary conditions. These are shown in Table 4.1 as a generic list and compared to the general reactor simulations based on Figure 4.2. It can be seen that these match those identified in the present modelling (See Section 3.5). The specified geometry and boundary conditions will be described in Chap. 6 for each case.

Table 4.1 Boundary conditions in FLUENT and proposed reactor model

Boundary Number	**Boundary Condition**
1	Internal or Interface boundary
2	Internal moving wall
3	Line of Symmetry
4	Pressure outlet
5	Internal wall
6	Velocity-inlet profile or Mass flowrate
7	Internal wall
8	Velocity-inlet profile or Mass flowrate

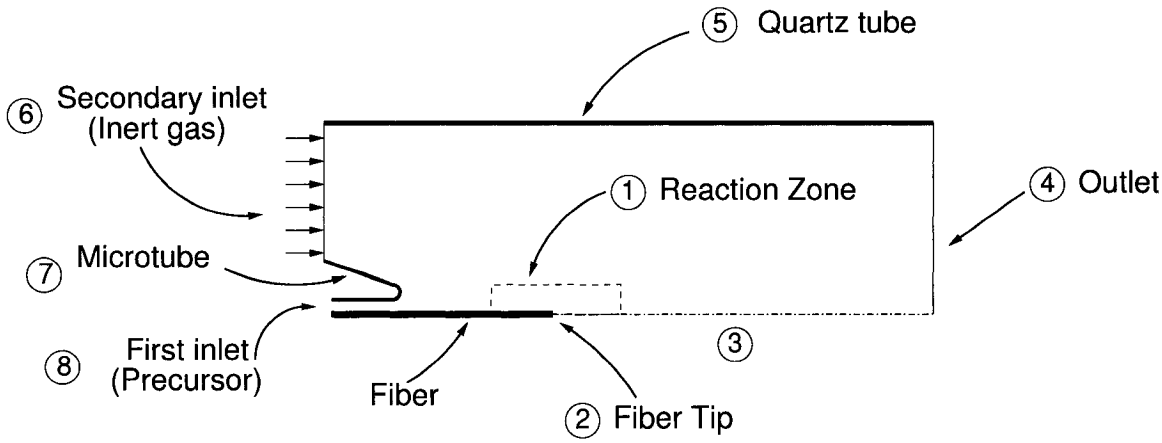

Figure 4.2 Boundary conditions in LCVD reactor modelling

Chemical kinetics Of primary interest for the present project, chemical species transport and reaction, including homogeneous and heterogeneous combustion models and surface reaction models are implemented. Within FLUENT, the material properties are specified with an extensive materials property database which can easily be complemented. In particular, it provides a comprehensive Modeling Surface Chemistry database, encountered in chemical vapor deposition (CVD) applications which is very similar to the present LCVD process.

In FLUENT, the reaction rate for gas-phase reactions is defined on a volumetric basis

and the rate of creation and destruction of chemical species become source terms in the species conservation equations. The rate of deposition is governed by both chemical kinetics and the diffusion rate from the fluid to the surface. Wall surface reactions thus create sources of chemical species in the bulk phase and determine the rate of deposition of surface species.

4.3 Development Activities

The rationale for the comprehensive undertaking in the computer simulation of the LCVD fiber growth process carried out in this study aims at complementing the experimental development and build upon the acquired know-how at the FFL. These virtual experiments can provide fundamental insights which can be used to establish guidelines for reactor design and control. From the discussions in the previous chapters, it can be concluded that a detailed understanding of the LCVD process for producing continuous fibers with high growth rates are clearly lacking to be applicable to an industrial context. From the literature review described in Chapter 2, this kind of modeling work has not been achieved previously at this level.

Even though the commercial package FLUENT has been selected for the reasons of its powerful capabilities and potential for saving much coding time, a LCVD simulation is not a straight forward application. Because of the interaction of the various physical processes, a successful numerical simulation must address its particular characteristics through specific physical and computational modelling procedures.

The particular issues that are raised and require the development of specific numerical techniques include:

1. the disparate scale of the phenomena, which range from the micro-meter for the detailed mass deposition at the fiber tip, to the meter for the global reactor;

2. the solution transfer for internal boundaries as required in the domain decomposition approach;
3. the unique chemical kinetics parameters in order to model and simulate the distinctive characteristics of the micro-scale thermodynamic and fluidic phenomena underlying fiber growth in LCVD;
4. the treatment of the fiber as a moving boundary;
5. investigating the accuracy and the convergence of the simulation results;
6. developing user-defined functions (UDF) to customize FLUENT to fit the LCVD modelling requirements.
7. investigating the material properties for the precursor gases and carbon under the range of the operating conditions of the reactors.

These cover the full range of computational and modelling techniques and have required extensive efforts to devise additional modules in the form of user defined functions or programs in the C computer language. These in turn required systematic validations to document the characteristics of these implemented modules and performing a critical review of their accuracy and validity, as well as their potential in light of the present application.

4.3.1 Mesh independency

Several numerical parameters control the solution of nonlinear problems . In the case of the grid, it should be established that the solution is independent of mesh. To this end, a number of solutions are obtained for a given sequence of varying meshes. These can be compared using a control variable.

Table 4.2 shows the dependence of the value of the velocity at one mesh point in the calculation zone with different grid sizes and other conditions. This approach to establish

Table 4.2 Effect of mesh size using a nodal value

Mesh faces	x-velocity	limit size	Iteration steps	Cont. resid.	x-vel. resid.	y-vel. resid.
20358	0.6272083	0.20mm	1426	1.0e-6	1.0e-6	1.0e-6
21190	0.6195994	0.175mm	1447	1.0e-6	1.0e-6	1.0e-6
21944	0.642261	0.15mm	1397	1.0e-6	1.0e-6	1.0e-6
23944	0.6348633	0.125mm	1395	1.0e-6	1.0e-6	1.0e-6
27310	0.6284549	0.10mm	1489	1.0e-6	1.0e-6	1.0e-6
34678	0.6415175	0.075mm	1752	1.0e-6	1.0e-6	1.0e-6
44040	0.6310591	0.06mm	2000	4.30e-4	3.56e-6	1.42e-6
55634	0.6284549	0.05mm	2500	5.0e-3	8.56e-5	3.77e-5
77072	0.6237606	0.04mm	3500	1.45e-2	2.26e-4	1.18e-4

mesh independency proved inadequate, so in the present study, a velocity profile placed at a critical location was chosen for this evaluation. Theses are shown for 9 different cases in Fig. 4.3.

A sequence of meshes of increasing size was used and the resulting velocity profiles were compared. It was found that beyond a mesh size of 20358 elements no significant effect resulted in the solution. This is illustrated for 9 different cases in Fig. 4.3. We can see that there is no big difference for the 9 cases. That means that going from a mesh size of 20358 elements to 77072 elements does not produce a significant effect in the results. Accordingly, the base mesh size for subsequent calculations was 27310 elements.

4.3.2 Meshing

The phenomena surrounding the fiber tip drives the process for the entire reactor. The resolution of the fine flow structure as well as the interaction of the energy and mass transfer in this inner region critically control the deposition rate. A methodology for the generation of a correspondingly fine grid adapted to the property gradient is required. This consisted in setting a sufficiently fine mesh at the fiber surface, and increasing this value in a geometric

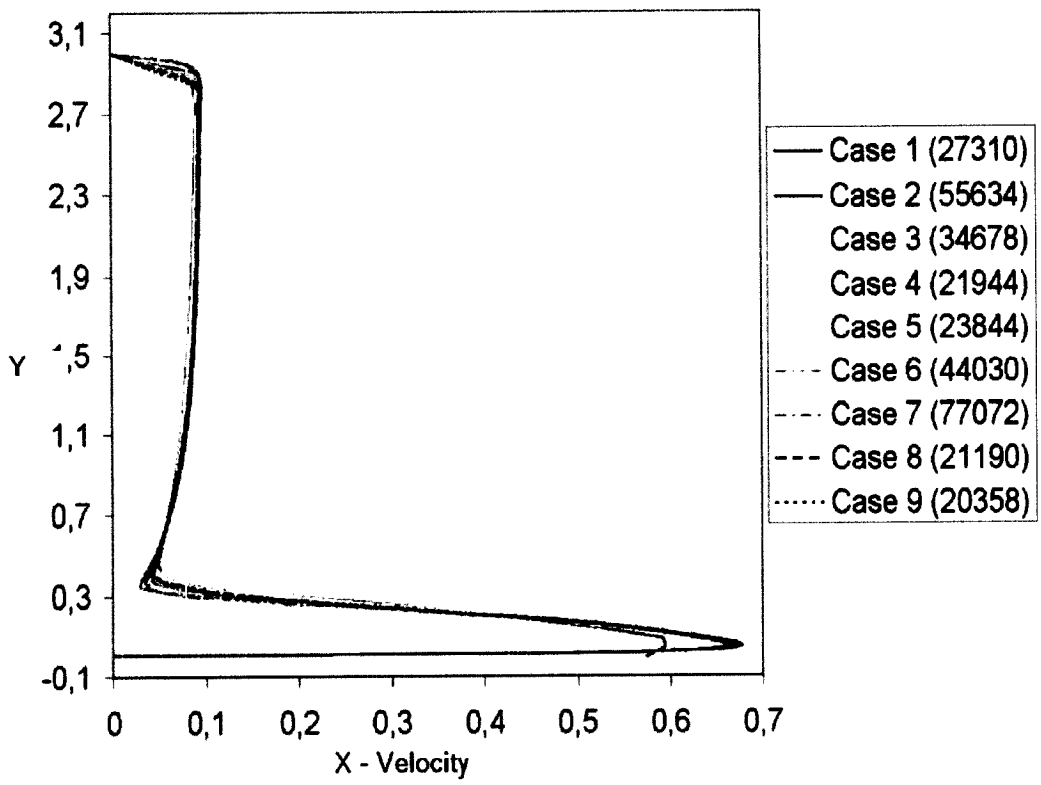

Figure 4.3 Effect of mesh size using the profile of a variable

fashion in the outward direction. This progression was applied until a limit value characteristic of the far field is reached, where the effects of the surface phenomena no longer dominate.

The fiber surface is used as the source edge of the size function as shown in Fig. 4.4. The parameters of the size function vary from case to case. Typical values of the size function are:

- Starting size = 0.005: this is the mesh-element edge length in the region immediately adjacent to the source entity.
- Growth rate = 1.2: this represents the increase in mesh-element edge length with each succeeding layer of elements.

- Size limit = 0.1: specifies the maximum allowable mesh-element edge length for the attachment entity either inside or outside the outer boundary of the size function.

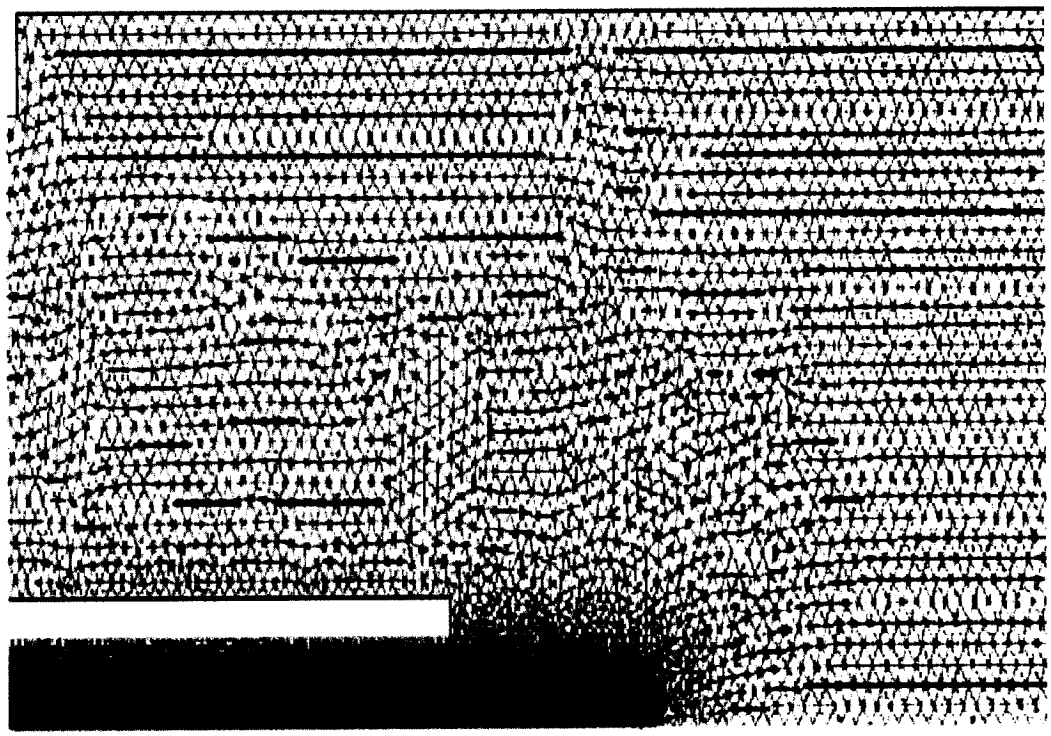

Figure 4.4 Typical mesh for the 2-tube open air reactor

4.3.3 Geometry domain decomposition

As described at Section 1.3, the widely varying scales of the exchange phenomena as they occur in the fiber tip region and in the far field of the reactor, require correspondingly varying grids. Indeed, the grid refinement necessary to capture the chemical kinetics dominated energy transfer at the tip is very fine and prohibitive if used throughout the entire domain. Consequently, the proposed approach is to decompose the overall domain into two subdomains: a small area in the vicinity of the fiber tip and an outer region of the reactor. These

zones will be computed separately, using different grids and distinct models. These are then coupled by matching the solution at their common internal boundary.

This required the development of computer modules for the transfer of solutions between the two computational domains, and these had to be tested and validated. The accuracy of transfering data between these two calculation zones was verified by a number of numerical experiments based on simplified cases.

Case 1 consisted of a simulation of a reactor with two species (methane and argon). The geometry for the overall domain was 3.0 m in length and 0.8 m in width. Case 2 consisted of another simulation, i.e. the subdomain for the fiber zone, whose dimension was 1.5 m in length and 0.5 m in width. The solution from Case 1 at the lines (x = 1.5 m and y = 0.5 m) is exported and becomes the boundary condition for Case 2 at the corresponding common boundary between the two domains. The entire solution is exported and includes all variables such as axial velocity, radial velocity and mass fraction of methane and argon as the boundary condition of Case 2.

Then Case 2 is computed for the same two species. The boundary type used for the zone boundary is a mass oulet flow. After importing the mass fractiom profiles and velocity profiles computed in Case 1, we obtained the results which match very closely with those of Case 1.

For further investigation, this procedure was repeated for several other variables. The mass fraction variation was extracted at x = 1.2 m for both cases, and is presented in Fig. 4.6. The good agreement indicates that the domain decomposition technique is sufficiently accurate for transfering data from one domain to another. This will lead to an increased computing efficiency as different grids and different models can be used in different domains, as appropriate.

4.3.4 The fiber as a moving boundary

If the fiber is not pulled, it will continue to grow until it deviates from the laser focus, and the growth stops. As described in Section 3.3, in high pressure LCVD simulation, it is expected that the fiber could be pulled continuously at a rate of 0.5 m/s. Therefore, the assumption of quasi-steady state no longer applies and the fiber is defined as a moving wall boundary condition.

In a situation of continuous fiber growth, the pulling translation speed is equal to the growth rate. Therefore, we may simplify this problem as a fixed boundary problem. Hence, the fiber geometry and the meshes are fixed. Although the boundary is fixed, the fiber material is moving with the pulling speed. FLUENT defines this problem as a moving wall boundary condition.

A particularity of FLUENT is that the moving wall condition cannot be used to model problems where the wall has a motion normal to the wall surface. In that case, all the normal components of wall motion are neglected. This illustrated with the simplified configuration of a flat fiber tip shown in Fig. 4.7(a). On the fiber side, the material velocity is null and not equal to the uniform pulling rate as required.

It was found that the techniques of Adapt-Boundary and Grid-Separate features in FLUENT could be utilized for solving the current boundary problem of a moving solid wall. These were used to mark the grids nodes adjacent to the fiber surface. Then, these grids were separated from the rest of the zone using the Grid–Separate–Cells tool. This resulted in two separated meshes or zones. One of them was a layer just adjacent to the solid fiber surface where the velocity was imposed as the uniform pulling speed as shown in Fig. 4.7(b).

This is illustrated more distinctly in Fig. 4.8 showing the fiber surface velocity around the fiber tip. It can be seen that the velocity on the fiber tip is uniform and equal to the pulling

speed (In this figure the vectors are scaled).

4.3.5 Convergence

Because of the nonlinearity of the equation set being solved, it is necessary to control the change of ϕ (ϕ represents the transported quantity). This is typically achieved by under-relaxation, which reduces the change of ϕ produced during each iteration. In a simple form, the new value of the variable ϕ within a cell depends upon the old value, ϕ_{old}, the computed change in ϕ, $\delta\phi$, and the under-relaxation factor, α, as follows:

$$\phi = \phi_{\text{old}} + \alpha\delta\phi$$

Figure 4.9 illustrates the convergence history of the H_2 concentration for two cases: under relaxation factors (URF) of 0.7 and 1.0 (default), respectively. It can be seen that with the default value the convergence is not smooth and that machine zero is not reached. In this instance, the choice of under relaxation factor greatly improves convergence showing the importance of correctly choosing its value for each variable.

Therefore, the under relaxation factor is very important for convergence and it should be carefully chosen for each variable.

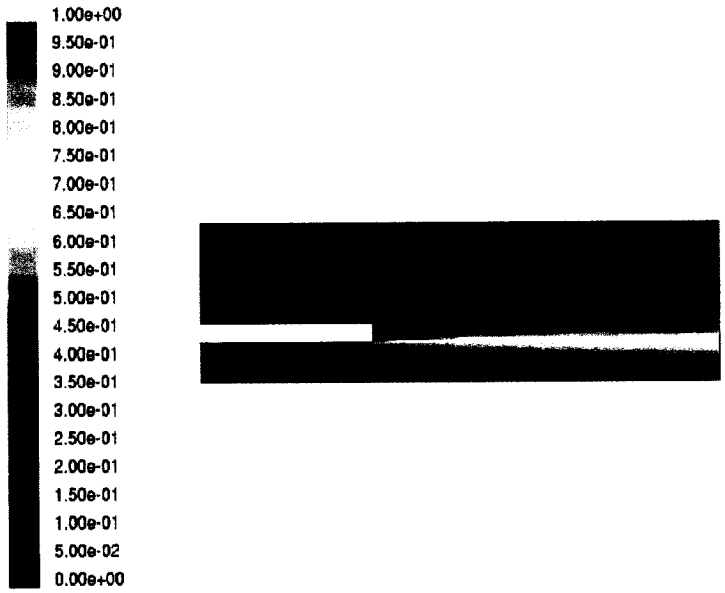

(a) Computational domain for overall reactor

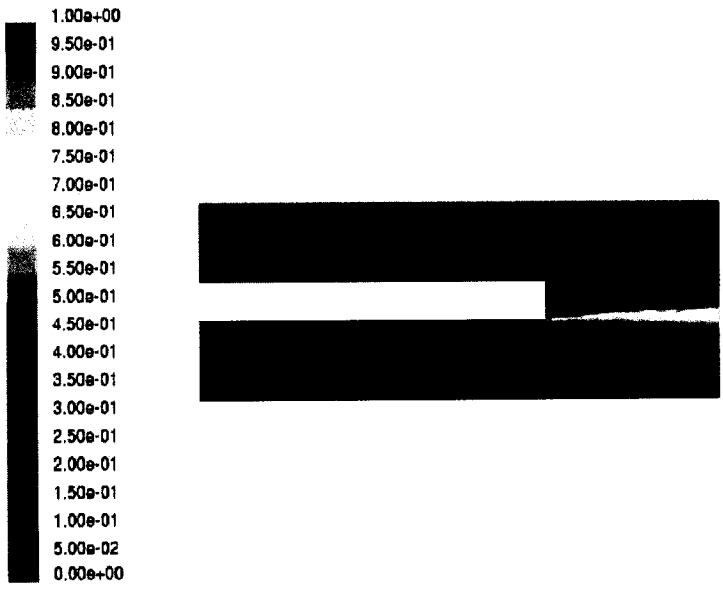

(b) Computational domain for the fiber region

Figure 4.5 Methane mass fraction for two different computational domains

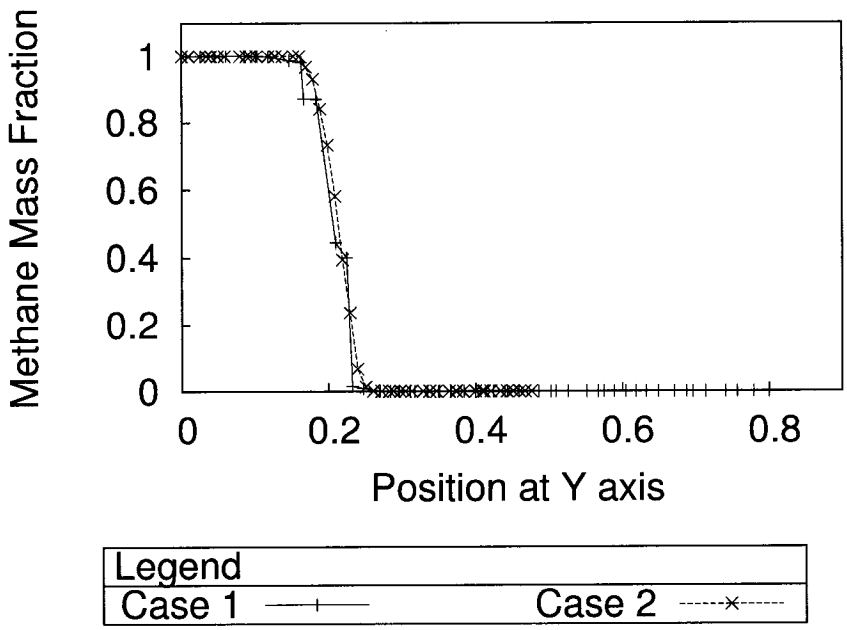

Figure 4.6 Comparison of the methane mass fraction for Cases 1 and 2

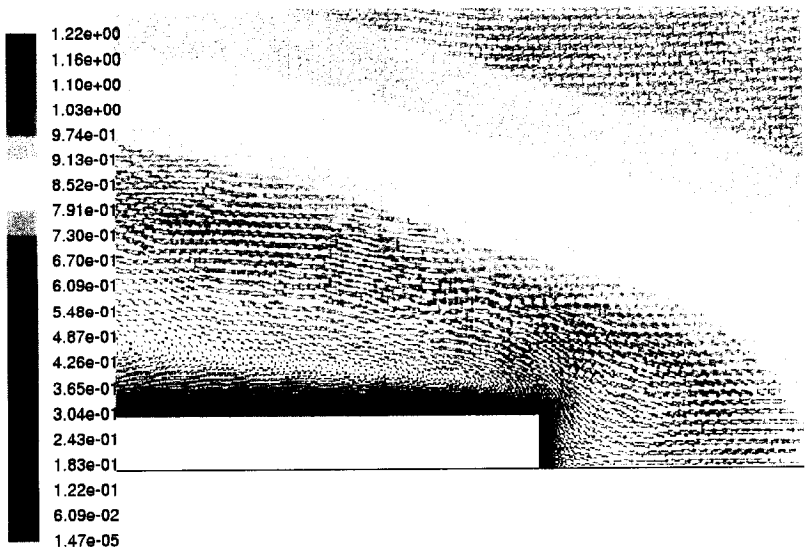

(a) Flow pattern without using grid-separate features

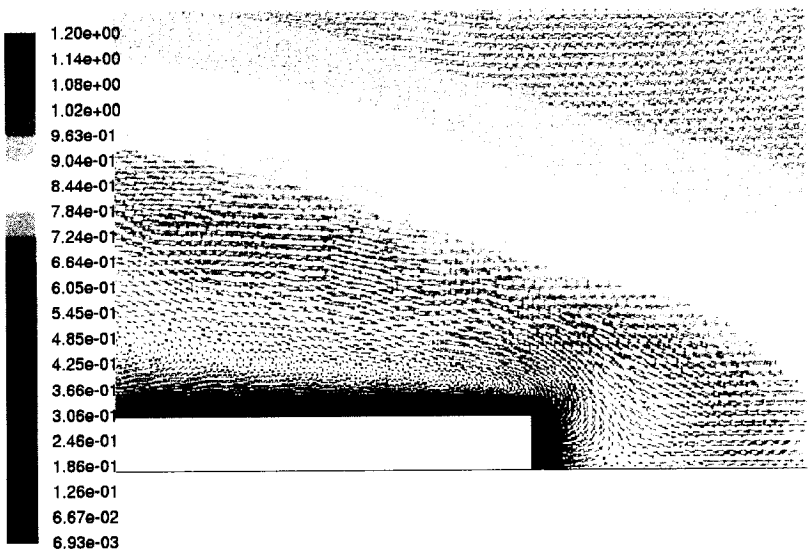

(b) Flow pattern with using grid-separate features

Figure 4.7 Flow velocity vector around the fiber tip

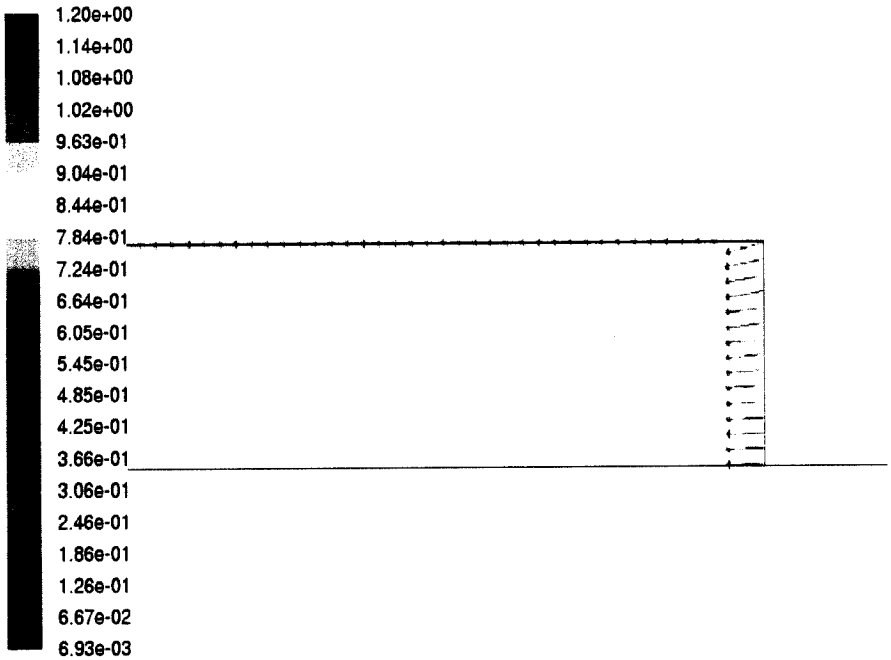

Figure 4.8 Velocity vector on the fiber surface

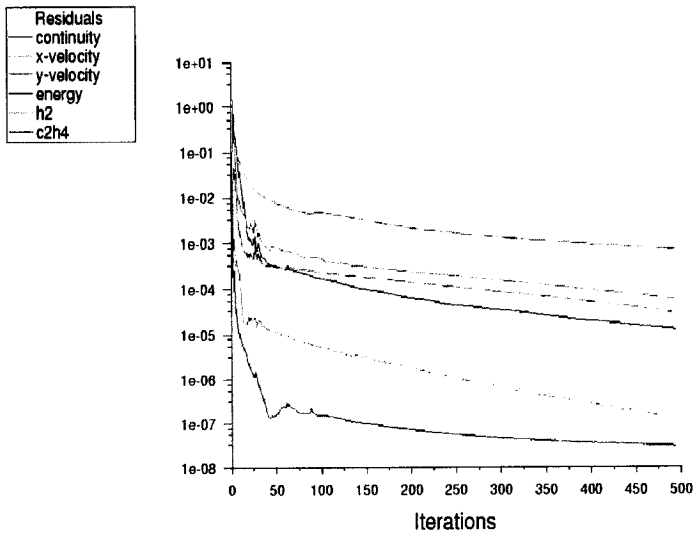

(a) Relaxation factor of 0.7

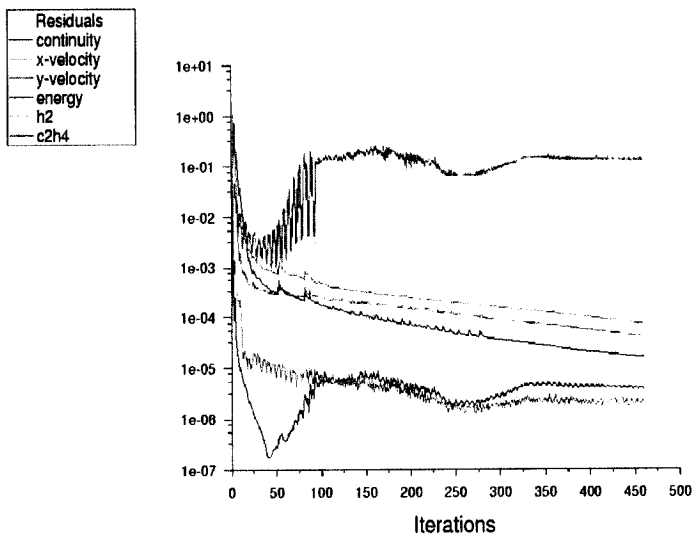

(b) Relaxation factor of 1.0

Figure 4.9 Effect of relaxation factor on the convergence for the solution of the H_2 concentration

CHAPTER 5

VALIDATION SIMULATIONS

The first step in the application of the proposed numerical approach is to establish its validity in terms of its predictive capabilities. Because of the complexity of the phenomena and in the absence of detailed measurements, this validation process can only be achieved indirectly and in global terms only. At steady state, the growth rate of the fiber should be equal to the deposition rate of the fiber. From existing measurements of the growth rate, such a comparison with the computed deposition rate will be used to validate the proposed physical and computational model.

The strategy of this validation is to simulate the fiber growth with the available data of Maxwell & Boman (2006) and compare the simulated fiber growth rate with the measured one. Since the configuration of the current model is different from that of Maxwell & Boman (2006), some adjustments are required to approach these experimental conditions as much as possible.

5.1 Experimental Facility

Figure 5.1 shows a simplified schematic of the experimental setup used at the Freeform Fabrication Laboratory (FFL) of Ecole Polytechnique de Montréal. This setup consists of a pressure reactor and a moveable target (the substrate). Through a complex beam steerer and expander, the laser beam (usually of Gaussian profile) is focused onto the substrate target.

The Ar^+ laser is chosen to be the laser beam provider because most gases are transparent

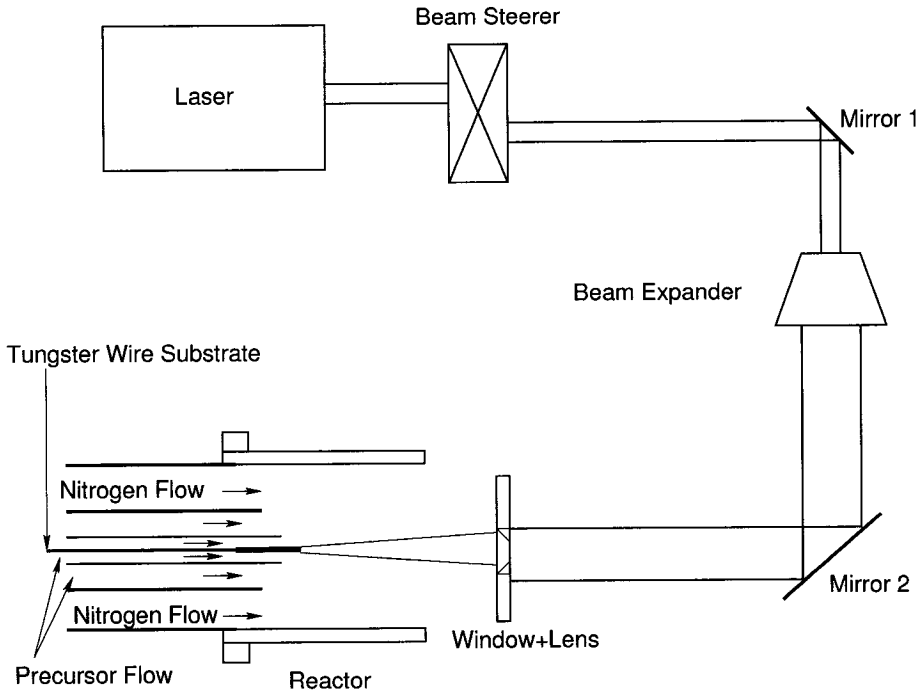

Figure 5.1 Simplified schematic of experimental setup

in the visible region. As a consequence, homogenous reactions within the precursor can be minimized, and deposition can therefore occur under normal or elevated pressures. In addition, due to the smaller wavelength (488.0 nm for Ar compared to 10600 nm for the CO_2 laser), the diffraction-limited diameter of the Ar^+ laser focus is smaller by a factor 20. Therefore, localization of heating is very much improved. Finally, the optics and adjustments are much simpler for visible radiation in comparison to infrared lasers (Leyendecker & Bauerle (1993)).

The measurements were carried out in such a reactor operating at ambient conditions described in detail in Goduguchinta (2006). The laser provided an output beam diameter of 3.97 mm and a maximum power output of 5 watts in the multiwavelength mode. The laser beam is focussed to a tungsten wire substrate located inside an inner tube. The substrate overhangs from the inner coaxial tube by about 1mm. The precursor (ethylene) gas is injected through this tube.

The system uses a coaxial flow configuration which is not enclosed in a chamber, and delivers a flow of nitrogen through an outer tube of 4.57 mm inner diameter. The reaction zone is shielded from the ambient flow by this coaxial flow of nitrogen, which acts as a shroud, The flow rates of ethylene and nitrogen are controlled by a combination of precision flow meters and metering valves interfaced with a data acquisition system. The emission from the reaction is monitored by a digital camera and a borescope that allows viewing only the region of interest.

The fiber growth takes place in a chamber-less open air environment where the reaction is restricted to the cloud of ethylene at the exit of the inner coaxial tube. The substrate is brought into the vicinity of the laser focus, and once growth is initiated, the position of the laser focus and the substrate is kept unchanged.

The methods of measuring the fiber growth rate are described in Goduguchinta (2006), where tracking of the emission spot during growth provided real time measurements of position, growth rate, and diameter of the deposited rod. Growth rates were obtained on the basis of the difference between consecutive centroid positions. The overlay of six emission images captured every 30 seconds during the rod growth. It gives a qualitative idea of the change in growth rate as the emission spot (rod growth front) travels across the digital camera screen. By scanning the picture from the left to the right, one can observe that the displacement of the emission spot in each interval.

Figure 4.5 of Goduguchinta (2006) represents the variation of growth rate (μm/s) with respect to the position along the rod axis or in other words, at different points in the focal region. Although all of these growth curves reach their peak value at approximately the same position along their length, the growth curves at lower values of laser power seem to exhibit a less drastic variation over their length. The reason of the subsequent decrease following the maximum is due to the laser beam focus moving away from the fiber tip.

The average fiber growth rate used for validation in the present study are from the data of

Table 5.1 Experimental average fiber growth rate versus laser power in FFL

Laser Incident Power(watt)	Average Fiber Growth Rate (μm/s)
0.6	12
1.0	16
1.4	27.5
1.6	37.0

Goduguchinta (2006) given in Table 5.1. Figure 5.2 gives a graphical representation of the relationship between the fiber growth rate and laser power from the data in Table 5.1.

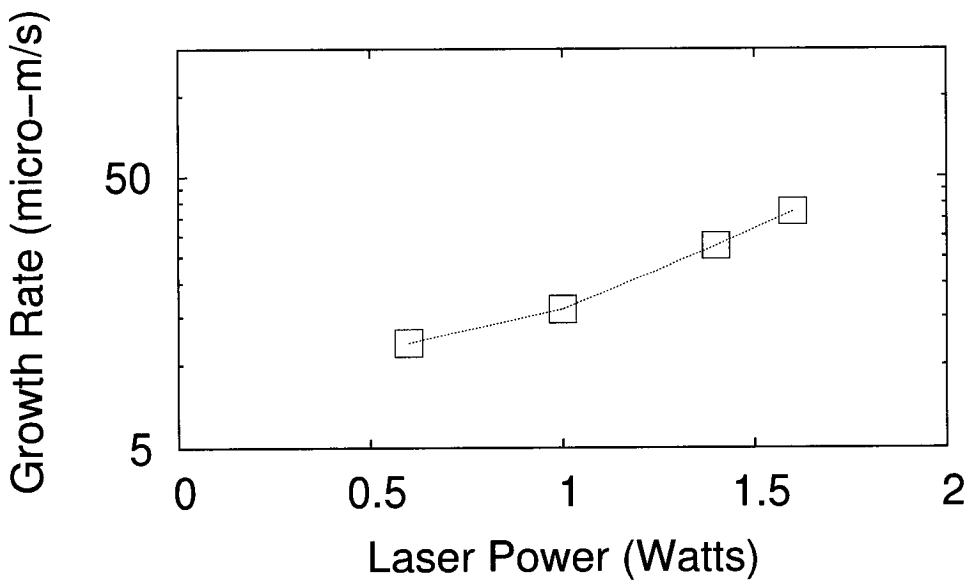

Figure 5.2 Growth rate versus laser power

5.2 Experimental Conditions for Validations and Calibrations

Validation of the modelling methodology cannot be achieved by direct comparison of the simulation results with the experimental measurements as these are not generally available.

For example, there are no thermometers for measuring the temperature of the laser spot and the fiber tip. This situation precludes the measurement and calculation of some important parameters relating to chemical kinetics, i.e. activation energy and pre-exponential factor.

The parameters which can be measured are global variables such as the flow rates of precursor and carrier gases, laser beam power, the fiber growth rate, and the geometry of the reactors.

The geometry of the design is shown in Fig. 5.3. It is made up of three concentric tubes: an outer resolver, an inner resolver and an inner micro-tube. The outer resolver provides the carrier gas (nitrogen). The inner resolver provides the precursor gas but also acts as a barrier to cool down the fiber tip and the sourrounding gas in order to avoid the detrimental effects of overheating. The gas from this inlet may be either a percursor gas or an inert gas. The inner tube provides the precursor gas (ethylene).

	Diameter
Outer Resolver	4.57mm
Inner Resolver	1.321mm
Inner tube	0.311mm
Fiber	0.200mm

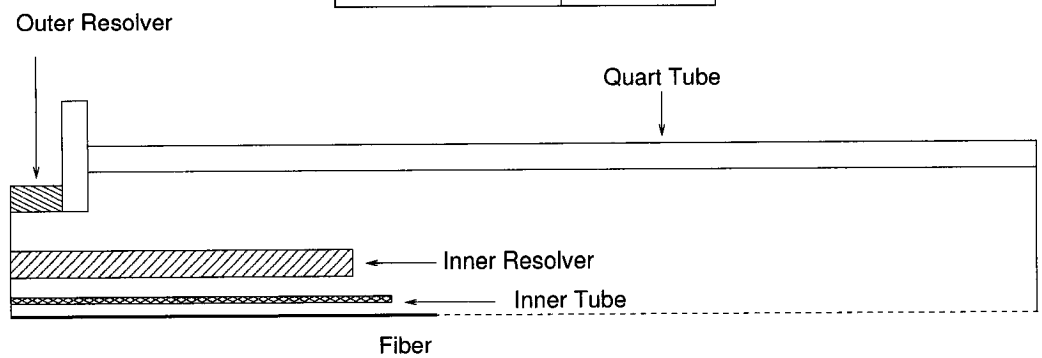

Figure 5.3 Geometry for the 3-tube open air reactor

Based on experimental observations, an elliptic profile is assumed for the shape of the fiber tip, with an aspect ratio of 1 to 2.

The mesh for this geometry, shown in Fig. 5.4, is obtained using the size function described in Section 4.3. The source edges of the size function are the fiber curve and the symmetry axis, giving a concentrated grid around these boundaries (Starting size = 0.005, Growth rate = 1.2, Size limit = 0.1). There are two grid domains: the flow domain and solid fiber domain. The resulting grid is composed of 70824 elements in the flow domain and 18386 elements for the fiber region. It was established in Section 4.3.1, that this discretization was sufficient to provide a mesh independent solution.

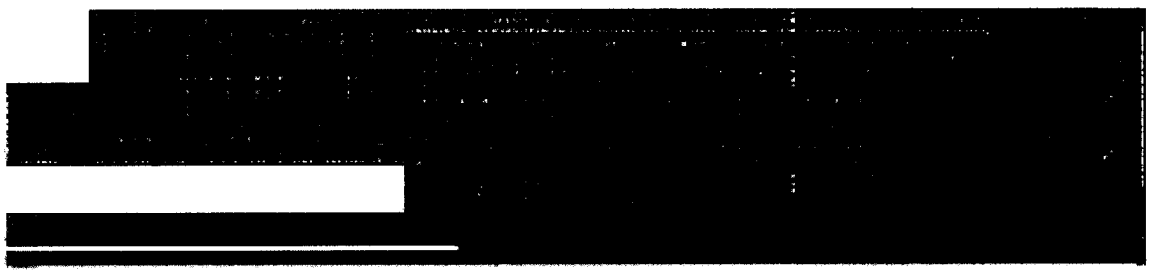

Figure 5.4 Mesh for the 3-tube open air reactor

The operating conditions are given in the table below:

Laser power	1.0 w
Fiber tip temperature	2150 K
Ambient temperature	18°C
Pressure	1.13×10^{5} Pascal
Flow rate of Inner tube	9.4746×10^{-8} kg/s
Flow rate of Inner resolver	1.136954×10^{-6} kg/s
Flow rate of Outer resolver	9.482954×10^{-7} kg/s

Following Mazumder & Kar (1995) and Duty (2001), the heat flux entering the surface of the fiber tip is set as the laser power input which is the specific power of a Gaussian

distributed laser beam as Eq. 5.1.

$$q(r)'' = \frac{2P_0(1-\rho)}{\pi {r_0}^2} e^{-2(\frac{r}{r_0})^2} \tag{5.1}$$

where P_0 is the laser power, ρ, the fiber reflectivity, r_0 the nominal laser radius, r the radial position.

Theoretically, the heat flux provided by the laser power can be computed with Eq. 5.1 which is widely used in the laser field. However, it was found that this equation was not always appropriate, especially in microscale or nanoscale fibers, because the heat flux is very sensitive to the laser spot diameter. In the current project, the laser spot diameter is very small, i.e. 20 μm and using the above equation could yield temperatures of the fiber tip high enough to initiate vaporation, with laser power as low as 1 watt. Even with power as low as 0.5 watt, the heat flux of the fiber tip calculated by Eq. 5.1 could reach values of the order of 10^9 (w/m^2). If the heat flux reached 3.0×10^7 (w/m^2), the temperature of the fiber tip could exceed temperatures of 5000 K which could initiate vaporation. However, throughout the experiments carried out at FFL, no vaporization of the fiber was observed. Therefore, it is believed that the temperature of the fiber tip is below the carbon boiling point (3000 K).

While it is clear that the temperature of the fiber tip is a very important parameter for the physical modeling, in the current situation, we can neither measure it, nor precisely calculate it. Maxwell & Boman (2005) described similar experimental conditions with laser incident powers of 0.2, 0.4, 0.6, 0.8, 1.0 and 1.2 watt and provided a relation between the average fiber tip temperature versus coupled laser power. The average fiber tip temperatures in the present study are estimated from the data which are given in Table 5.2.

Another important parameter for chemical kinetics is the reaction rate k of Eq. 3.24.

$$Ln(k) = Ln(k_0) - \frac{E_a}{RT}$$

Table 5.2 Average fiber tip temperature versus coupled laser power from the data of Maxwell & Boman (2005)

Laser Incident Power (watt)	**Average Fiber Tip Temperature (K)**
0.2	1100
0.4	1500
0.6	1800
0.8	2000
1.0	2200
1.2	2500
1.4	2700

Table 5.3 Activation energy (E_a), rate constant (k_0), reaction order (n) of ethene from the data of Maxwell & Boman (2006)

	Region I (1250 K to 2000 K)	**Region II** (2200 K - 3300 K)
E_a (kJ/mol)	70.34	94.37
$\ln(k_0)$ (μm/s)	6.76	7.21
n	1.65	1.65

The activation energy E_a, the constant rate k_0, and the reaction order n in this equation are typically determined from a kinetic analysis of experimental data, not available at FFL. However, Maxwell & Boman (2006) provided such data under the conditions of 2.0 bars pressure and 0.95 watt laser power with natural convection. These authors give the average reaction order for alkenes as 1.65, and the activation energy and the pre-exponential factor (rate constant) of ethene (ethylene) are given in Table 5.3. These data can be used to validate the current model for comparing the simulated growth rate with the measured growth rate from the experiments done by Maxwell & Boman (2006).

5.3 Validation of the modeling methodology

For the present validation, the measurements and conditions from the experiments described in Section 5.2 will be used for comparison with the computed values. However, other important parameters such as temperature, activation energy, and chemical rate constant were not avalaible for the above experiments. Consequently these had to be obtained from other measurements, which could not be exactly those of the experiments conditions in the present study. Thus, the modeling results may not match the experimental results, and the trends or variations for both modelling and experiments becomes the only comparable information for the present validation.

The simulation results were carried out using the numerical methodology of Chap. 4. This consisted in numerous computations to validate grid independence, numerical convergence of all computed variables etc... The results are the spatial distribution of the velocity, temperature and pressure fields, as well as the various species concentrations. From these, detailed information can be extracted about the variables which affect the fiber growth process.

The strategy of this validation is to simulate the fiber growth with the available data of Maxwell & Boman (2006) and compare the simulated fiber growth rate with the measured one. Since the configuration of the current model is different from that of Maxwell & Boman (2006), some adjustments are required to approach these experimental conditions as much as possible. The boundary condition of the outer resolver was replaced by a wall because only precursor gas is introduced into the reactor. The flow rates were adjusted to be at very low speed in order to approach natural convection.

Two examples from Maxwell & Boman (2006) representing two temperature ranges a) Region I (1250 K - 2000 K), and b) Region II (2200 K - 3300 K) were used to carry out these validations. From this data, the fiber growth rate was about 100 μm/s at 2000 K and

Table 5.4 Comparison of simulated growth rate with experimental data

Growth rate (μm/s)	**Region I** (2000 K)	**Region II** (2200 K)
Experimental	100	120
Simulation	93.20	108.84

120 μm/s at 2200 K. The reason for selecting these two temperatures is that they are in the middle of the total temperature range of Region I and II (1250 K - 3300 K). The reaction order at these temperatures was obtained by Maxwell & Boman (2006) through regression analyses of extensive data equal to a value of 1.65. However, according to Wright (2004), the reaction order is not constant and may vary with the operating conditions.

The growth rates obtained by the proposed numerical model at operating conditions of 2 bars, temperatures of 2000 K and 2200 K, and using the chemical parameters taken from Table 5.3, are given in Table 5.4. This comparison shows that the simulation results are in good agreement with the experimental data.

For this simulation, the temperature profile at the fiber tip surface was assumed constant (not Gaussian), resulting in a uniform surface deposition rate of carbon. It was found by simulations that the difference on the fiber deposition rate for Gaussian temperature profile and constant temperature profile was only the deposition rate distribution on the fiber surface tip. The constant temperature profile results in a uniform surface deposition rate. If the constant temperature is equal to the peak temperature of a Gaussian profile, the uniform surface deposition rate will be equal to the maximum deposition rate resulting from a Gaussian temperature profile.

Figure 5.5 shows the simulated results of the carbon fiber deposition for the experimental conditions of Maxwell & Boman (2006). These results yield a mass deposition rate per section area of 0.137 kg/m^2/s at 2000 K and 0.160 kg/m^2/s at 2200 K. Dividing by the car-

bon density (1470 kg/m^3), the mass volume rate per section area is obtained which gives a length growth rate of 93.20 μm/s and 108.84 μm/s, respectively. These simulated values of growth rate are in good agreement with the experimental growth rate of $100.00\mu m/s$ at 2000 K and $120.00\mu m/s$ at 2200 K. From this, it can be concluded that the modelling methodology and the establishement of the physical parameters of the model are convincing.

5.4 Calibration

The activation energy and the rate constant can be obtained from the experimental growth rates at the corresponding temperature. The experimental growth rates are known from Table 5.1 and the assumed temperature at the corresponding temperature can be deduced from Table 5.2. Therefore, the only unknown kinetic parameter is the reaction order which needs to be calibrated .

These are always found experimentally (Wright (2004)) by plotting the logarithm of the growth rate as a function of the logarithm of the varied precursor pressure, from Eq. 3.13. The reaction order is obtained from the slope of the plot.

However, the experiment data of deposition rates for the four laser powers were measured at ambient conditions at FFL, hence, the method of using varied precursor pressures cannot be used. The only way to obtain the reaction order is through calibration.

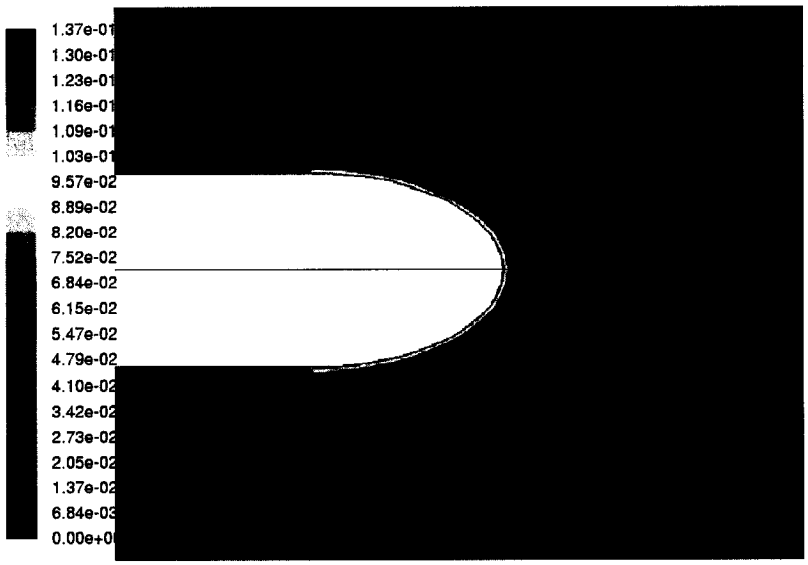

(a) Region I

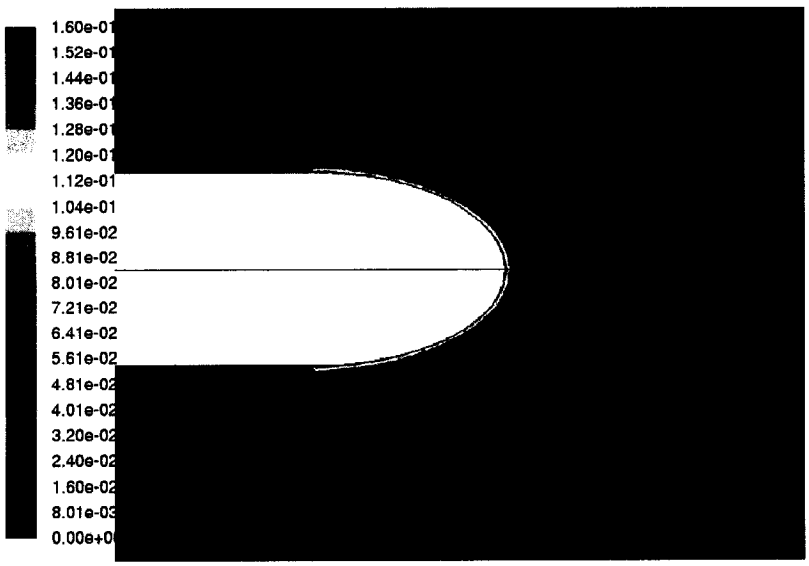

(b) Region II

Figure 5.5 Carbon deposition rates for validation simulations

The first step for the calibration is to calculate the activation energy and the rate constant. Eq. 3.12 shows that the relationship between the logarithm of reaction rate ($ln(k)$) and $\frac{1}{T}$ is linear. From this relation, the activation energy can be obtained from the slope and the pre-exponential factor from the intercept. However, this is limited to a narrow temperature range as discussed by Doppelbauer & Bauerle (1986) who demonstrated that different temperature ranges (about 250 K) had different activation energies, resulting in different pre-exponential factors.

Based on the data of Tables 5.1 and 5.2 summarized in Table 5.5, the logarithm of the growth rate is expressed as a function of the inverse of temperature, and shown in Fig. 5.6.

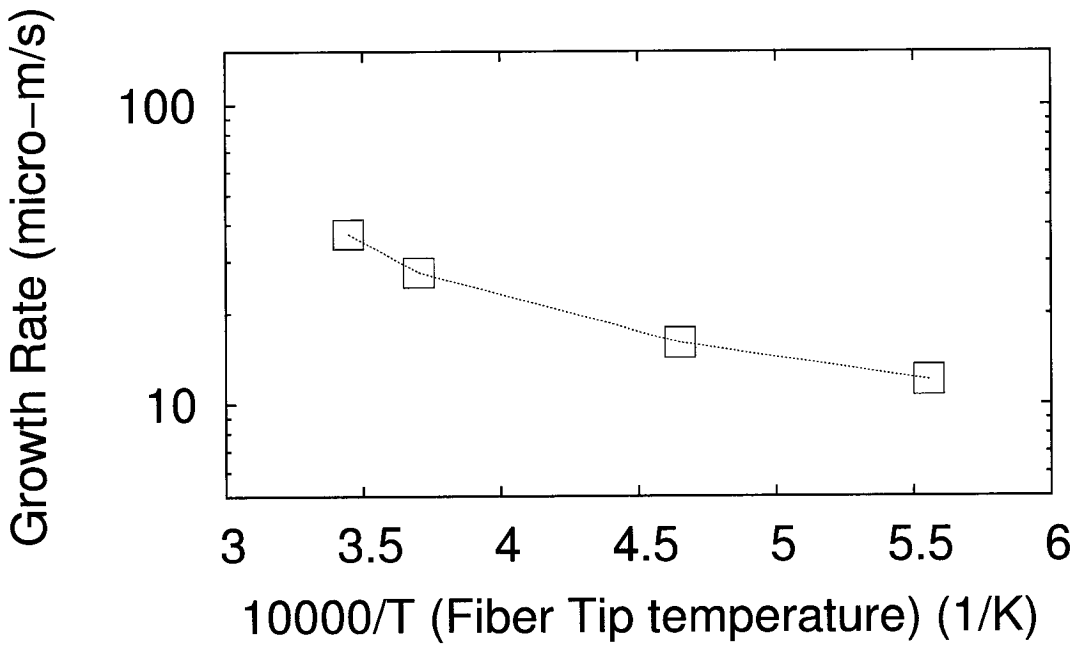

Figure 5.6 Experimental growth rate versus fiber tip temperature

With the linear relation of ln k and $\frac{1}{T}$ shown in Table 5.5 and Fig. 5.6, two points can yield a slope and an intercept from which the activation energy and the rate constant (pre-exponential factor) can be obtained. Table 5.6 gives these calculations.

Table 5.5 Growth rate versus fiber tip temperature

Laser Power (watt)	**Growth Rate (μm/s)**	**T (K)**
0.6	12.0	1800
1.0	16.0	2200
1.4	27.5	2700
1.6	37.0	2900

Table 5.6 Activation energies and pre-exponential factors from the data of Table 5.5

Laser Power (watt)	**Activation Energy (J/kgmol)**	**Pre-exponential Factor**
0.6	0.6630835×10^{6}	5.839697×10^{7}
1.0	1.0425134×10^{6}	1.224983×10^{8}
1.4	1.7787575×10^{6}	4.662666×10^{9}
1.6	2.7047882×10^{6}	2.032943×10^{9}

Doppelbauer & Bauerle (1986) measured the reaction order to be 0.8 for ethylene as a LCVD precursor gas for conditions of pressure of 300 mbar to 1000 mbar and a laser temperature range of 2000 K to 2250 K.

Maxwell & Boman (2005) measured the reaction order to be 2.0 for ethylene as a LCVD precursor for conditions of pressure of 500 mbar to 1.2 bar and with laser power of 0.4 watt to 1.0 watt.

As a first attempt, the reaction orders are assumed to be constant, 0.8 and 2.0. Using the chemical parameters of Table 5.6, two sets of simulation results of the fiber growth rates are computed. The comparison with the experimental data is shown in Fig. 5.7.

It can be seen that the experimental data lies between the two simulation results, meaning that the reaction order of the experiments at FFL must be in the range between 0.8 and 2.0, and probably closer to 2.

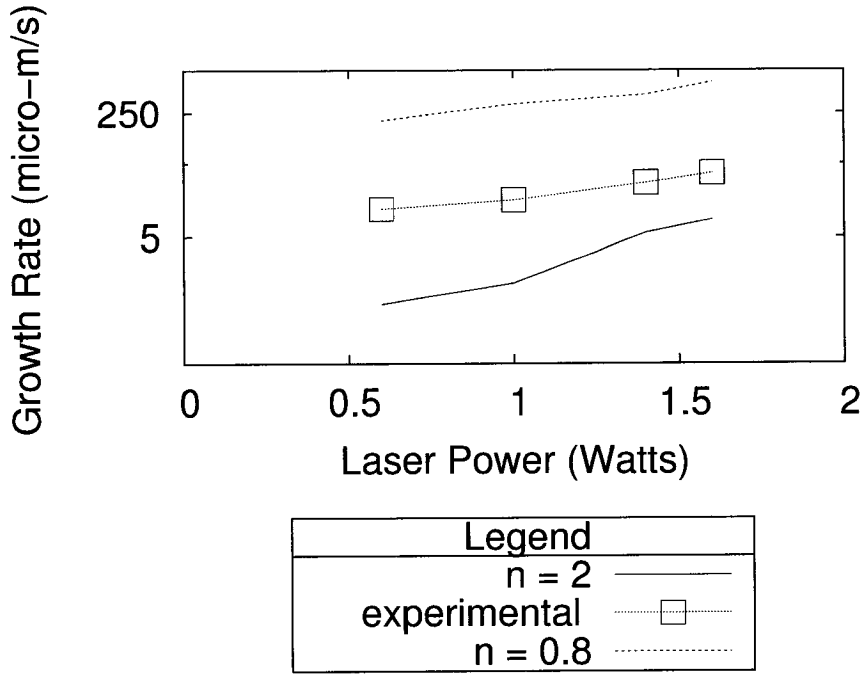

Figure 5.7 Comparison of experimental and computed growth rates for reaction orders of 0.8 and 2.0

The reaction order at different laser power by calibration are shown in Table 5.7.

5.5 Chemical Kinetics Regime

With the configuration described in Section 5.2 and the chemical reaction parameters of Section 5.4, a typical solution at 1.0 watt laser power is given in Fig. 5.8 for the mole

Table 5.7 Reaction order and simulated growth rate

Laser Power (watt)	**Growth Rate Exp.(μm/s)**	**Growth Rate Sim.(μm/s)**	**Reaction Order**
0.6	12.0	11.90	1.395
1.0	16.0	16.05	1.42
1.4	27.5	27.48	1.49
1.6	37.0	36.53	1.67

fraction distribution for the ethylene specie in the entire reactor. This shows how the mass diffusion takes place at the edge of inner resolver and the presence of a precursor (ethylene) jet around the axis since the flow rate of the precursor is much higher than that of the carrier gas (nitrogen).

Figure 5.8(b) shows detailed information in the vicinity of the fiber tip. At the surface, these results show a small region where a slight decrease in the fraction (illustrated by a lighter color) which means that the presursor was consumed in some degree. Adjacent to this area, the concentration is 100% ethylene, indicating that there is enough precursor gas to feed the reaction. Hence the reaction is kinetically controlled.

According to the discussion presented by Shaarawi (2001), the reaction rate versus temperature is governed by a relation of the form given in Fig. 5.9. At low temperatures, the deposition rate is primarily a function of temperature and the deposition process is reaction limited and proportional to temperature. As temperature increases, mass transport of the precursor into the reaction zone limits the deposition rate resulting in relatively constant deposition rate, independent of temperature. Finally, further increase in temperature causes a significant decrease in the deposition rate as a result of a change in the equilibrium products of the system. This is in agreement with the present simulation, as well as with the experimental results shown in Table 5.1 that show that with the increase of laser power, the growth rate is increased.

Therefore, both simulations and experiments agree and show that the reaction was kinetically controlled in accordance to the discussion of Section 3.2.

5.6 Effect of precursor flow rate on growth rate

The effect of precursor flow rate on the growth rate was investigated experimentally by Goduguchinta (2006). This consisted of growing several carbon fibers at a constant laser

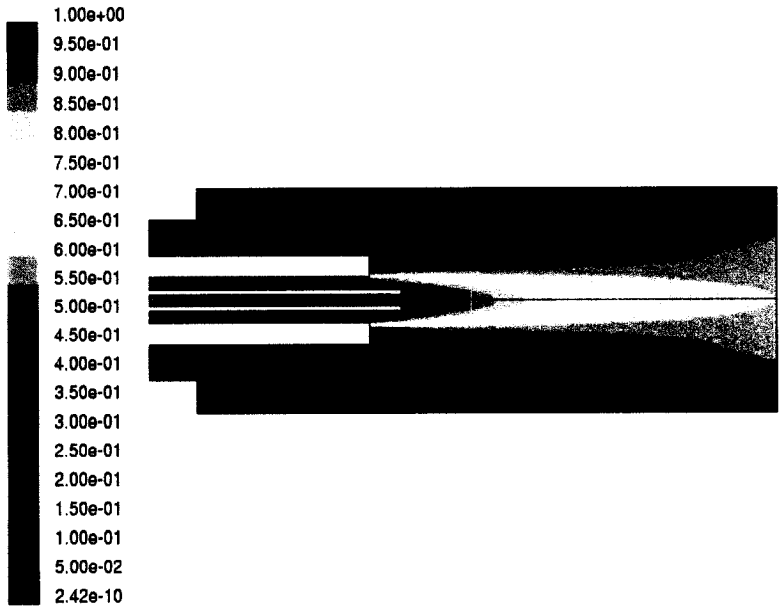

(a) Entire reactor

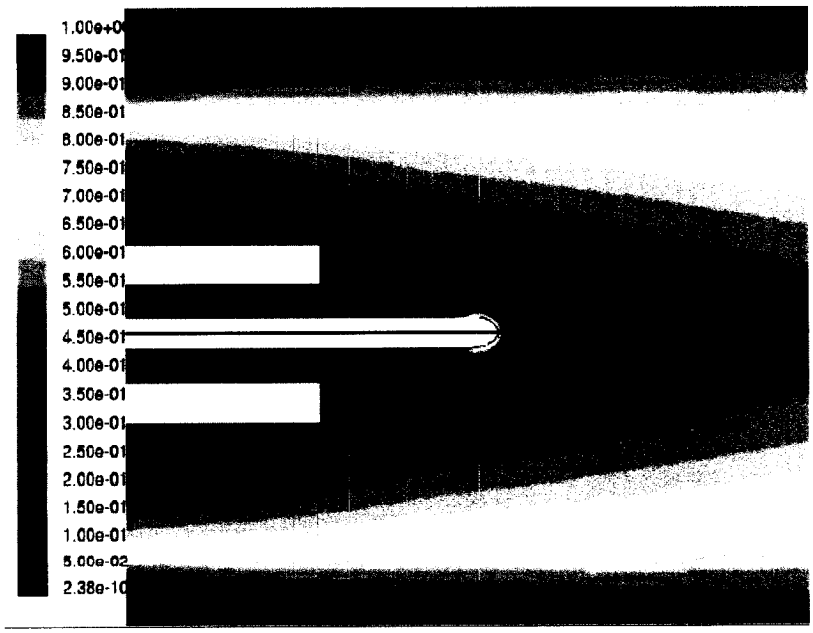

(b) Fiber tip region

Figure 5.8 Ethylene mole fraction in the reactor

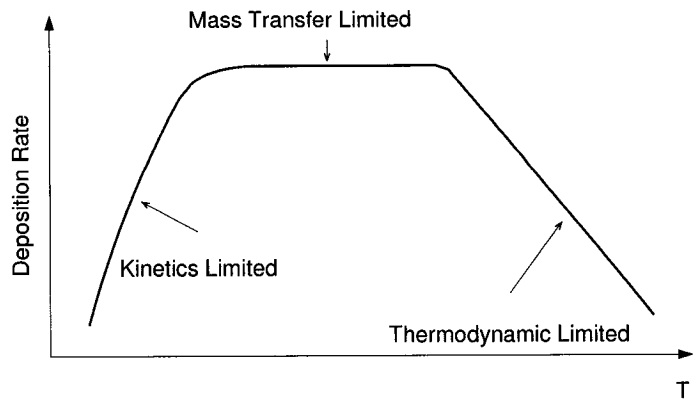

Figure 5.9 Relation between reaction rate and temperature

Table 5.8 Experimental growth rates versus primary precursor flowrate

Precursor Flowrate (Re)	**Growth Rate (μm/s)**
37.5	30
75	30.5
152	31
313	32.5

power, with varying primary precursor flow rate (Inner-tube flow rate). Table 5.8 shows such results at laser power of 1.2 watt from Fig.2.14 of Goduguchinta (2006) which illustrates that the corresponding increase in the growth rate is small. All the experiments reported in Table 5.8 were carried out at a constant secondary precursor flow rate (Inner-resolver flow rate) at a Reynolds number of 83.

With the adjusted configuration to match the experimental setup and the same method of calculating and calibrating the chemical kinetics parameters described in Section 5.4 at 1.2 watt laser power, the chemical kinetics parameters were obtained from Table 5.9. The simulated results of growth rates varying with the primary flow rates are given in Table 5.10.

Table 5.9 Activation energy (E_a), rate constant (k_0), reaction order (n)of ethylene at 1.2 watt from the data of Goduguchinta (2006)

Activation Energy (J/kgmol)	**Rate Constant**	**reaction Order**
701499.8	1.02636×10^8	1.22

Table 5.10 Simulation growth rate versus primary precursor flowrate

Precursor Flowrate (Re)	**Growth Rate (μm/s)**
37.5	33.06
77	33.88
152	34.63
313	35.17

Figure 5.10 shows the trends and variations for both computations and experiments which become another comparable information for the present validation. It can be seen that both simulated and experimental growth rates are increased but not much with the primary precursor flow rate increment for a given precursor flow.

In summary, the validation shows good quantitative and qualitative agreement between measured and numerical results. It can be concluded that the parameters of the model and the simulation methodology are globally correct and yield convincing results.

For these validation computations, typical calculations required about 19000 iterations for a CPU time of 855 min. The computer model is IBM 6230-56U. Figure 5.11 shows the convergence history of the residual of continuity, x-velocity, y-velocity, temperature, hydrogen concentration, and ethylene concentration.

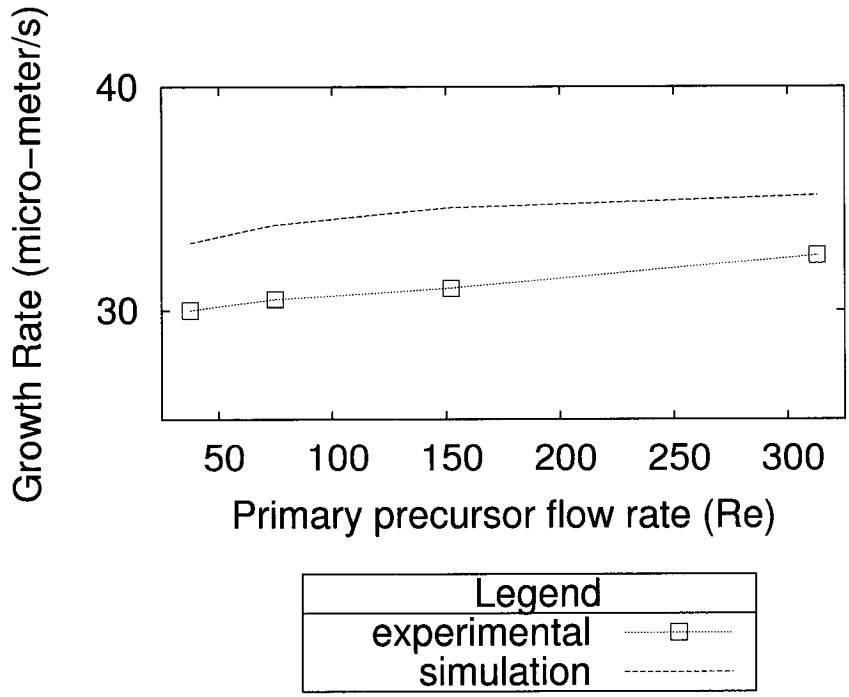

Figure 5.10 Growth rate versus primary precursor flowrate

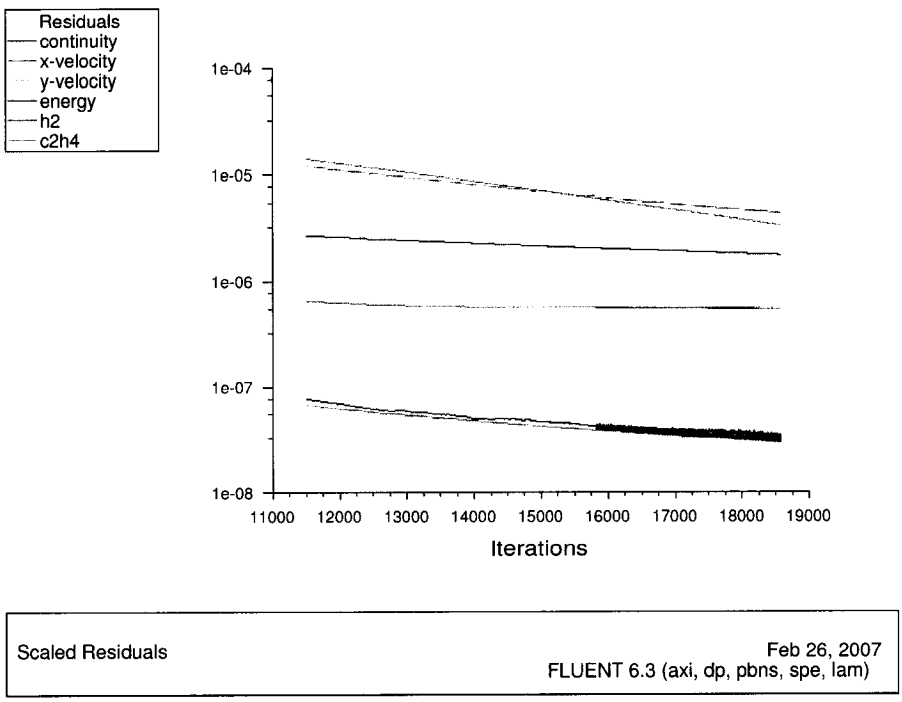

Figure 5.11 Convergence of the solutions for modelling validation

CHAPTER 6

APPLICATION TO REACTOR DESIGN AND ANALYSIS

Following the validation and calibration of the proposed methodology described in the previous chapter, it is now applied to assess separately the various phenomena which occur in a simplified reactor; namely the flow field, the energy exchange mechanisms and the chemical kinetics. Investigation of the contribution of each of these will help to gain insight into the LCVD process. Specifically, we will study how the growth rate (deposition rate) depends on such parameters as the laser power (or tip temperature), precursor flow rate and the position of the laser beam focus. Similarly, we will try to investigate how the detailled flow properties and species concentration affect the deposition rate.

Next, different design and operating conditions will be analysed in the context of two forced convection configurations (along and against the fiber growth directions) to assess the working hypothesis described in Chapter 1.

Finally, to illustrate its usefullness to reactor design, an optimisation procedure will be described.

6.1 Parametric analysis

The first step in the simulation methodology is to verify the behaviour of the model under a set of simplified geometric and physical conditions. The objective of such simplified simulations is to investigate separately the effects of flow, heat transfer, chemical reaction parameters and fiber tip initial position on the species concentrations.

1. the fiber tip (or laser focus) positions are investigated.

2. the mixture characteristics of the precursor and the carrier gas are investigated considering only the flow effects. Then, the effect of the laser heat is analyzed for species concentrations and temperatures.

3. the effects of the chemical reaction are analyzed and discussed.

These investigations will be carried out using an open air configuration (Goduguchinta (2006)) whose geometry is shown in Fig. 6.1. It is an axisymmetric design made up of two concentric tubes which are the outer tube and the inner tube. The outer tube provides the carrier gas (argon), while the inner tube provides the precursor gas (ethylene). The shape of the fiber tip is assumed to be an elliptic profile with an aspect ratio of 1:2.

	Diameter
Tungsten wire	75 μm
Fiber	317 μm
Inner tube	800 μm
Outer tube	4570 μm

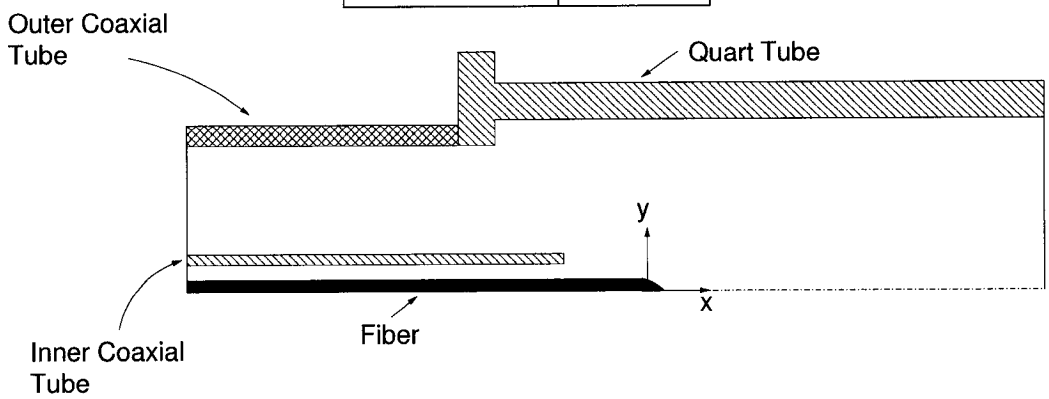

Figure 6.1 Geometry for 2-tube open air reactor

The operating conditions[1] are given in the table below:

[1]Gas flows are usually measured in the unit of **sccm**: standard cubic centimeters per minute.

Laser power	0.3 w to 2.5 w
Fiber tip temperature(Gaussian distribution)	Maximum 2000 K
Ambient temperature	18°C
Pressure	1.13×10^{5} Pascal
Flow rate of Inner tube (ethylene)	4.7375×10^{-7}kg/s (25 sccm)
Flow rate of Outer tube (argon)	1.758×10^{-5}kg/s (650 sccm)

The average inlet velocity for ethylene is 0.963 m/s and 0.4625 m/s for argon. These are in the range of 0.01-10.0 m/s, giving Reynolds numbers less than 1500. Therefore, it is laminar flow.

The temperature profile of the fiber tip is assumed to be a Gaussian profile with the maximum temperature of 2000 K.

6.2 Effect of the fiber tip position

The precursor concentration around the fiber tip controls the deposition process and hence the growth rate. The purpose of the following calculations is to investigate the effect of different tip positions on the precursor concentration around the fiber tip in order to find an optimum position. The calculations are carried out for three different cases, corresponding to three initial positions of the fiber tip of 1, 2 and 3 mm ahead of the edge of the inner tube, respectively. To adequately capture the physics in the vicinity of the fiber, a concentrated mesh is obtained using the size function with parameters given in Table 6.1.

The geometry and the resulting mesh for these cases are given in Fig. 6.2.

Moving the fiber tip, from 1 mm to 2 mm ahead of the position of Case 1, results in a significant change of the precursor concentration. The comparison of three fiber tip positions (1, 2, and 3 mm ahead of the edge of the inner tube) under the same precursor flow rate (50

Table 6.1 Mesh parameters for grid concentration

		Size range	Adaptation rate	Mesh elements
Case 1	Flow	0.005 to 0.10	1.2	42360
	Fiber	0.005 to 0.05	1.2	15794
Case 2	Flow	0.005 to 0.10	1.2	45285
	Fiber	0.005 to 0.10	1.2	31440
Case 3	Flow	0.005 to 0.10	1.2	48242
	Fiber	0.005 to 0.10	1.2	34236

sccm) and the same carrier gas flow rate (650 sccm) are shown in Figs. 6.3(b), 6.4(a), and 6.4(b). It can be seen that the precursor mole fraction is between 0.85 and 0.90 for Case 1, between 0.70 and 0.75 for Case 2, and between 0.60 and 0.65 for Case 3. That means that the closer the fiber tip position to the edge of the inner tube, the higher the mole fraction of the precursor gas.

These results indicate very clearly that the location of the tip controls in a direct way the mixing of the precursor gas and the inert gas, and adjusting the laser focus position is a good mechanism to optimize the concentration.

The upper and lower halves of each map of Fig. 6.5 represent mole fraction and mole concentration of ethylene, respectively. The units for the mole concentration are kmol/m^3 while there are no units for the mole fraction which ranges between 0 to 1. These concentration maps clearly indicate that overhang and tip temperature have an influence on the concentration in the region of interest. These numerical results also show that beyond 5 mm from the nozzle exit, in the worst case, mixing is almost complete. The minimum distance at which mixing is complete (>80 percent argon molar concentration) thus effectively defines the micro-reactor chamber as a cylinder 1 mm in diameter by 5 mm long. This analysis further demonstrates that the micro-reactor's effective length shortens with increasing overhang between 1 and 3 mm, and with increasing tip temperature. Above 3 mm, neither overhang nor temperature seem to have a significant effect.

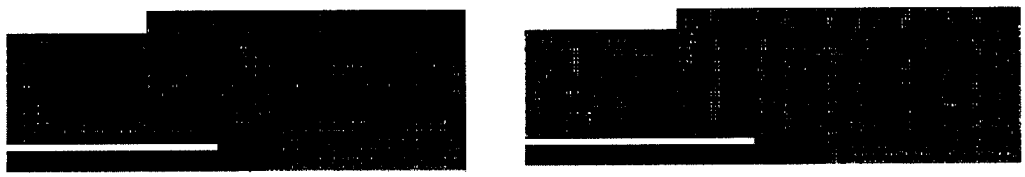

(a) Geometry and mesh for Case 1

(b) Geometry and mesh for Case 2

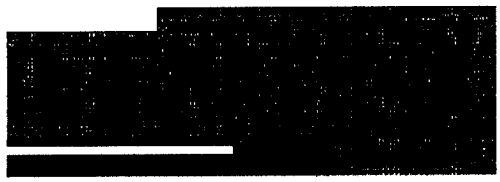

(c) Geometry and mesh for Case 3

Figure 6.2 Geometry and mesh for the three cases of the two-tube open-air reactor

The fiber tip position affects significantly the heat transfer on the fiber tip surface. The closer the tip to the inner tube edge, the stronger the convection to the fiber tip. For a constant heat flux of 2.0×10^5 w/m^2 applied to the fiber tip, Table 6.2 shows the fiber maximum temperature for three overhang positions.

This investigation on the effect of fiber tip position has been utilized to guide the LCVD process control and reactor design, and the results published in "Position Dependence of Growth Rate in Convection Enhanced Laser CVD of Carbon Rods" (Goduguchinta (2006)).

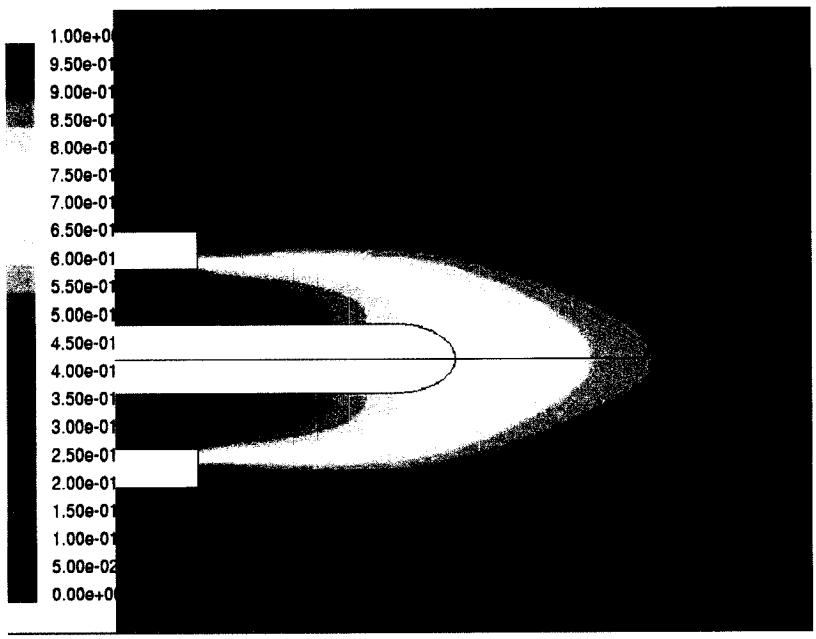

(a) Precursor input flow rate of 25 sccm

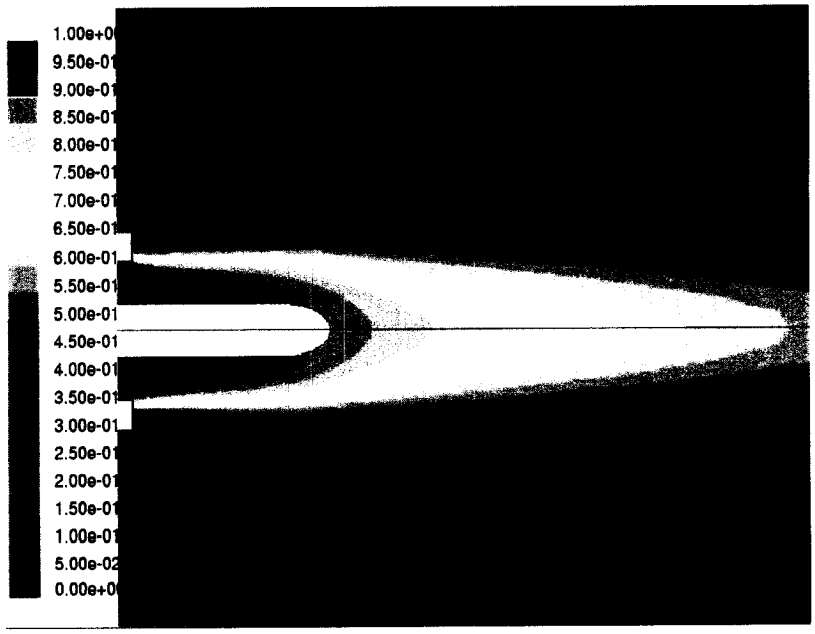

(b) Precursor input flow rate of 50 sccm

Figure 6.3 Effect of flow rate on ethylene mole fraction distribution in 2-tube open-air reactor

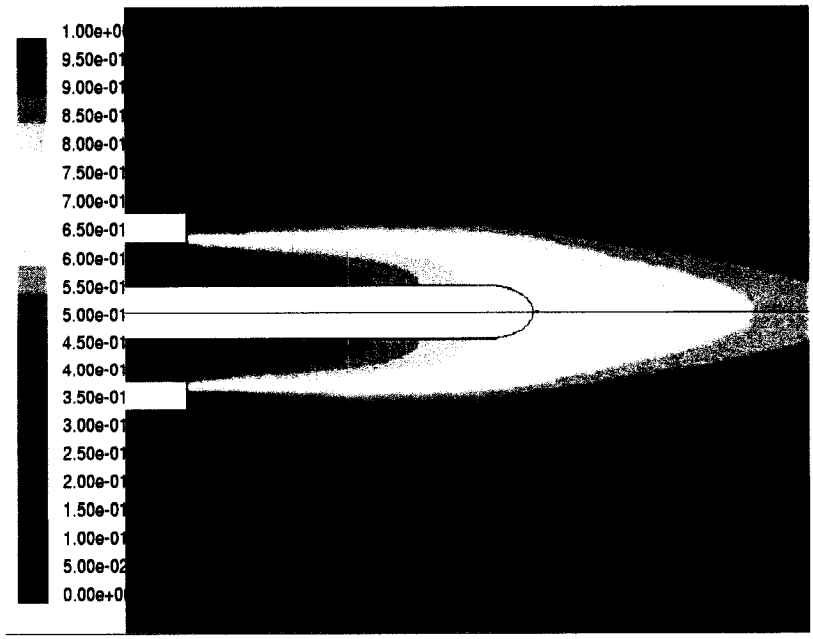

(a) Fiber position Case 2

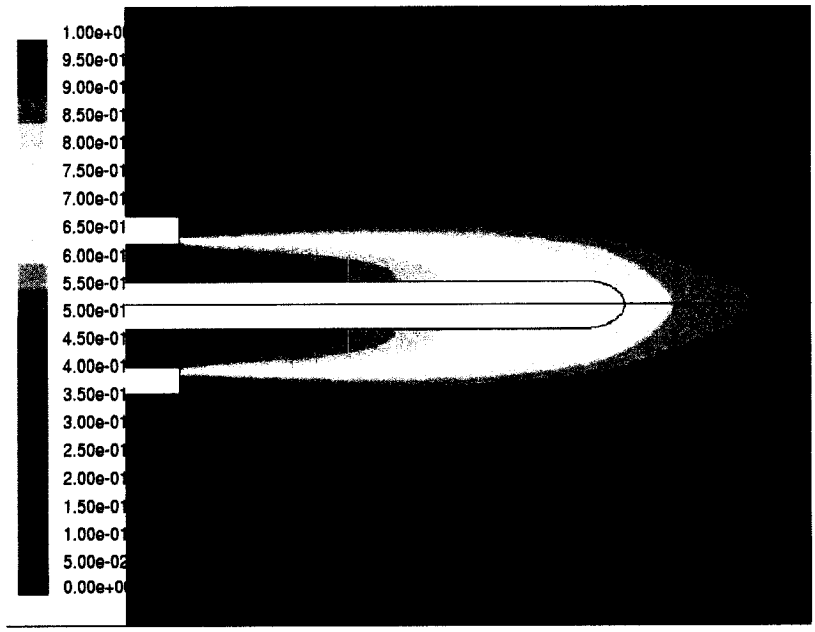

(b) Fiber position Case 3

Figure 6.4 Effect of fiber position on ethylene mole fraction distribution in open-air reactor at 50 sccm input flow rate

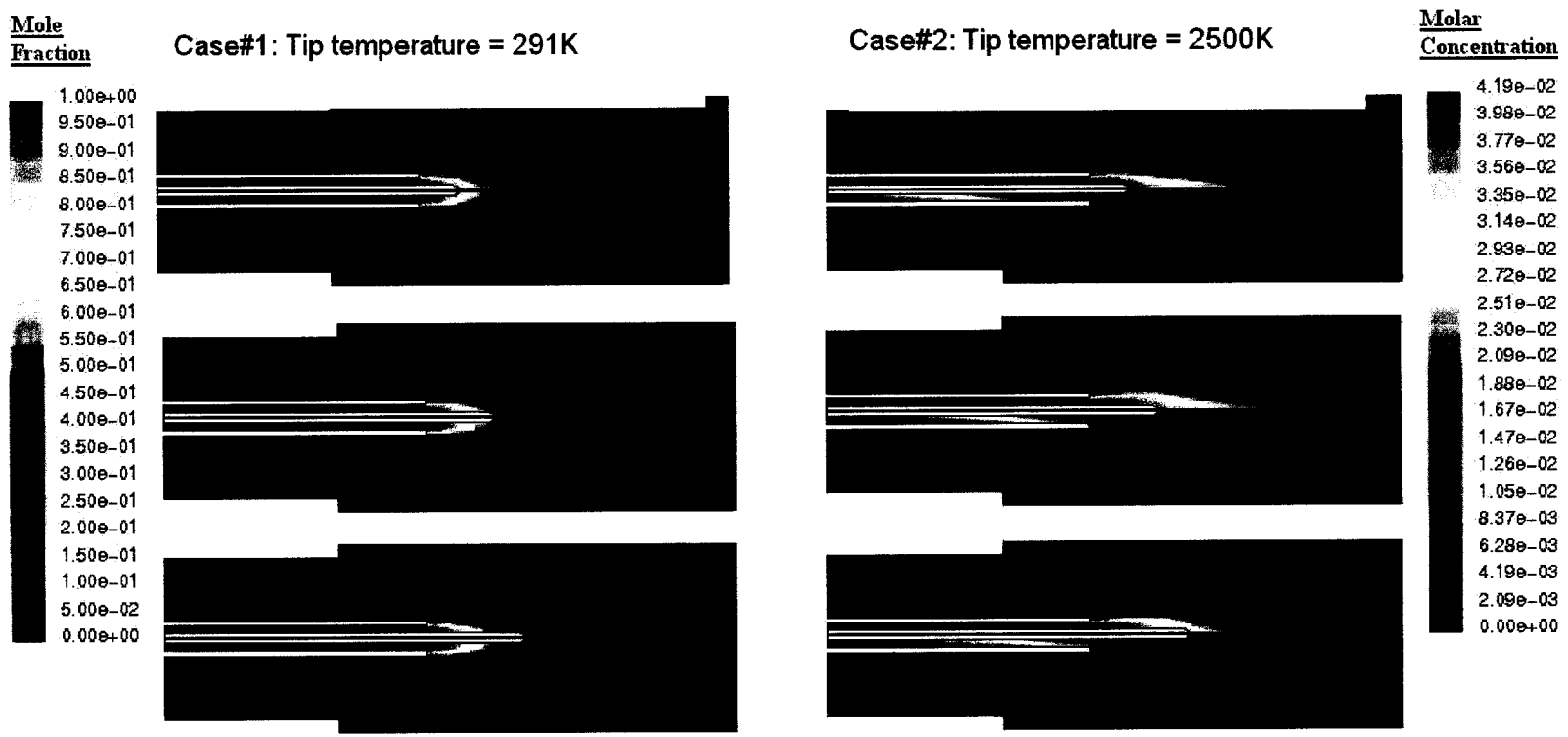

Figure 6.5 Mole fraction and concentration maps of Ethylene in the 2-tube reactor for varying overhang and assumed tip temperature

Table 6.2 Maximum fiber tip temperatures for a constant heat flux of 2.0×10^5 w/m^2

	Maximum fiber tip temperatures (K)
Case 1	1410
Case 2	1590
Case 3	1670

6.3 Effect of flow rate and laser heat

The purpose of the calculations in this section is to investigate how the various variables around the fiber tip are affected by:

- laser heat;
- flow rates of the precursor gas on the precursor concentration;
- flow rates of the carrier gas on the precursor concentration.

First, the effect of the laser heat on the flow in the reactor without considering the chemical reaction is investigated. This is an assumed situation, as local heating is required to enable chemical reaction. However, numerical simulations allow us to analyze these effects separately. Figure 6.6 provides the comparison of the velocity fields, with and without heat addition, for the case with 25 sccm ethylene and 650 sccm argon input flow rates.

As expected, heat addition from the laser makes a significant contribution to the flow around the fiber tip. The maximum velocity increases from 1.38 m/s to 3.92 m/s. It can be observed that the divergence of the flow around the tip is enlarged. That means heat addition increases the kinetic energy of the gas around the fiber tip and can affect the regime of the reaction.

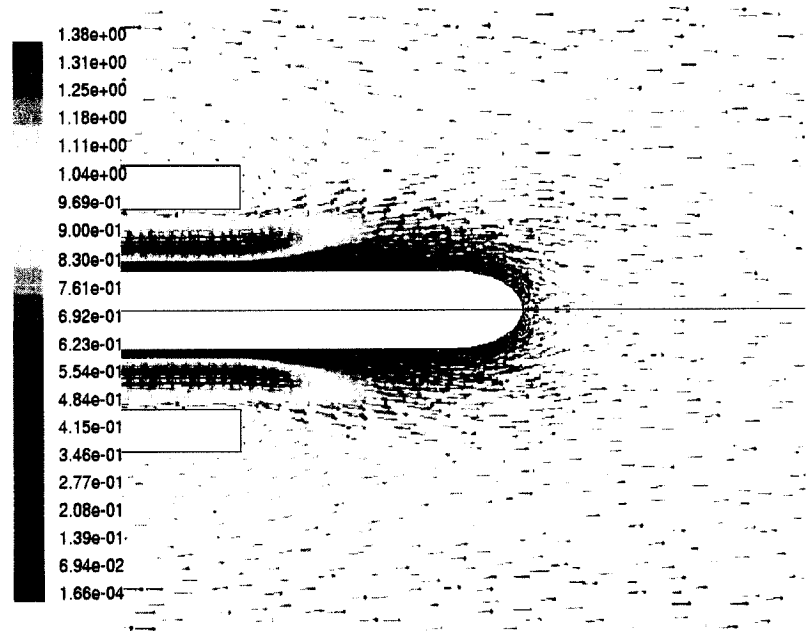

(a) Without laser heat

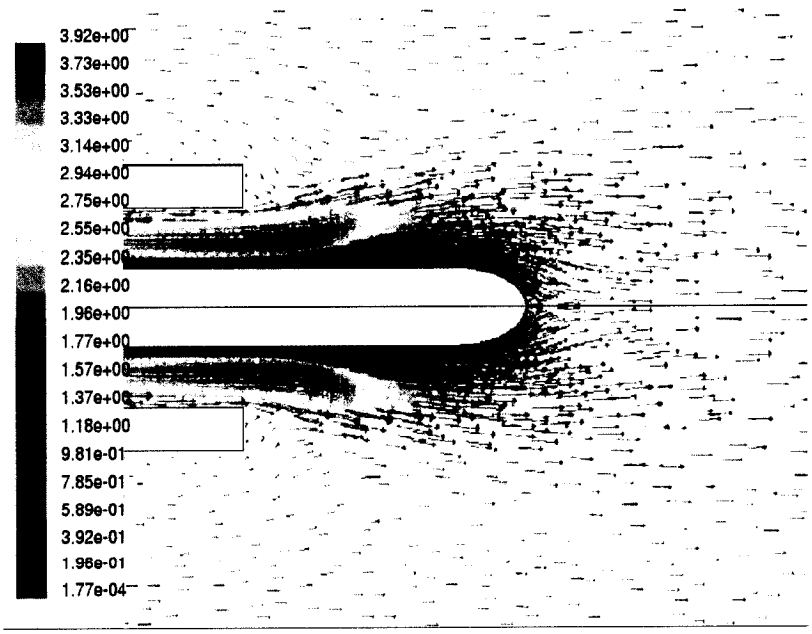

(b) With laser heat

Figure 6.6 Effect of heat addition on the flow field

This effect is illustrated more quantitively by observing the variation of the velocity profile with the axial distance along a cut 0.2 mm radially above the axis (0.041 mm above the fiber surface), as shown in Fig. 6.7. The velocity magnitude remains the same along the fiber length and drops at the tip for the case without laser heat. With heat addition, the opposite behaviour is observed; the velocity increases at the region around the fiber tip. This is due to the higher temperature in that region, inducing a local pressure increase.

Figure 6.3(a) shows that the ethylene mole fraction distribution around the fiber tip varies between 0.70 and 0.75. While doubling the flow rate of the ethylene from 25 sccm to 50 sccm and keeping the other parameters constant, the precursor mole fraction range is increased to 0.85 and 0.90 (see Fig. 6.3(b)). That means the species distribution depends sensitively on the flow rate of the precursor gas. Therefore, to obtain a sufficient precursor gas concentration around the fiber tip to result in ideal fiber growth, the flow rate of the ethylene should be increased.

The effect of the flow rate of carrier gas is also investigated. Decreasing the flow rate of the carrier gas from 650 sccm to 325 sccm or doubling the flow rate from 650 sccm to 1300 sccm, the simulation results show no significant changes on the species distribution in the area of the fiber tip. Thus, doubling the carrier gas flow rate has no significant effect on the precursor concentration around the fiber tip.

However, when the flow rate of carrier gas is increased 10 or 100 times that of the precursor gas (650 sccm), the situation is significantly different. Figure 6.8 shows the effect of high flow rates of the carrier gas on the precursor gas mole fraction distribution. It reveals that the high speed carrier gas decreases the precursor concentration around the fiber as a result of mass diffusion of the two species and the extensive strong jet of the carrier gas.

To further investigate the effect of flow rate, the 3-tube open-air reactor configuration of Section 5.2 was used (see Fig. 5.3). Computations were carried out with a constant laser heat flux of 1.0×10^{7} w/m^{2} and with several flow rates of precursor and carrier gases. From

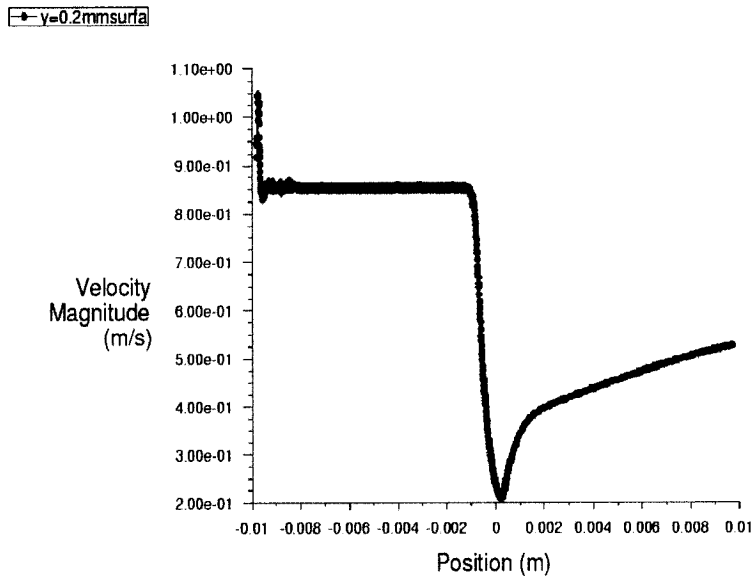

(a) without laser heat

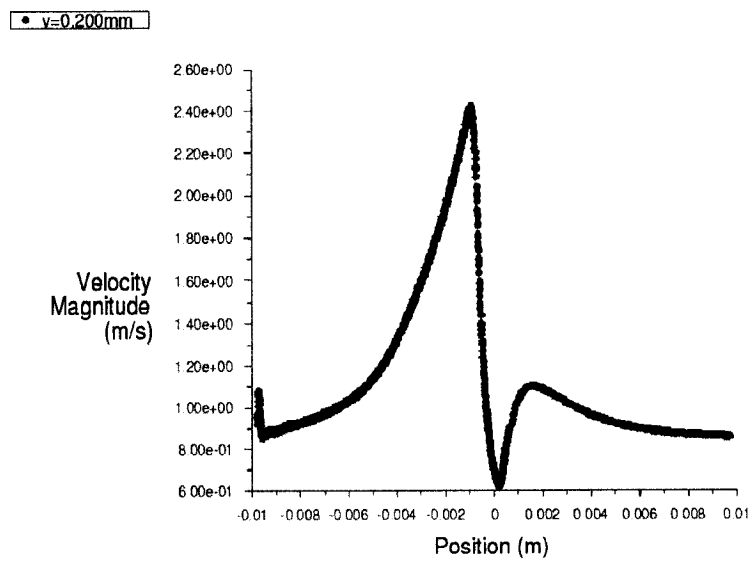

(b) with laser heat

Figure 6.7 Effect of heat addition on the velocity profile at 0.041 mm above the fiber surface

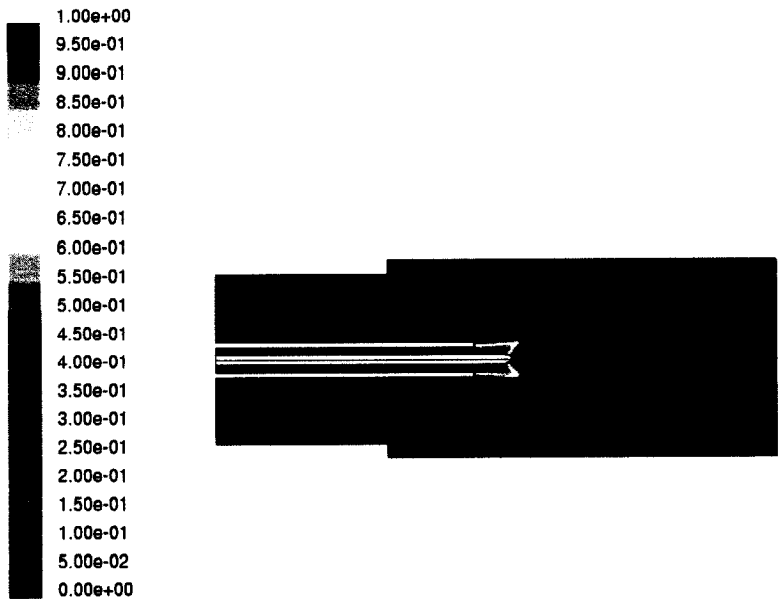

(a) Argon flow rate increased 10 times of 650 sccm

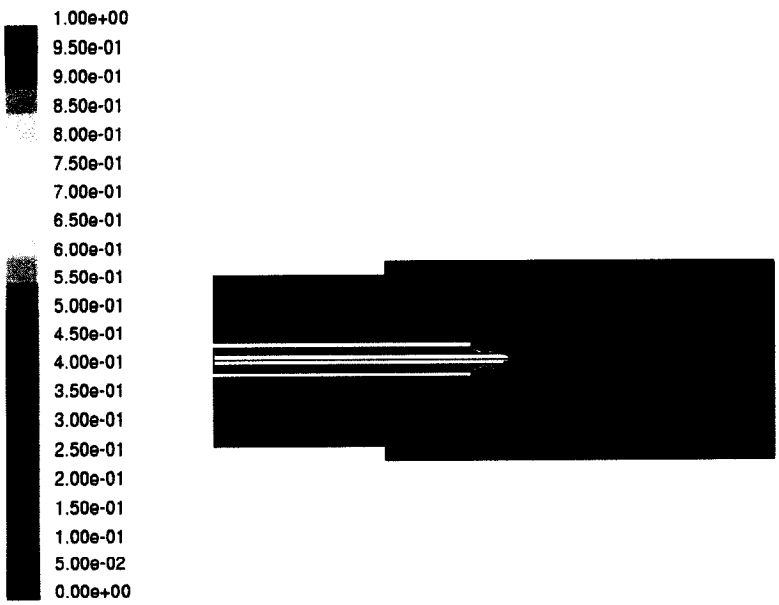

(b) Argon flow rate increased 100 times of 650 sccm

Figure 6.8 Effect of argon flow rate on ethylene mole fraction distribution

Table 6.3 Fiber tip temperature versus gas flow rate

Case No.	**Inner Resolver** (sccm)	**Outer Resolver** (sccm)	**Inner Tube** (sccm)	**Fiber tip temp.** (K)
1	30	50	5	1920
2	60	50	5	1920
3	90	50	5	1920
4	120	50	5	1910
5	150	50	5	1910
6	180	50	5	1920
7	210	50	5	1920
8	60	200	5	1920
9	60	200	2.5	2210
10	60	50	2.5	2210
11	600	500	25	1560

the experimental setup at FFL, the flow rate of the nitrogen from the outer resolver inlet is either 50 sccm or 200 sccm and the flow rate of the inner tube gas (C_2H_4) is either 5 sccm or 2.5 sccm. The flow rate of the precursor gas from the inner resolver inlet is varied from 30 sccm to 210 sccm. Table 6.3 shows the results of the temperature of the fiber tip with the constant heat flux of 1.0×10^7 w/m^2 and with varying gas flow rates.

It can be seen from Table 6.3 that the flow rate of the inner tube gas has an apparent effect on the fiber tip temperature. However, in the range of the adjustable flow rates of experiments in FFL, the change of the flow rates of the inner and outer resolver gases are not sufficient to significantly affect the fiber tip temperature. This could be because the range of variations is small. Case 11 is an extreme example for which the flow rates of the precursor and the carrier gases are 10 times higher than those of Case 1 to 7. It can be seen that the fiber tip temperature decreases significantly because of the strong forced convection flow. For these cases, the flow rates of the precursor and the carrier gases will affect the fiber tip temperature.

Cases 1 to 7 correspond to flow rates of 30 sccm to 210 sccm with intervals of 30 sccm. During these simulations, different flow patterns were observed. A recirculation zone appeared in the reactor outlet, whose size increased with the precursor flow rate. We can induce that the back flow of the air can reach the reactor zone and affect the phenomena.

Figure 6.9 is the mole fraction map of N_2 with conditions of 30 sccm (Case 1), 60 sccm (Case 2), and 210 sccm (Case 7) precursor flow rates. It can be seen that the case of 30 sccm has no air back flow, but the case of 60 sccm has a little back flow in the reactor outlet. For the case of 210 sccm, this effect is very large.

Figure 6.10 is the map of the nitrogen mole fraction for Case 8 of Table 6.3. Comparing it with Case 2 (Fig. 6.9(b)), it can be seen that if the carrier gas flow rate is much higher than the percursor flow rate, the carrier gas concentration will mainly occupy the reactor space and the precursor gas concentration will be compressed near the axis. There is no inverse flow at the outlet.

From these simulations, we can conclude that the relative flow rates for the carrier gas to the precursor gas are very important. The flow rate of the precursor jet should be high enough to push away the carrier gas to reach the sufficient concentration on the fiber tip. However, if the precursor flow rate is much higher than the carrier gas flow rate, a reverse flow will result, bringing air into the reactor zone.

If the flow rate of the carrier gas is too low, it cannot push away the soots of the deposition. Therefore, the good adjustment of the flow rates of the precursor and carrier gases is a very important operating condition for the LCVD process. From the current simulations, ratios of carrier to precursor flow rates in the range of 0.1 to 0.5 seem appropriate according to these parametric calculations.

The investigation of the effects of flow rates can provide insights for the LCVD process which can be used to guide the LCVD process control. The paper "On the Importance

of Focus Tracking in LCVD Growth of Carbon Rods" (Goduguchinta (2006)) used the modelling results of the mixture concentration distributions in the reactor to support the assumption that the ethylene (precursor) shrouds the secondary flow (argon as the carrier gas) to prevent diffusion of argon into the reaction zone.

6.4 Effects of Chemical Kinetics

The chemical reaction has a significant effect on the flow pattern and the species distribution around the fiber tip. The first difference is the presence of a new specie, H_2, as a by-product of the reaction. This will be investigated using the 3-tube reactor configuration (as in Section 5.2). The chemical kinetics parameters are based on Table 5.6 and Table 5.7 described in detail in Section 5.4. The fiber tip temperature is assumed to be constant of 2150K.

Figure 6.11 shows the mole fraction distributions of precursor (ethylene) around the fiber tip with and without chemical reaction. In the absence of chemical reaction, the mole fraction of the precursor is 1, while with chemical reaction, the mole fraction of the precursor takes on values below 1 because the precursor gas is consumed by the chemical reaction. The hydrogen concentration distribution and carbon deposition rate are shown in Figs. 6.12 and 6.13 which are not present without the chemical reaction.

Figure 6.14 shows the velocity vector field in the area of fiber tip, with and without chemical reaction. It can be seen that without chemical reaction, the no-slip condition between the gas flow and the solid fiber is verified, with the presence of a stagnation point at the fiber tip. In the presence of a chemical reaction, there is a gas velocity "sink" at the fiber tip because of the carbon deposition, and a small velocity source in the front of the fiber tip because of the by-production of hydrogen.

This effect of the chemical reaction on the velocity field is illustrated more quantitively by

observing the variation of the velocity magnitude distribution with the axial distance along a cut 0.2 mm radially above the axis (0.041 mm above the fiber surface), as shown in Fig. 6.15.

It can be seen that there is no significant difference for the general velocity magnitude distribution between the two cases with and without chemical reaction. This is because the by-production gas is in small quantity.

6.5 Proving the Working Hypothesis

In Section 1.2, a working hypothesis was presented which is that forced convection of the precursor gas along the direction of fiber growth contributes to enhance cooling, increases growth rate and provides better mechanical support of the growing fiber.

In the present section, we will compare the two cases of forced convection along and against the direction of the fiber growth. Based on the 3-tube reactor configuration of Section 5.2, the fiber and the laser beam focus direction are reversed, resulting in a new configuration where the fiber growth direction is against the precursor jet. The same procedures and operating parameters are used for this case.

The velocity pattern in Fig. 6.16(a) shows the presence of a velocity "sink" at the surface of the fiber tip resulting from the carbon deposition. However, this does not appear in the other case shown in Fig. 6.16(b) because of strong convection. It can be seen from Fig. 6.17 that the carbon deposition rate for the case of a precursor jet along the axis jet is higher. The numerical values are 2.16×10^{-2} kg/m$^2/s$ and 5.83×10^{-3} kg/m^2/s for axial jets along and against the fiber tip, respectively.

The result is a decrease of precursor mole fraction and an increase in the production of hydrogen for the case of the counter precursor jet compared with the case of the precursor

jet along the direction of fiber growth which was shown in Figs. 6.18 and 6.19.

Also, because the fiber is very thin, vibrations will be easily induced in such a strong convection jet. Therefore, we can conjecture that the precursor jet along the fiber growth direction provides better mechanical support.

It can be seen that for a constant heat flux (2.5×10^5 w/m^2) applied on the fiber tip, the case of counter precursor jet naturally results in a higher convection and consequently the temperature of the fiber tip is lower as shown in Fig. 6.20. Based on these simulation results of forced convection along and against the direction of the fiber growth, it can be observed that forced convection of the precursor gas along the direction of fiber growth increases the growth rate by a factor of 3.7 times that of precursor counter flow.

6.6 Summary of Ambient Simulation Results

The simulation results for the reactor operating at the ambient conditions are as follows:

1. The validation results show good quantitative and qualitative agreement between measured and numerical results. The growth rate of simulation for Maxwell & Boman (2006) is very close to the experimental maximum growth rate which means that the modelling methodology and the establishment of the physical parameters of the model are convincing.

   The simulation results show there is enough precursor gas to feed the reaction from which it can be deduced that the reaction is chemical kinetics controlled. This is in agreement with the experimental results that show that with the increase of laser power, the growth rate is always increased.

2. Flow rates of the precursor and the carrier gas have a significant effect on the concentration distributions of the precursor in the area of reaction zone. The precursor

concentration increases when increasing the precursor flowrate.

3. The concentration distributions of the precursor in the area of reaction zone are very sensitive to the laser focus position (initial fiber tip position). The closer the fiber tip position to the edge of the inner tube, the higher the mole fraction or the concentration of the precursor is reached.

4. The laser heat affects to the flow around the fiber tip. The maximum velocity of the flow from the inner tube is increased and the divergence of the flow around the exit of the inner tube is enlarged as a result of heat addition.

5. The overhang and tip temperature of the fibers have an influence over species concentration in the reaction region. The micro-reactor's effective length shortens with increasing overhang, and with increasing tip temperature. However, beyond a certain distance from the edge of the inner tube (i.e. 3 mm), neither overhang nor temperature seems to have a significant effect.

6. The flow rate of the precursor and the carrier gases influence significantly the species concentration distribution. If the flow rate of the carrier gas is much higher than that of precursor gas, the precursor gas will shrink its divergent space. If the precursor flow rate is much higher than the carrier gas flowrate, a reverse flow results and the recirculation flow could draw air into the reaction zone.

7. The chemical reaction at the fiber tip affects the velocity field in the reaction zone through a velocity "sink" because of the carbon deposition replacing the no-slip condition on the fiber tip. There is no significant macroscopic effect in the velocity field of the entire reactor because of the small quantity of by-product gas produced.

8. The working hypothesis which is that forced convection of the precursor gas along the direction of fiber growth contributes to enhance cooling, increases growth rate and provides better mechanical support of the growing fiber is verified.

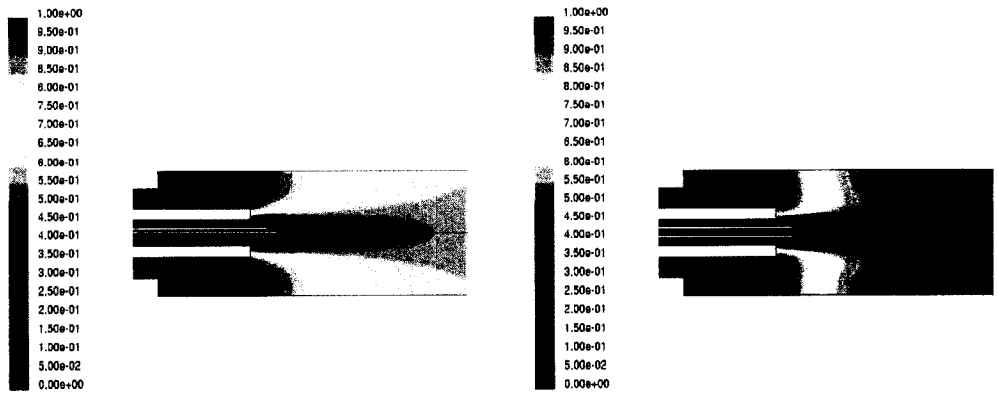

(a) 30 sccm precursor flow rate

(b) 60 sccm precursor flow rate

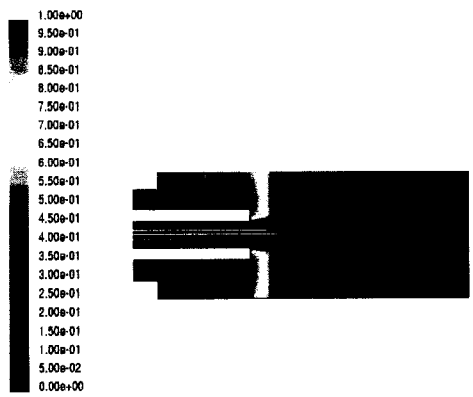

(c) 210 sccm precursor flow rate

Figure 6.9 Effect of precursor flow rate on nitrogen mole fraction for the 3-tube open air reactor

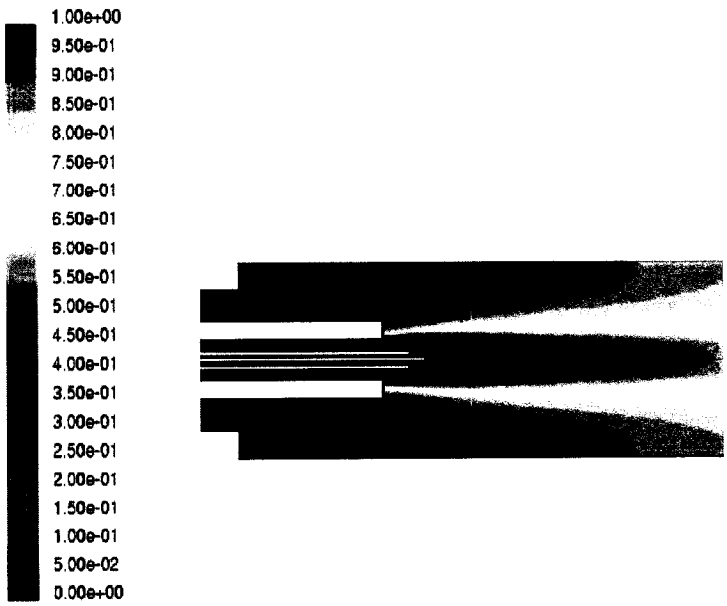

Figure 6.10 Map of nitrogen mole fraction for 200 sccm carrier and 60 sccm precursor

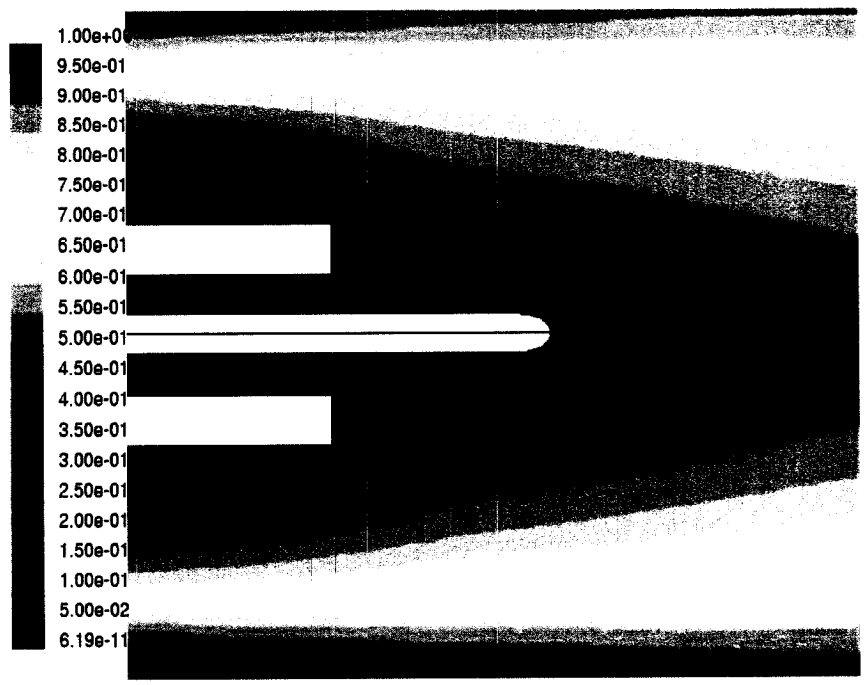

(a) Without chemical reaction

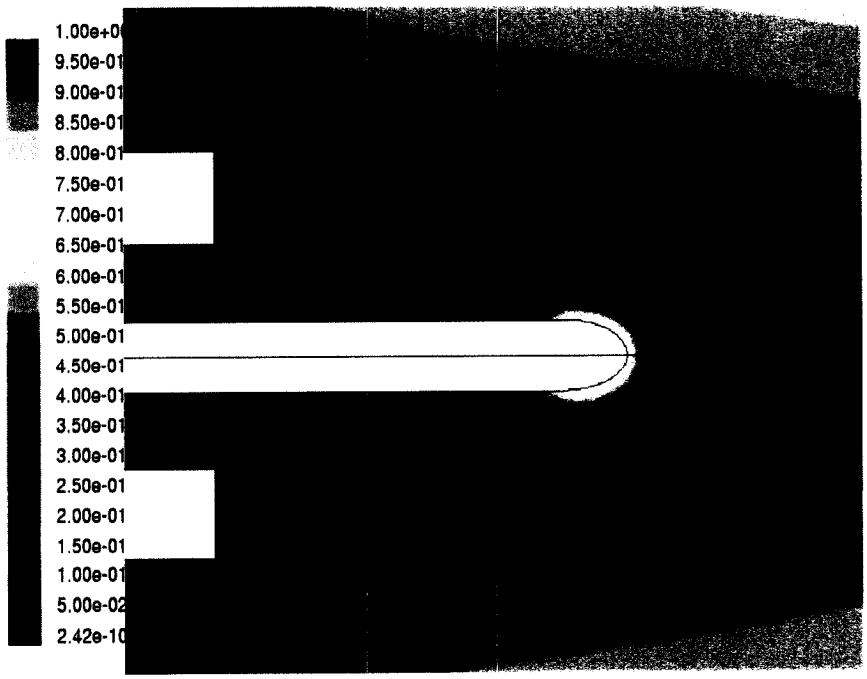

(b) With chemical reaction

Figure 6.11 Effect of chemical reaction on the precursor mole fraction around the fiber tip

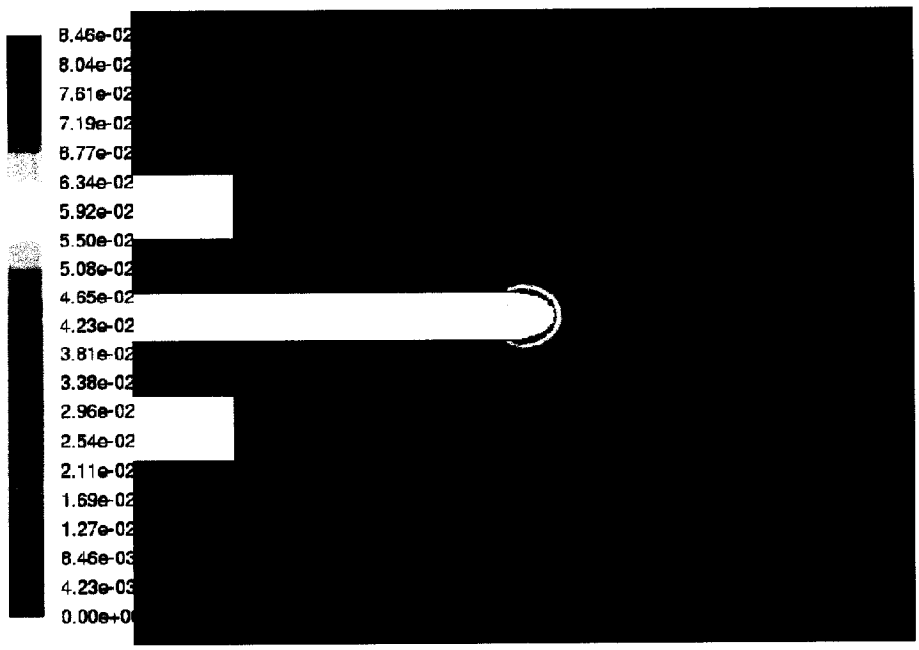

Figure 6.12 By-production (hydrogen) mole fraction

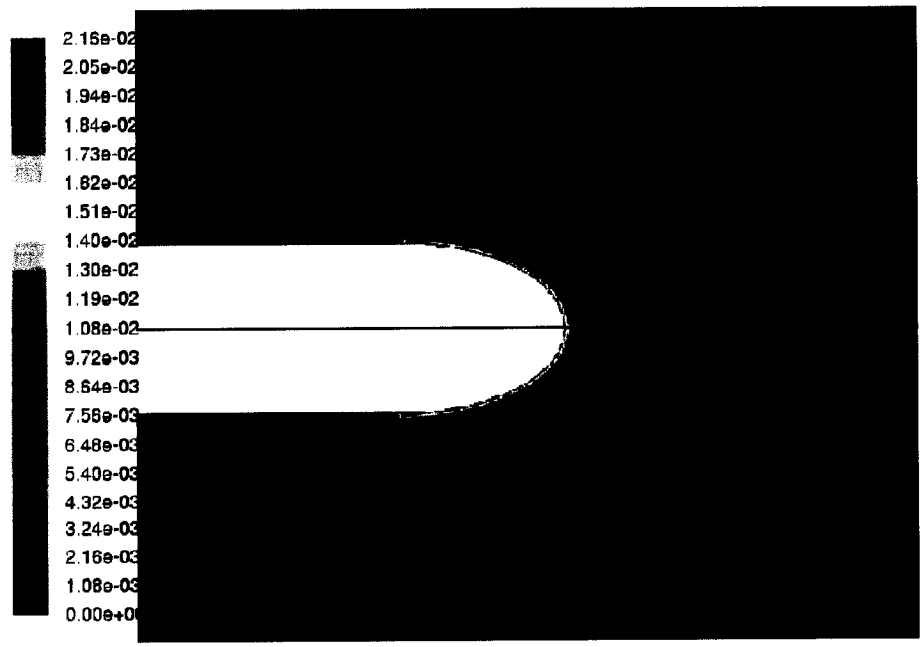

Figure 6.13 Map of the carbon deposition rate ($kg/m^2/s$)

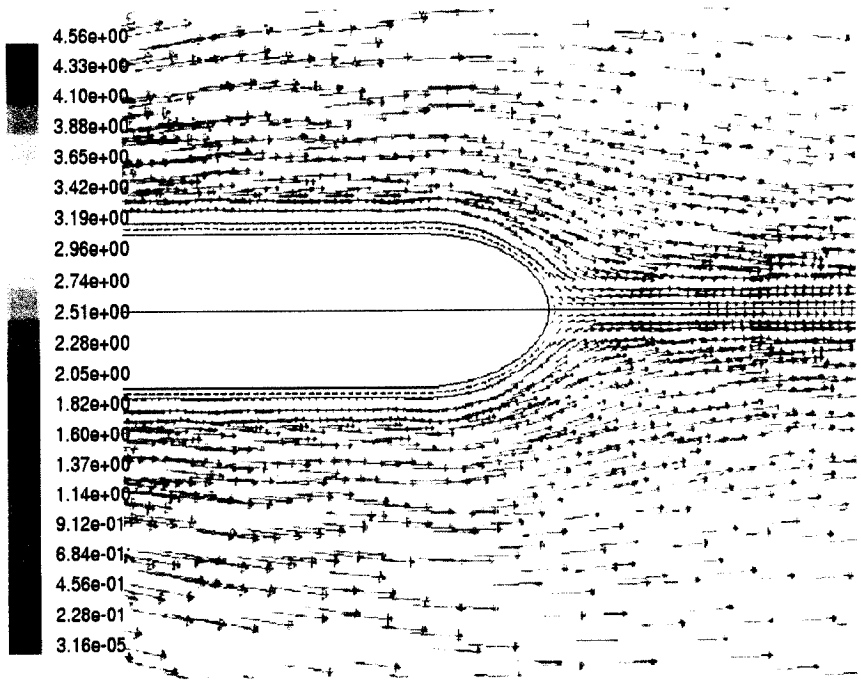

(a) Without chemical reaction

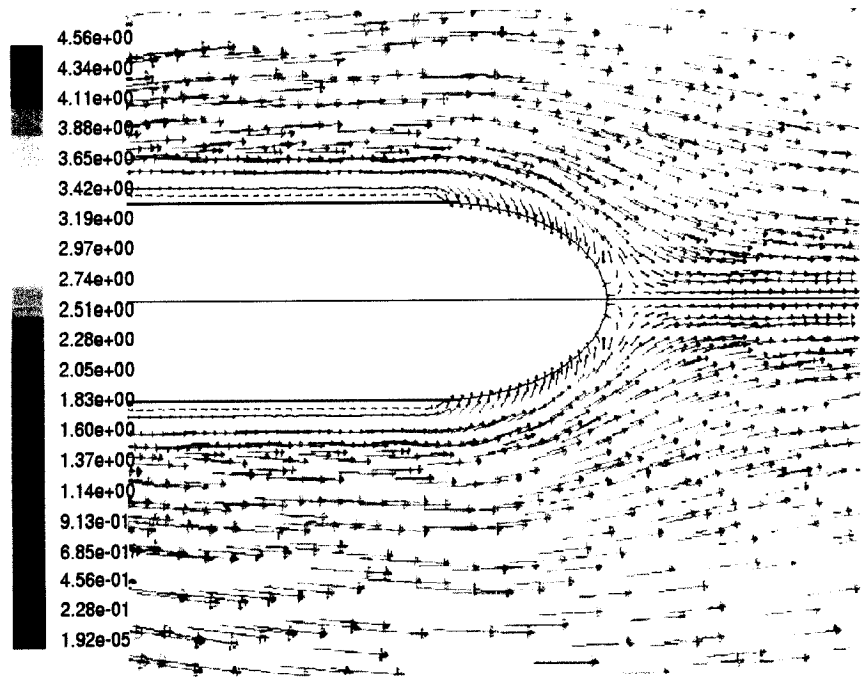

(b) With chemical reaction

Figure 6.14 Effect of chemical reaction on the velocity field at the fiber tip

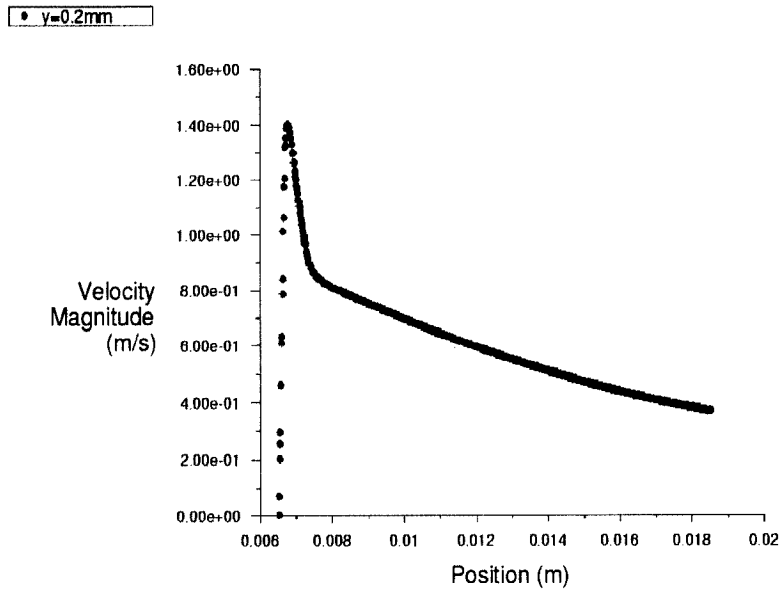

(a) without chemical reaction

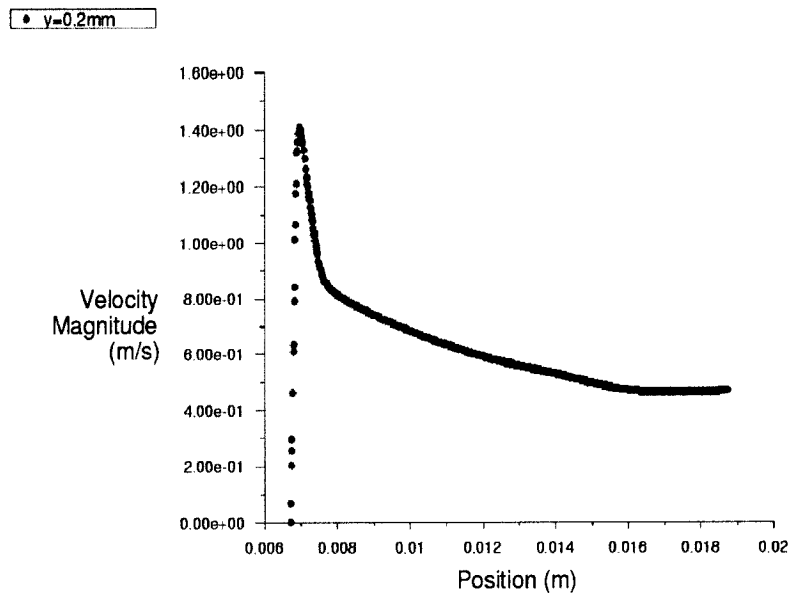

(b) with chemical reaction

Figure 6.15 Comparison of the velocity magnitude without and with chemical reaction

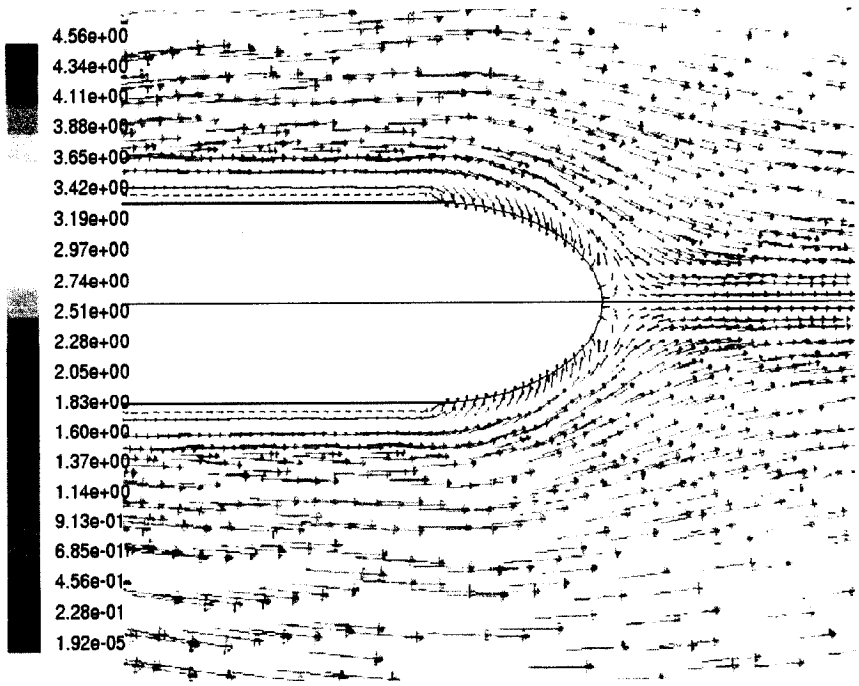

(a) Precursor jet along the fiber growth direction

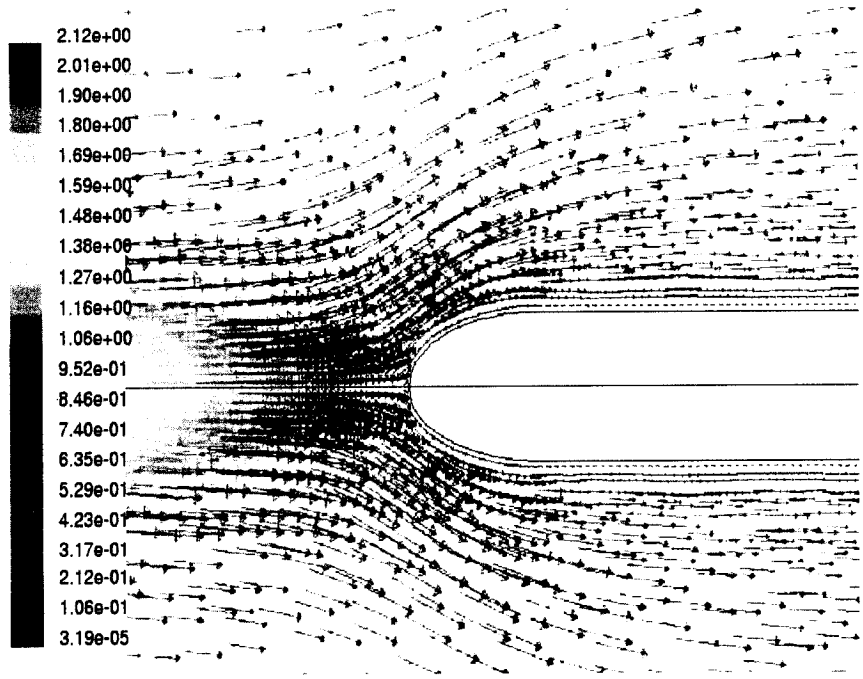

(b) Precursor jet against the fiber growth direction

Figure 6.16 Effect of flow direction of precursor gas on the flow pattern at the fiber tip

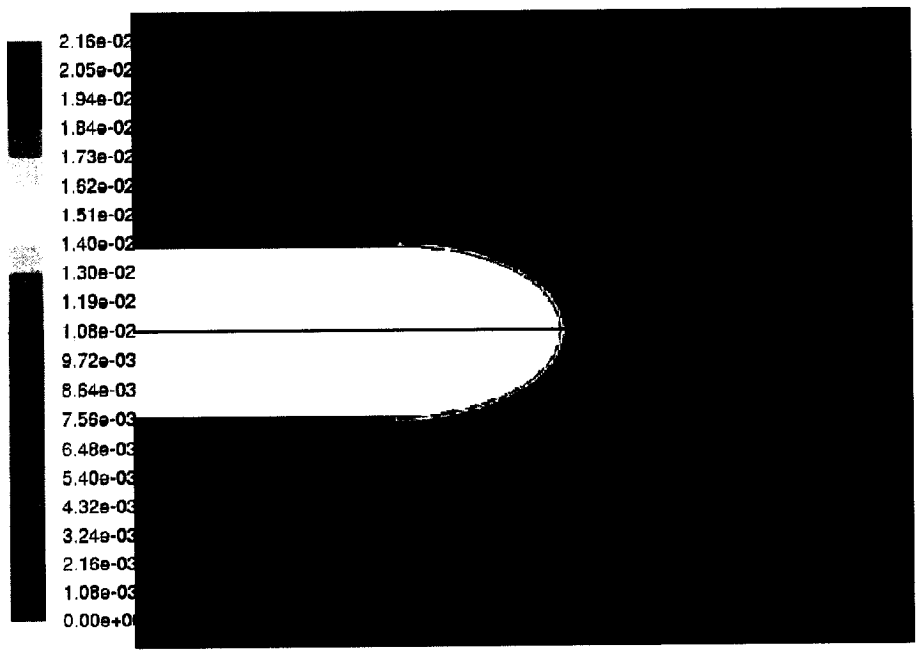

(a) Precursor jet along the fiber growth direction

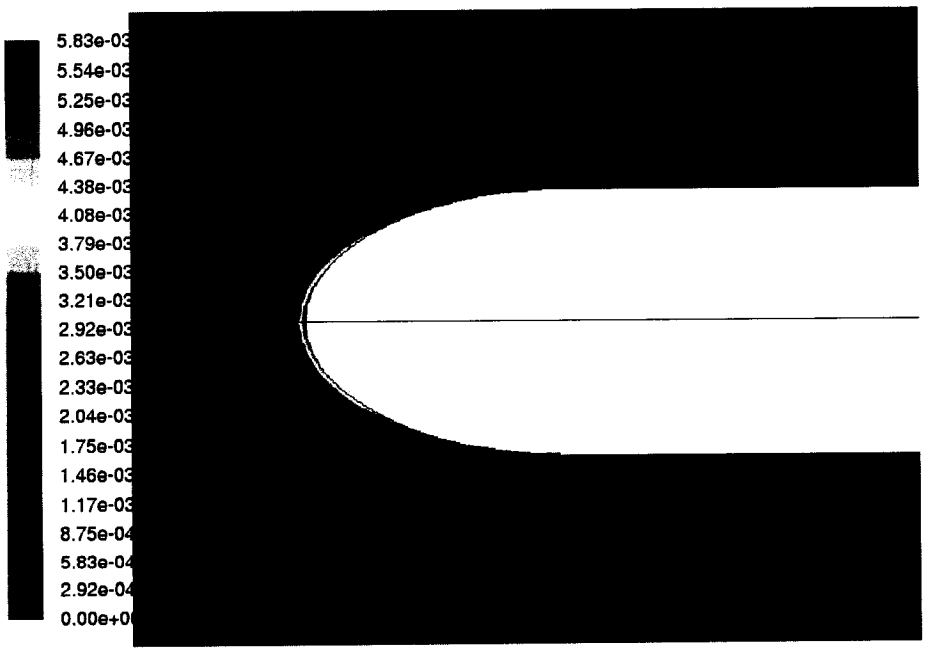

(b) Precursor jet against the fiber growth direction

Figure 6.17 Effect of precursor flow direction on the carbon deposition rate

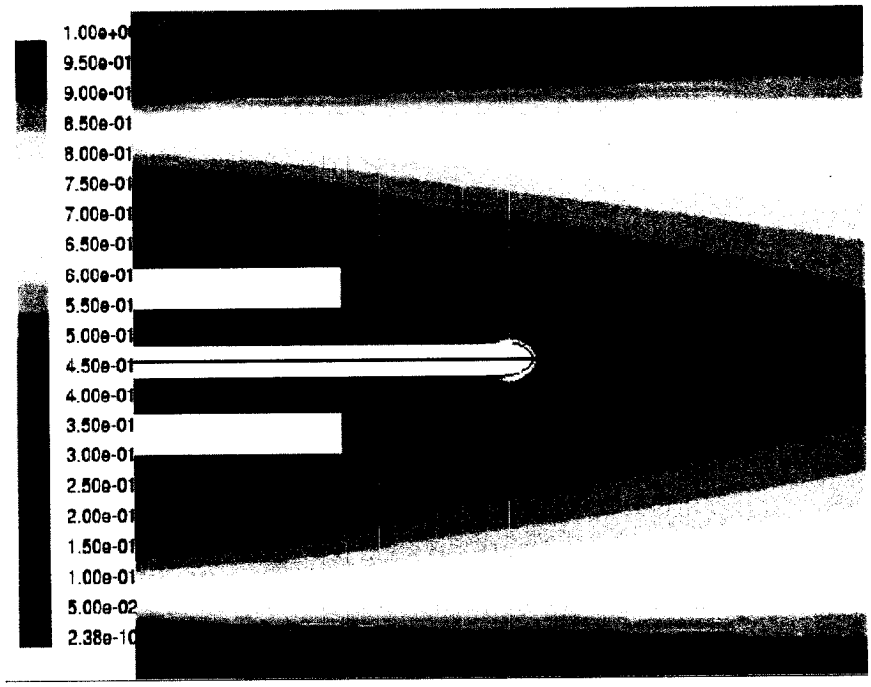

(a) Precursor jet along the fiber growth direction

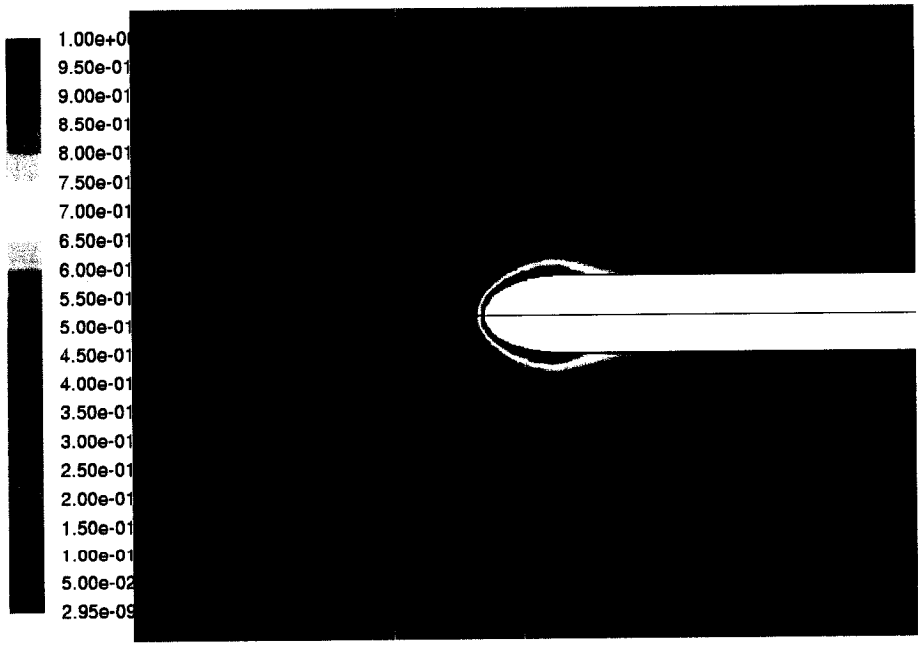

(b) Precursor jet against the fiber growth direction

Figure 6.18 Effect of precursor flow direction on the mole fraction of precursor

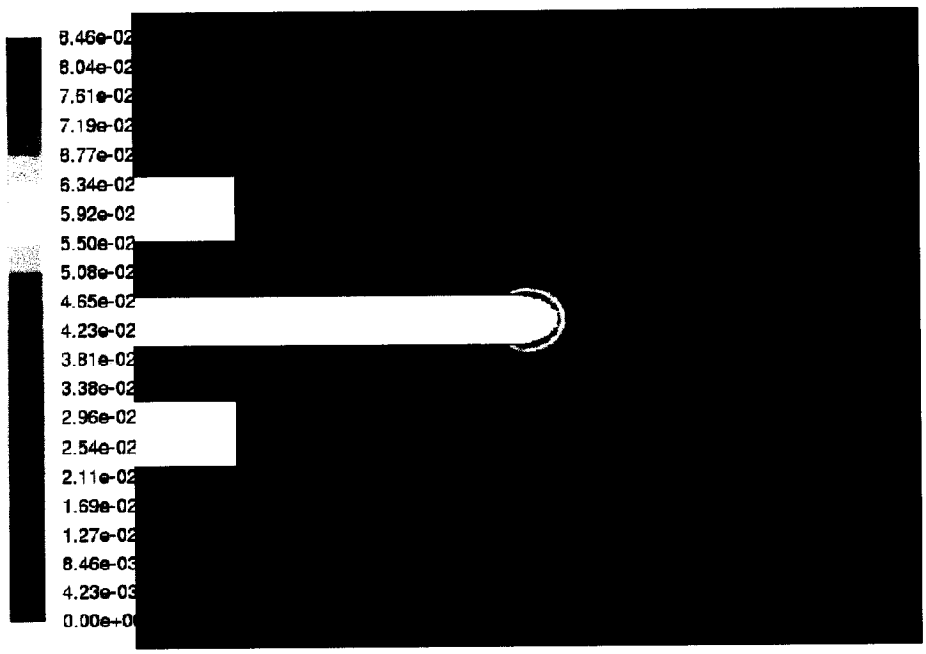

(a) Precursor jet along the fiber growth direction

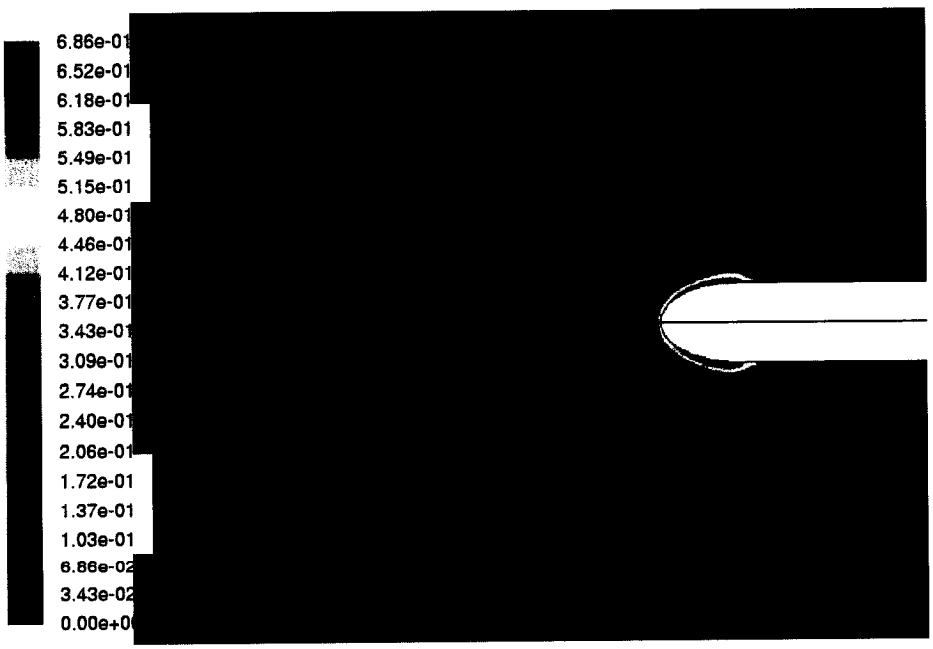

(b) Precursor jet against the fiber growth direction

Figure 6.19 Effect of precursor flow direction on the mole fraction of hydrogen

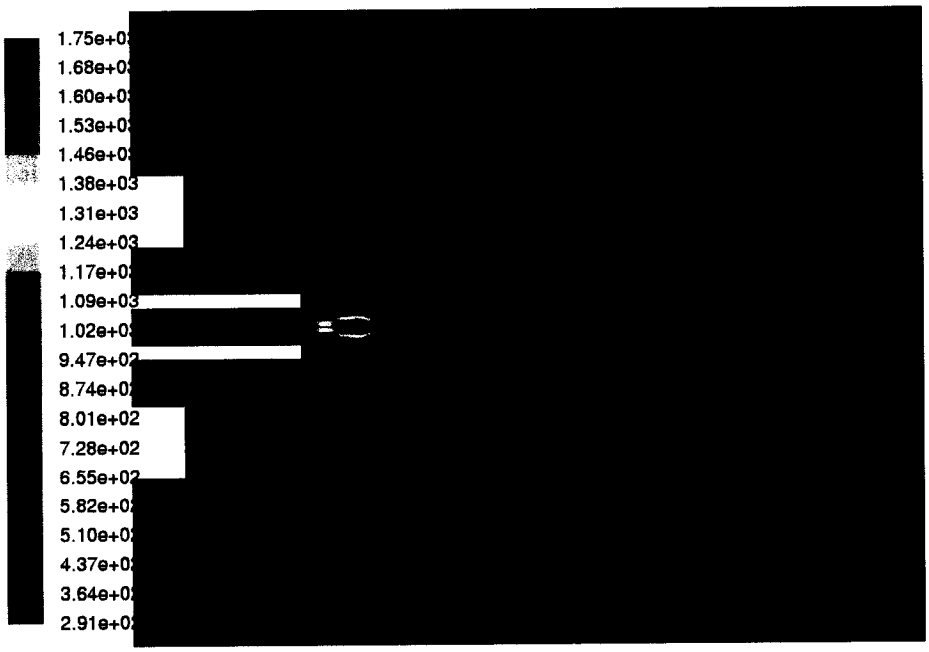

(a) Precursor jet along the fiber growth direction

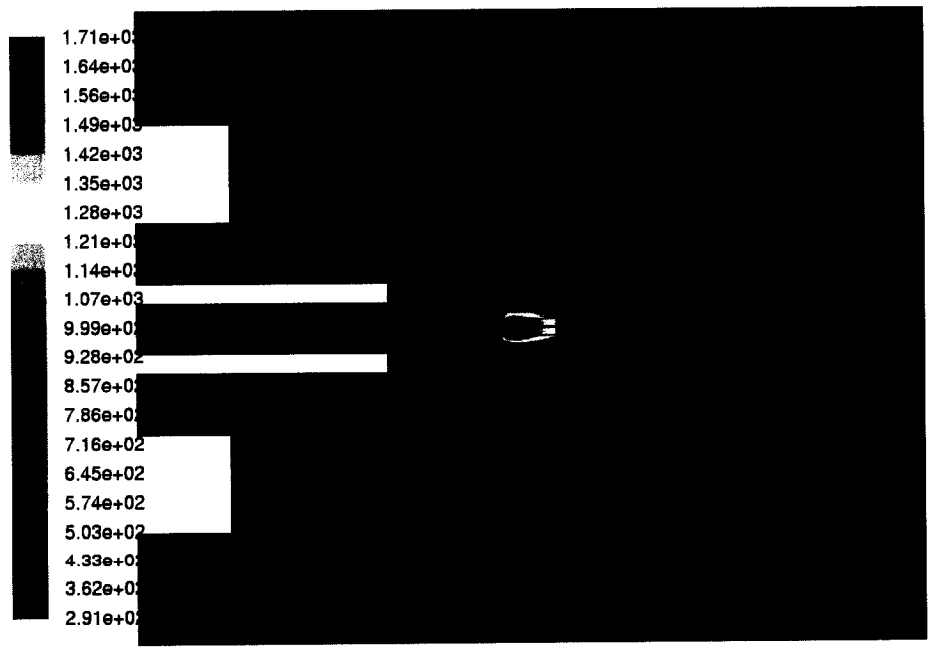

(b) Precursor jet against the fiber growth direction

Figure 6.20 Effect of precursor flow direction on fiber tip temperature

CHAPTER 7

SIMULATION OF A HIGH PRESSURE REACTOR

It has been reported by Longtin (2003) that fibers produced by LCVD at atmospheric and sub-atmospheric pressures have low hardness and elastic modulus. These poor mechanical properties can be improved by HP-LCVD process in addition to the potential of increasing substantially the deposition rate.

The model developed and validated in the previous chapters is extended to conditions of high pressure conditions, in order to establish the performance characteristics of such a reactor compared to those at ambient conditions.

Therefore, the objective of this chapter is to extend and establish the modelling and simulation methodology to the HP-LCVD process. While incomplete due to the lack of experimental data, this will nevertheless show that computing flow, temperature, and species distributions and deposition rate in a virtual high pressure LCVD reactor is possible. In general, it will provide the basis for understanding the process of the fiber growth in very high pressure conditions.

Thus this modelling and the results are not to be considered as predictive but rather they are intended to show the capability and feasiblity of such extensions, together with the validation of the specific computational developments necessary to address the particularities of HP-LCVD modelling requirements (scale disparity, adaptive grids, material and reaction parameters...).

7.1 Modelling the HP-LCVD Process

The differences in simulating between HP-LCVD reactor and ambient reactor are described below:

Operating conditions: 50 bar and 193.15 K for a HP-LCVD reactor compared to atmospheric pressure and room temperature for ambient reactor.

Properties: All the properties of the gases are changed for the HP-LCVD reactor as given by the real gas laws.

Moving boundary : In the ambient reactor, since the fiber growth rate is very low (about 10 μm/s), stationary boundary conditions are assumed. However, in the HP-LCVD simulations, the fiber pulling rates can be as high as 50cm/s, therefore, a moving wall boundary conditions must be implemented.

The inlet mass flow rate boundary conditions for the ambient reactor are known from experimental measurements. No such experimental data are available for HP-LCVD as no such reactor is yet available. However, from the design configuration, these conditions can be deduced from the fact that the two gases streams are fully developed flows.

Domain decomposition: The size of the ambient reactor is about 2.3 mm in radius and 5 mm in length for 100 μm fiber in radius while that of HP-LCVD is 3 mm in radius and 20 mm in length for 10 μm fiber in radius. This difference in size is more than a scaling factor in the geometry, and has a very important impact in the discretisation process. As discussed in Chap. 4, this requires to decompose the computational domain in two sub-domains.

Since for the high pressure LCVD reactor, the magnitude of the fiber radius is about 10 μm, therefore, the mesh size around the fiber tip should be less than 1 μm. However, the

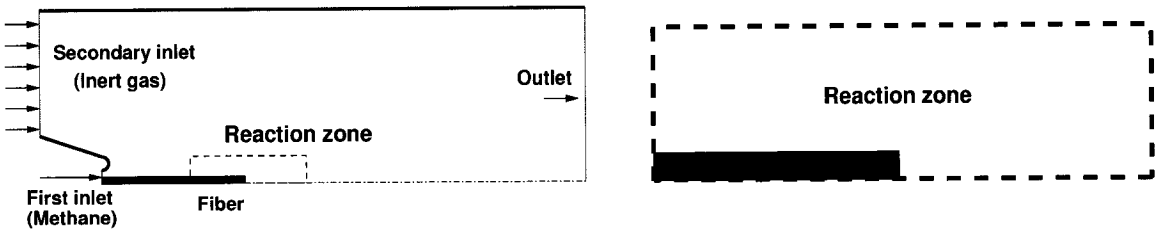

Figure 7.1 Domain decomposition

magnitude of the reactor radius is about 3 mm, a ratio of 3000. An appropriate grid size for a correct numerical simulation in the vicinity of the fiber would be of the order of 1.2-1.5. Clearly, this would be much too small for the entire reactor domain. The disparate scales encountered in this problem rule out the possibility of using a uniform grid. An approach to this contradictory requirement is a decomposition of the domain into an outer and inner problem as shown in Fig. 7.1. Thus the overall problem is decomposed into a distinct flow problem in each of these two regions and to make them inter-dependent by coupling them through permeable boundary conditions. The formulation of these separate problems will be based on appropriate grids and flow characteristics. Regions will be treated by exponentially varying mesh size, in order to account for the order of magnitude differences in computed quantities.

The strategy of the simulation is to break up the entire chamber into an overall domain and a small area in the vicinity of the fiber tip. The numerical simulation of the outer reactor region is carried out without considering the chemical reaction and the results will provide the boundary data for the inner region in the vicinity of the fiber tip. In this area a more detailed calculation will be carried out around the fiber tip with chemical kinetics and energy transfer mechanisms.

In a summary of this section, there are three key problems needing to be solved for a successful simulation.

1. Domain decomposition

2. Moving boundary condition

3. Determination of kinetics parameters

7.2 Simulation of the Outer Reactor Region

The objective of these simulations is to investigate the flow and the mixture situations of the precursor gas and the carrier inert gas, and species concentration distribution for the entire HP-LCVD reactor and to provide the boundary flow and species data for the simulation of the inner reaction zone.

The geometry and meshing of this axisymmetric configuration are shown in Fig. 7.2. The initial position of the fiber tip has been set at 1.6 mm ahead of the edge of the microtube. The shape of the fiber tip is a circular profile whose diameter is equal to the fiber height. The other main geometry parameters (Croteau (2005)) are as below:

	Diameter
Tungsten wire	75 μm
Fiber	20 μm
Microtube	340 μm
Quart tube	6000 μm

The grid has been generated with source edges at the fiber surface and outer tube wall. The mesh concentration around the fiber and the outer tube wall is specified with the meshing functions given in the table below:

	Starting size	Growth rate	Limit size	Mesh faces
Mixture flow	0.005	1.2	0.10	89464

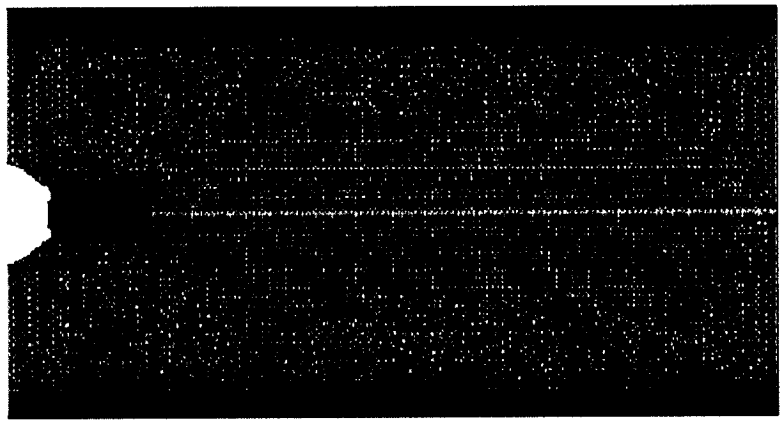

Figure 7.2 Geometry and meshing for HP-LCVD reactor

The operating conditions are given in the table below:

Laser power	0.3w to 2.5 w
Fiber tip temperature(Gaussian distribution)	Maximum 2200 K
temperature	193.15 K
Pressure	50 bar
Flow rate of Quart tube (argon)	Parabolic profile
Flow rate of Microtube (methane)	Parabolic profile+Pulling velocity

The temperature profile of the fiber tip was assumed to be Gaussian with 2200 K at the fiber center. Using a velocity in the range of 0.01 to 10.0 m/s, the Reynolds number is estimated at less than 1500. Therefore, it is laminar flow. The inlet velocity profiles for the carrier and precursor streams are taken as fully developed laminar flow and these were derived by

Croteau (2005) as,

$$v_{Ar}(r) = \frac{V_{Ar(max)}[a^2 - r^2 + \frac{a^2-b^2}{ln(b/a)} ln(a/r)]}{[a^2 - (a+b)^2/4 + \frac{a^2-b^2}{ln(b/a)} ln(\frac{2a}{a+b})]} \tag{7.1}$$

where,

$v_{Ar}(r)$ = the velocity of carrier gas (argon) at the inlet;

$V_{Ar(max)}$ = the maximum velocity (the peak of the parabolic profile);

a = the interior radius of the quartz tube;

b = the exterior radius of the microtube;

r = the radial position;

For the precursor gas, the velocity profile is:

$$\begin{aligned} v_{CH_4}(r) &= V_{pull} \frac{ln\frac{a}{r}}{ln\frac{a}{b}} \\ &+ (V_{CH_4(max)} - V_{pull} \frac{ln\frac{2a}{(a-b)}}{ln(a-b)}) \frac{[a^2 - r^2 - (a^2 - b^2)\frac{ln\frac{a}{r}}{ln\frac{a}{b}}]}{[a^2 - (a-b)^2/4 - (a^2 - b^2)\frac{ln\frac{2a}{(a-b)}}{ln(a-b)}]} \end{aligned}$$

where

$v_{CH_4}(r)$ = the velocity of carrier gas (argon) at the inlet;

$V_{CH_4(max)}$ = the maximum velocity (the peak of the parabolic profile);

a = the radius of the microtube;

b = the radius of the fiber;

r = the radial position;

V_{pull} = moving speed of the fiber

It is noted that these are not parabolic as the streams are annular. The velocity profiles at the inlets are shown in Fig. 7.3.

Figure 7.4 shows computed results for the velocity vector field in the entire reactor. Comparing with the velocity vector shown in Fig. 6.6, the precursor velocity is less divergent. It means the gases were compressed due to the high pressure.

Another important simulation result for the outer reactor region is the species distribution of the precursor and carrier gases as shown in Fig. 7.5. The results calculated by Croteau (2005) under the same operating conditions (Fig. 4.3 of Croteau (2005)) showed a "waving" boundary line between the two gases. This is not a real phenomena but rather the result of lack of convergence. The current calculation shows that the two species are gradually mixed and without any "waving" interface.

Comparing with the open air reactor results shown in Fig. 6.9, it can be seen that the two species are less diffusive. Even though they are not the same precursor and carrier gases, a large difference is observed since the binary mass diffusivity between argon and methane in ambient conditions are even higher than the binary mass diffusivity between nitrogen and ethylene. The reason why the two species have less diffusion for the HP-LCVD reactor is because the mass diffusivity decreases at high pressure. This is as expected, because the high precursor concentration can be reached more easily in the fiber tip region, providing enough precursor for the chemical reaction. This is another advantage for using HP-LCVD reactor for producing fibers.

7.3 Simulation of the Reaction Zone

As described in Section 7.1, the disparate scales of the entire reactor and the reaction zone require a decomposition of the overall domain into an outer region of the reactor and an inner small area in the vicinity of the fiber tip as shown in Fig. 7.1. Thus the overall problem is decomposed into a distinct flow in each of these two regions and these are coupled through permeable boundary conditions. This coupling was investigated and found to be accurate (Section 4.3.3). The boundary data of flow and species distribution was transferred as follows:

- creating the iso-surfaces at the same dimensions of the reaction boundaries at the entire reactor. Except for the symmetry axis, there are two radial lines and one axial line. The dimensions are 680 μm $\times$ 170 μm with the edge starting at 100 μm distance away the fiber tip.
- writing the profiles of the three iso-surface with coordinates, velocity, and mole fraction of each specie in the reactor region simulation.
- providing these data from the outer region as boundary conditions in the inner region.

7.3.1 Configuration of the reaction zone

Figure 7.6 shows the geometry and the meshing for the reaction zone.

As expected (see Section 1.2), the deposition rate of the fiber at high pressure (50 bar) is very fast (0.5 m/s was initially assumed) due to the high pressure and the forced convection. Therefore, the assumption of quasi-steady state no longer applies. The moving boundary condition described in Section 4.3.4 was used.

As described in Section 4.3.4, all the normal components of wall motion are neglected by

FLUENT. This is illustrated with Fig. 7.7. The velocity on the circular fiber surface is gradually increased with the quadrant angle until it equals to the pulling speed as shown in Fig. 7.7(b) (scaled and skipped velocity vector just on the fiber tip surface).

With the techniques of Adapt-Boundary and Grid-Separate features in FLUENT described in details in Section 4.3.4, an uniform translational velocity is applied on the entire surface of the fiber, as shown in Fig. 7.8.

7.3.2 Chemical kinetics parameters

Normally, the activation energy and the pre-exponential constant should be obtained from related experiments, but this kind of experiments at very high pressure (> 11 bar) are not available.

Maxwell & Boman (1999) reports experiments at high pressure 3D-LCVD where carbon was grown from ethylene at pressures of 1 - 11 bar; fine free-standing fibers of diamond-like carbon were grown at linear rate exceeding 12 cm/s. This report provides the figures of fiber axial growth rates versus ethylene pressures between 4 -11 bar with 0.95 watt laser power. In this case, the growth rate rises linearly from 4 bar to 6 bar, then begins an exponential rise in axial rate which continues until approximately 9 bar. Above 9 bar, a discontinuity in growth rate occurs, and the reaction proceeds at a much higher activation energy.

As described in Section 5.4, we need the data of growth rates versus laser power (or fiber tip temperature) for obtaining the activation energy and rate constant. These important information, directly from experiments at high pressure (> 4 bar), are missing in Maxwell & Boman (1999), and we have to seek other ways to investigate the chemical kinetics parameters. Two different ways have been tried to investigate these in high pressure conditions. One is based on one set of kinetics parameters of low pressure from Jean & Duty (2002),

the other is to estimate these data or to calibrate them based on the same method as used in Section 5.4.

7.3.2.1 Method I

According to Jean & Duty (2002), the apparent activation energy for methane fiber growth is 176 kJ/mol, the pre-exponential constant under the pressure of 78.4 kPa with 95 percent concentration was estimated to be 2.66×10^{13} and the reaction order is 3.47, which are in the range of typical values of a kinetically controlled system. Accordingly, we set the data from Jean & Duty (2002) for the HP-LCVD simulation in the table below:

Pre-exponential factor	2.66×10^{13}
Activation energy	176 kJ/kgmol
Reaction order(CH_4)	3.45
Pressure	50Mpa

However, the resulting calculations were divergent which means this set of data from low pressure conditions are not appropriate for simulating the high pressure process.

To obtain reasonable kinetics parameters, many trial and error computations were made in order to find the correct range. It was found that the activation energy did not play the key role in the deposition rate, but the pre-exponential factor and the precursor reaction order did affect significantly the deposition rate. Thus the activation energy was still set at 176 kJ/kgmol, the reaction order as 2.45, fiber tip temperature as 2200 K, while varying the pre-exponential factor.

Under these conditions, according to Eq. 3.24, we know the term $e^{-E_a/RT}$ will remain the same and the deposition rate will be proportional to the term $k_0 C^n$. We define a function $A = k_0 C^n$. Table 7.1 shows the simulation results. Figure 7.9 shows the plot of deposition

Table 7.1 Deposition rates with varying pre-exponanial factors

Pre-exp.factor	**deposition rate kg/m^2-s**	**CH_4 mole concentration kmol/m^3**	**Function A**
1.0×10^{8}	0.882	0.261	3.7220×10^{6}
5.0×10^{8}	3.69	0.236	1.4541×10^{7}
1.0×10^{9}	6.55	0.220	2.4490×10^{7}
1.5×10^{9}	9.04	0.209	3.2390×10^{7}
2.0×10^{9}	11.3	0.200	3.8775×10^{7}
2.5×10^{9}	13.2	0.193	4.4418×10^{7}
3.0×10^{9}	15.0	0.186	4.8689×10^{7}
3.5×10^{9}	16.5	0.179	5.1708×10^{7}
4.0×10^{9}	17.8	0.172	5.3593×10^{7}
5.0×10^{9}	20.3	0.160	5.6113×10^{7}
7.0×10^{9}	22.8	0.143	5.9658×10^{7}
1.0×10^{10}	28.3	0.128	6.4963×10^{7}
1.5×10^{10}	33.7	0.112	7.0255×10^{7}
2.0×10^{10}	37.0	0.100	7.0963×10^{7}
2.5×10^{10}	40.2	0.0917	7.1737×10^{7}
3.0×10^{10}	42.2	0.085	7.1482×10^{7}
3.5×10^{10}	44.6	0.0798	7.1446×10^{7}
4.0×10^{10}	46.6	0.0756	7.1522×10^{7}

rate in terms of Function A. The pre-exponential factor was incremented in order to reach a deposition rate close to the one we expected in 50 bar (0.5 m/s or 735 kg/m^2/s). However, when the pre-exponential factor reached 5.0×10^{10}, the results did not converge. The deposition rate was about 50 kg/m^2/s which was much less than the expected one (735 kg/m^2/s). When the pre-exponential factor was increased to 7.0×10^{10}, the results diverged. We can get two points from this procedure:

- Under the current operating conditions, the maximum deposition rate would be obtained from the virtual experiment testing. This could be another benefit and contribution for the numerical simulation.

- The pre-exponential factor has its own range and the appropriate data may be ob-

tained from the virtual experiment testing.

To find the appropriate pre-exponential factor requires an analysis from the information of Table 7.1 and Fig. 7.9. It can be seen that the proportional relation could be kept with different slopes from Function A = 4.50×10^{7} until Function A = 7.0×10^{7}. For this range, the pre-exponential factor lies between 2.50×10^{9} and 1.50×10^{10}. We selected the maximum datum for keeping the proportional relation of the deposition rate and Function A, because we wanted to obtain the maximum deposition rate.

Next, keeping the pre-exponential factor as 1.50×10^{10} the reaction order was varied between 1.8 and 4.0 in order to find the appropriate value. From trial and error simulations, values of the reaction order below 2.0, resulted in non-convergence of the computations. For the reaction order values beyond 4.0, the deposition rate was very small. We define a new function B = C^{n}. From Equation 3.24, we can induce that the deposition rate should be proportional to Function B if we keep the same pre-exponential factor. Table 7.2 shows the simulation results.

Table 7.2 Deposition rates with varying reaction orders

Reaction order	**Deposition rate (kg/m^2/s)**	**CH_4 mole concentration (kmol/m^3)**	**Function B**
1.80	54.0	0.0555	5.49196×10^{-3}
2.00	45.7	0.0726	5.27076×10^{-3}
2.20	39.7	0.0901	5.01643×10^{-3}
2.40	34.1	0.107	4.68297×10^{-3}
2.45	33.7	0.112	4.68365×10^{-3}
2.60	30.0	0.124	4.39437×10^{-3}
2.65	29.0	0.128	4.30630×10^{-3}
2.80	26.2	0.140	4.06592×10^{-3}
2.85	25.4	0.143	3.91478×10^{-3}
3.00	22.9	0.155	3.72388×10^{-3}
3.50	14.8	0.190	2.98977×10^{-3}
4.00	9.01	0.211	1.98212×10^{-3}

The variation of deposition rate in terms of Function B is shown in Fig. 7.10. The appropriate reaction order, was found by an analysis of the information of Table 7.2 and Fig. 7.10. It can be seen that the proportional relation could be kept with different slopes from Function B = 3.5×10^{-3} until Function B = 5.0×10^{-3}. For this range, the reaction order was between 2.2 and 3.0.

From trial and error simulations, it can be seen that for the given geometry, under the conditions of the gas flow rate, laser power and the high pressure and low temperature and the activitation energy, the precursor reaction order should be in the range of 2.2 to 3.0; the pre-exponential factor should be in the range of 2.5×10^{9} to 1.5×10^{10}; the maximum carbon deposition rate in the kinetics controlled regime should be about 40 kg/m^2/s or 27.21 mm/s. This gives the adjusted data as below:

Pre-exponential factor	1.0×10^{10}
Activation energy (J/kgmol)	176000
Reaction order	2.45
Tip temperature (K)	2200 (constant)
Pressure(Mpa)	50

The constant carbon deposition rate was obtained as 27.4 kg/m^2/s (0.01864 m/s) which was much less than the expected value of 0.5 m/s.

Therefore, for using the activation energy which is measured in low pressure to simulate high pressure, the information of the varying range and the appropriate datum of the reaction order and rate constant, and the maximum deposition rate would be obtained from the virtual experiment testing. But the simulated fiber growth rate may never reach the expected value for the same operating conditions.

Table 7.3 Activation energy and pre-exponential factor at 50 bar

Laser Power (watt)	**Activation Energy (J/kgmol)**	**Pre-exponential Factor**
0.6 - 1.0	138286	8.01712×10^{11}

7.3.2.2 Method II

The other method to estimate these data is to calibrate them using the same method as in Section 5.4. This consists of solving two linear equations for the activation energy (E_a) from the slope and the rate constant (k_0) from the intercept. These equations are obtained from two known fiber growth rates versus the corresponding $\frac{1}{T}$.

Hence, at least two possible growth rates should be given to calculate the activation energy and the rate constant. Maxwell & Boman (1999) reports a carbon growth rate of 12 cm/s with 0.95 watt laser power at 11 bar. We expect that the growth rate can reach 0.5 m/s with 1 watt laser power at 50 bar. Hence, one possible growth rate can be 0.5 m/s for 1 watt laser power. From Fig. 5.2 and Maxwell & Boman (1999), the growth rate at 0.6 watt laser power must be lower than the one at 1 watt laser power even in high pressure. At ambient conditions in FFL, Table 5.1 shows the growth rates to be 12μm/s at 0.6 watt laser power and 16 μm/s at 1 watt laser power. If we assume we have the similar linear proportional relationship in high pressure, the growth rate at 0.6 watt at 50 bar should be 0.375 m/s. However, Maxwell & Boman (1999) reports that the growth rate has an exponential rise with the pressures higher than 6 bar and even higher with the pressures higher than 9 bar. Consequently we estimate that the growth rate at 0.6 watt laser power should be higher than 0.375 m/s but lower than 0.5 m/s. We set it as 0.45 m/s.

Therefore, two possible growth rates: 0.5 m/s at 1.0 watt laser power and 0.45 m/s at 0.6 watt laser power, at a pressure of 50 bar, were set to calculate the chemical kinetics parameters given in Table 7.3. Thus, the only remaining unknown parameter is the reaction

order. With the parameters of Table 7.3, this can be established to be 1.73 and the simulated growth rate was 0.50 m/s exactly.

7.3.3 Simulation results for the reaction zone

From the boundary conditions of Section 7.3.1 and the kinetics parameters of Table 7.3, simulations for the HP-LCVD reactor were carried out. We have to declare that these results are not reliable since the kinetics parameters were calculated by assumed growth rates, but we can still obtain a qualitative information inside the HP-LCVD reactor through this simulation.

The carbon deposition rate was obtained to be 7.35×10^2 kg/m^2/s (0.5 m/s) with the stable convergence results shown in Fig. 7.11. The mole fraction of the precursor (methane), the carrier gas (argon) and the by-product (hydrogen) are shown in Fig. 7.12, Fig. 7.13, and Fig. 7.14 for these conditions.

Fig. 7.12 shows the precursor (methane) mole fraction. Comparing with Fig. 6.11 in ambient reactor, the methane concentration is less but more divergent in HP-LCVD because there is more precursor gas consumed due to the high reaction rate.

Figure 7.14 shows the hydrogen mole fraction. Comparing with Fig. 6.12, the hydrogen mole fraction in the ambient reactor, there is a greater quantity of hydrogen produced in the HP-LCVD reactor, and the hydrogen concentration is more divergent in HP-LCVD because there is more hydrogen produced. The velocity vector field with chemical reaction in the reaction zone is shown in Fig. 7.15 . Comparing with Fig. 7.8, it can be seen that there are gas jets in the center. This is because the chemical reaction occurs here with a by-production of hydrogen. The velocity of the gas from this "source" is much higher than that of the other gases in the reactor.

For HP-LCVD simulation, typical calculations required about 5000 iterations for a CPU time of 111 min for inner reaction zone and about 2000 iterations for a CPU time of 60 min for inner reaction zone. The computer model is IBM 6230-56U.

7.3.4 Effect of the flow rate on the fiber growth rate

A parametric analysis was carried out to investigate the effect of the flow rate of the precursor and carrier gases on the carbon deposition rate. These results are summarized in Table 7.4 for 10 cases for the carbon deposition rate varying with different precursor and carrier gas flow rates.

Table 7.4 Deposition rate with varying gas flowrate

Case	Methane flow rate (kg/s)	Argon flow rate (kg/s)	Deposition rate (m/s)
1	1.158116×10^{-5}	8.4824×10^{-5}	0.5966
2	2.316232×10^{-5}	1.69648×10^{-4}	0.6279
3	3.474348×10^{-5}	2.54472×10^{-4}	0.6463
4	4.632464×10^{-5}	3.39296×10^{-4}	0.6653
5	5.790580×10^{-6}	4.24120×10^{-5}	0.5524
6	1.447645×10^{-6}	1.0603×10^{-5}	0.5238
7	2.316232×10^{-5}	8.4824×10^{-5}	0.7075
8	5.79058×10^{-6}	8.4824×10^{-5}	0.5524
9	1.158116×10^{-5}	1.69648×10^{-4}	0.5959
10	1.158116×10^{-5}	4.2412×10^{-5}	0.5973

Case 1 is the reference case where the flow rates of the precursor and the carrier gases are almost the same as in Fig. 7.3. The precursor and carrier gas flow rates of Case 2, Case 3, Case 4 are 2, 3 and 4 times those of Case 1. The gas flow rates of Case 5 and Case 6 are 0.5 and 0.125 time of those of Case 1. It can be seen that the deposition rates depend strongly on the gas flow rates. The question is: which gas is more important for the deposition rate?

Cases 7 and 8 are the situations keeping the same flow rates of the carrier gas. In Case 7,

the precursor flow rate is double that of Case 1 while the precursor flow rate of Case 8 is half that of Case 1. Comparing Case 1 with Case 7 and Case 8, the deposition rates are increased with the increased precursor flow rates.

In Cases 9 and 10 the carrier gas flow rates are double and half those of Case 1 but keeping the same precursor gas flow rate. Comparing Case 1 with Case 9 and Case 10, although the flow rate of the carrier gase change significantly, the deposition rates do not vary much. Therefore, we can conclude that the deposition rates are more dependent on the precursor gas flow rates. Fig. 7.16 shows the deposition rates varying with the precursor flow rates.

7.4 Summary of the High Pressure Simulation Results

The summary of the simulation results with high pressure is as follows:

1. A demonstration model of the high pressure LCVD modelling was established.
2. The problem of domain decomposition was solved and converged results for outer and inner reaction zones were obtained.
3. The problem of moving boundary was solved successfully by utilizing the special techniques of Adapt-Boundary and Grid-Separate features in FLUENT.
4. The information of the varying range and the appropriate datum of the chemical kinetics parameters, and the maximum deposition rate can be obtained by trial and error.
5. The two species of the precursor and the carrier gas are less diffusive in HP-LCVD reactor than they are in the ambient reactor. This is because at high pressure, the mass diffusivity is becoming much less. This situation could result in high precursor concentrations in the region of fiber tip which can provide enough precursor for

the chemical reaction. This is another advantage for using HP-LCVD reactor for producing fibers.

6. The fiber deposition rates depend on the flow rates of the precursor gas.

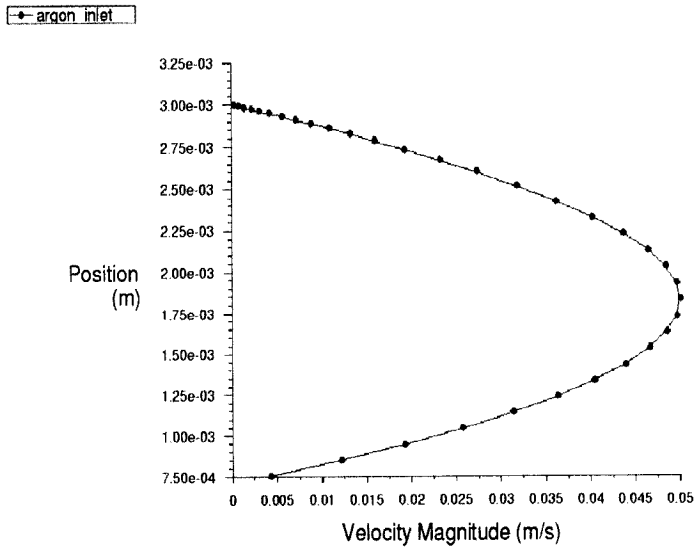

(a) Carrier gas velocity profile

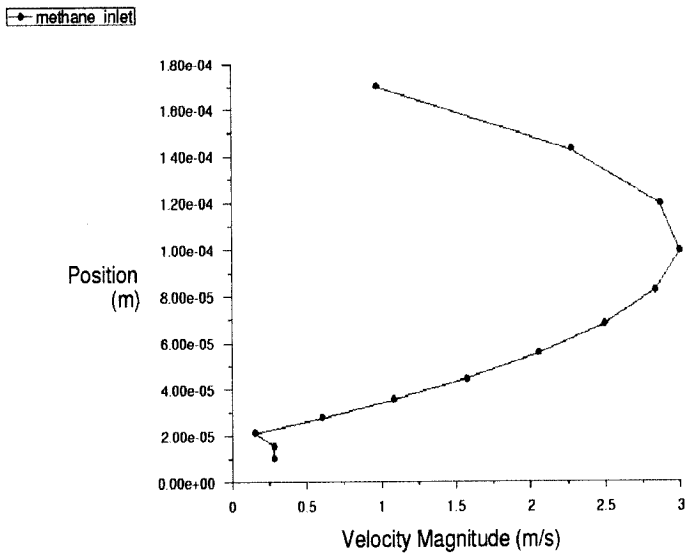

(b) Precursor velocity profile

Figure 7.3 Inlet velocity profiles for the HP-LCVD reactor

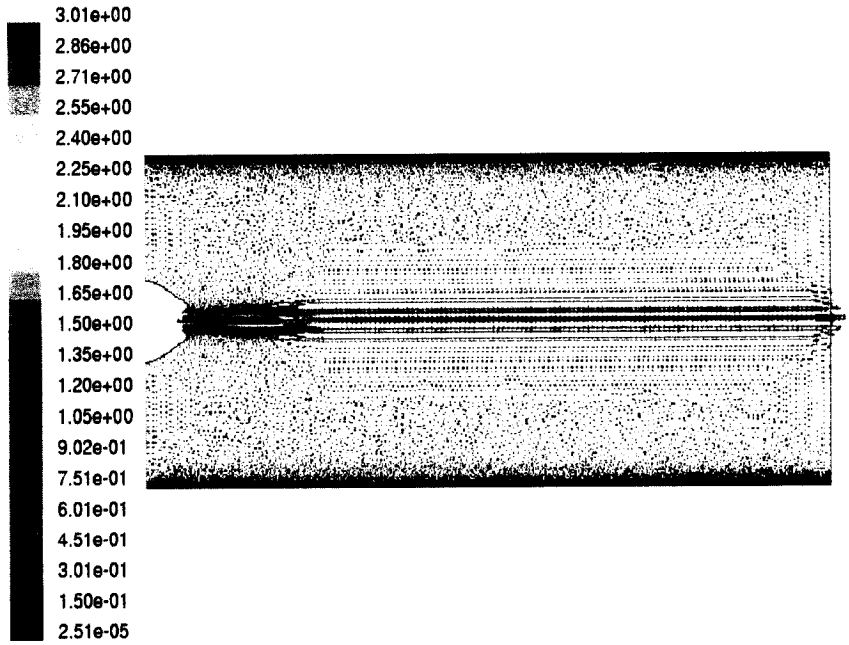

(a) Entire HP-LCVD reactor

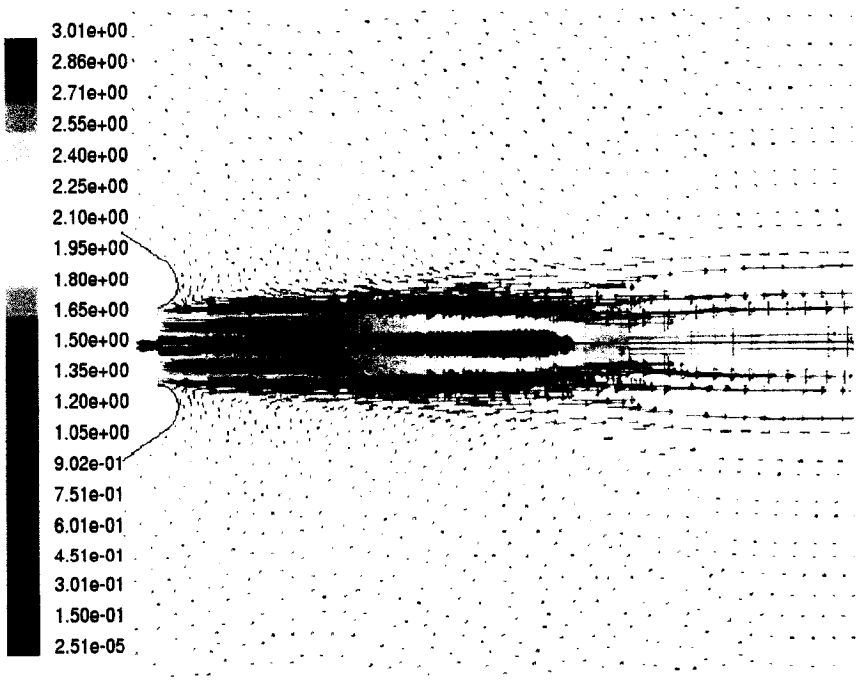

(b) Reaction zone around the fiber

Figure 7.4 Velocity vector field for the HP-LCVD reactor

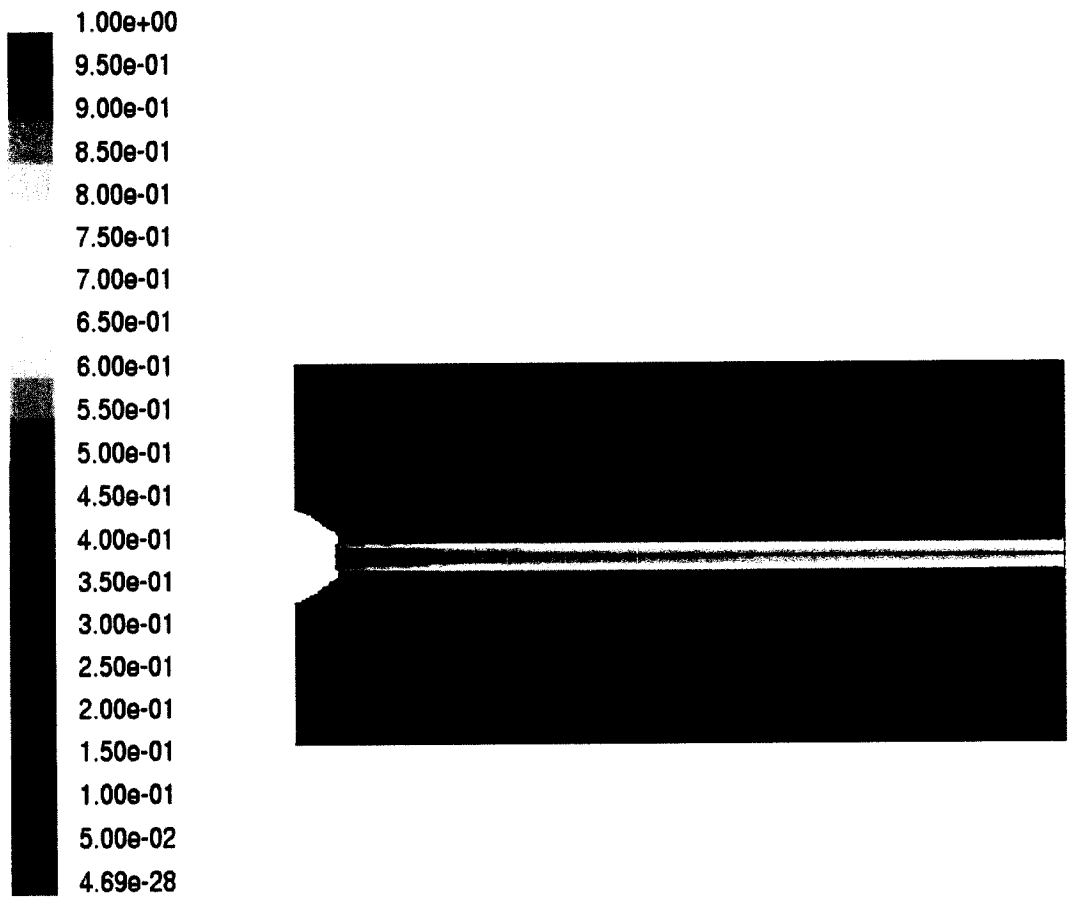

Figure 7.5 Map of methane mole fraction in the HP-LCVD reactor

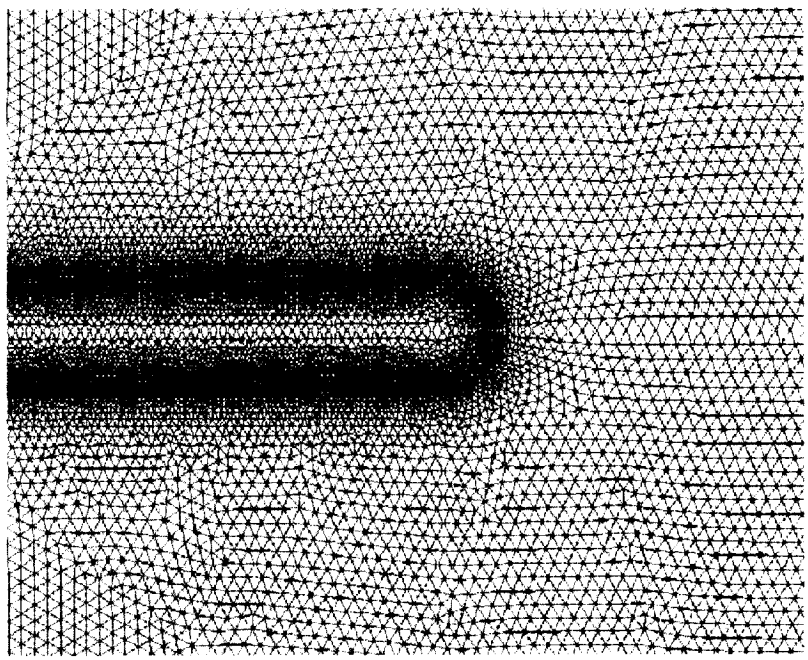

Figure 7.6 Geometry and mesh for the HP-LCVD reaction zone

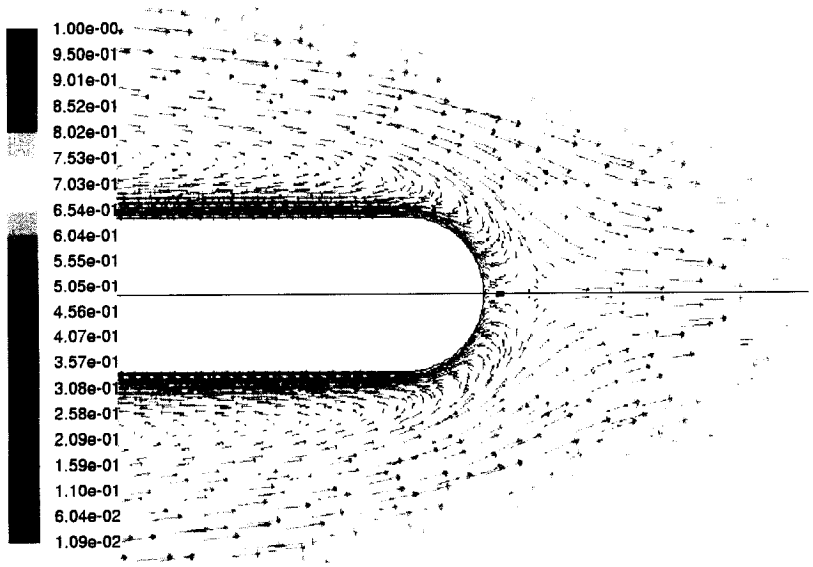

(a) Flow pattern without using grid-separate features

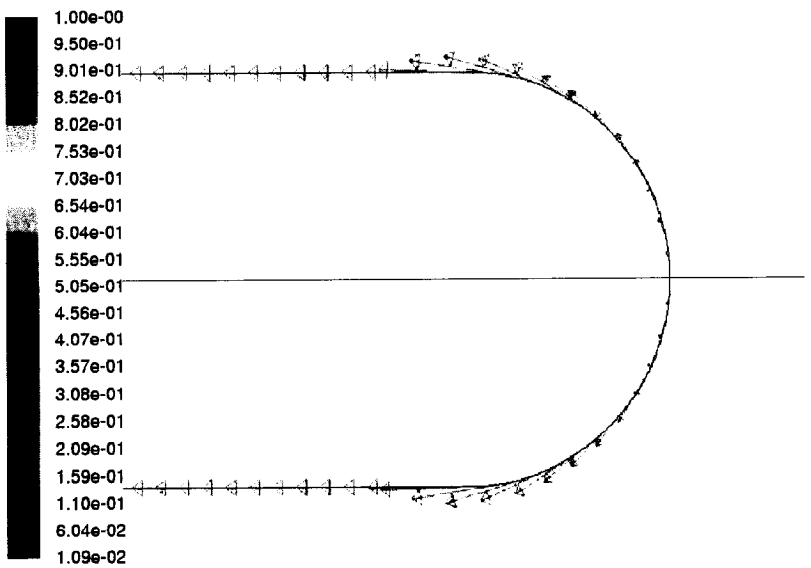

(b) Zoom of flow pattern without using grid-separate features

Figure 7.7 Flow velocity vector around the fiber tip in high pressure reaction zone

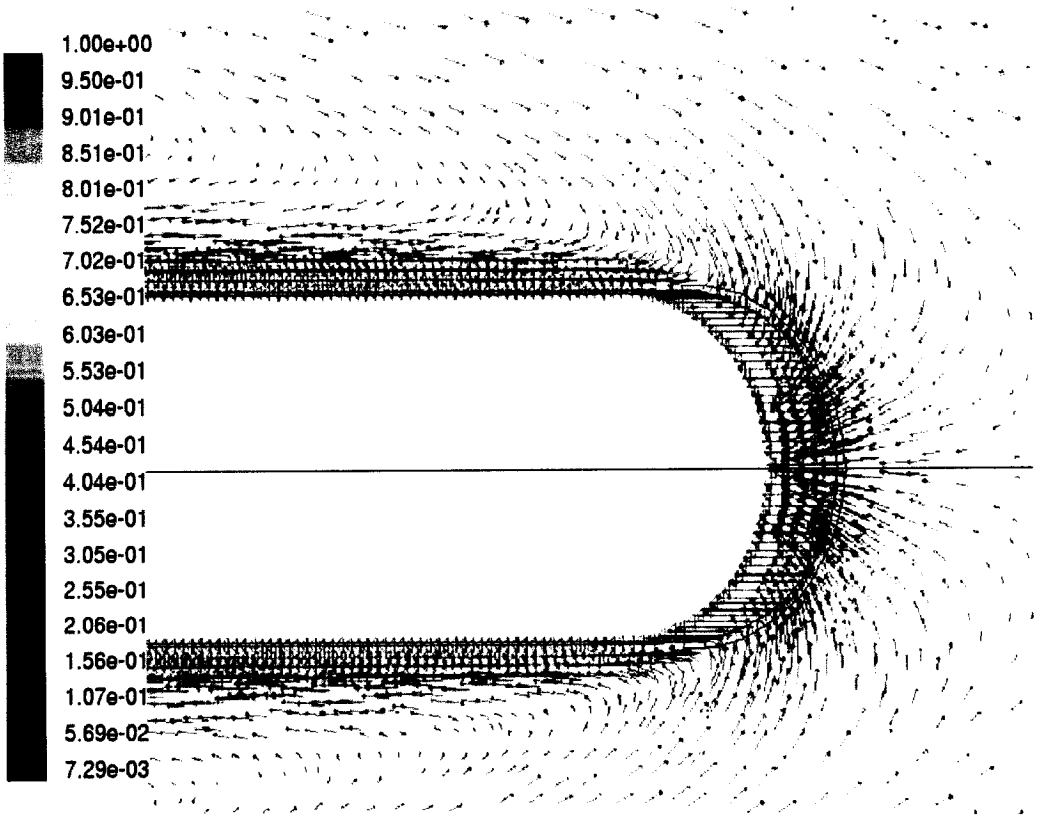

Figure 7.8 Fiber tip zone velocity vectors

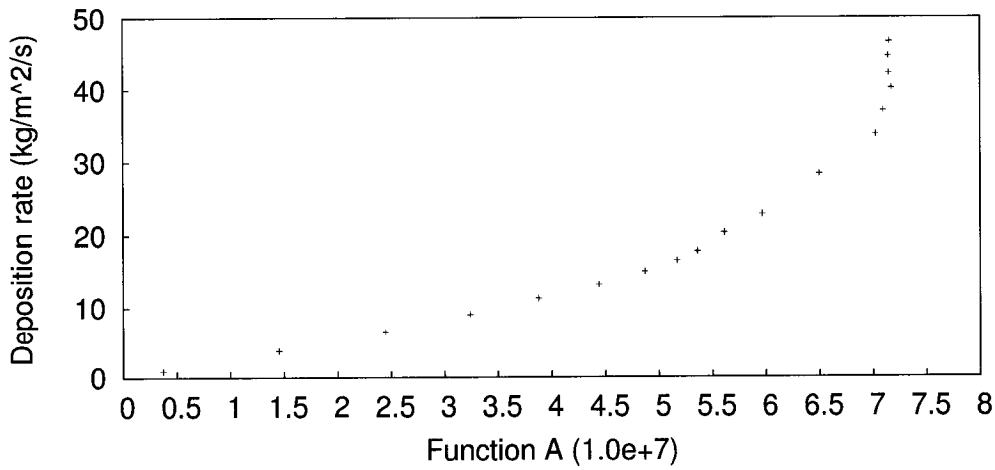

Figure 7.9 Deposition rate versus Function $A = k_0 C^n$

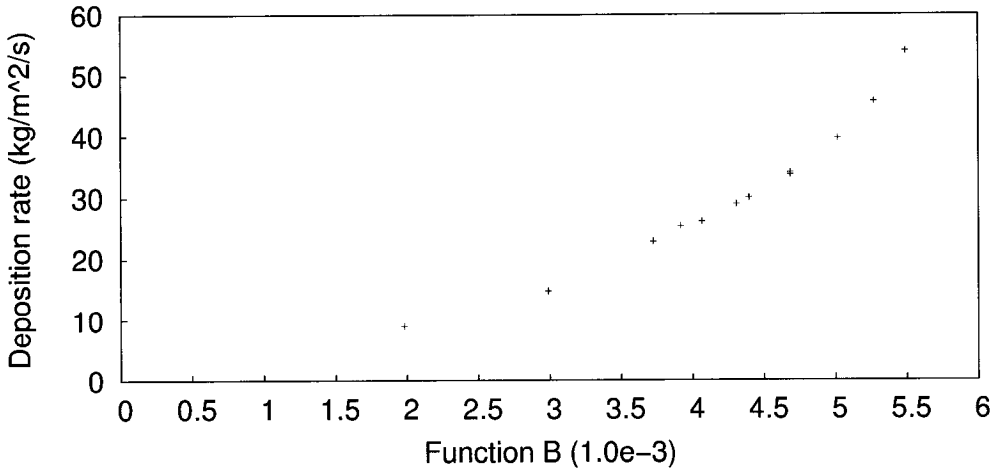

Figure 7.10 Deposition rate versus Function B = C^n

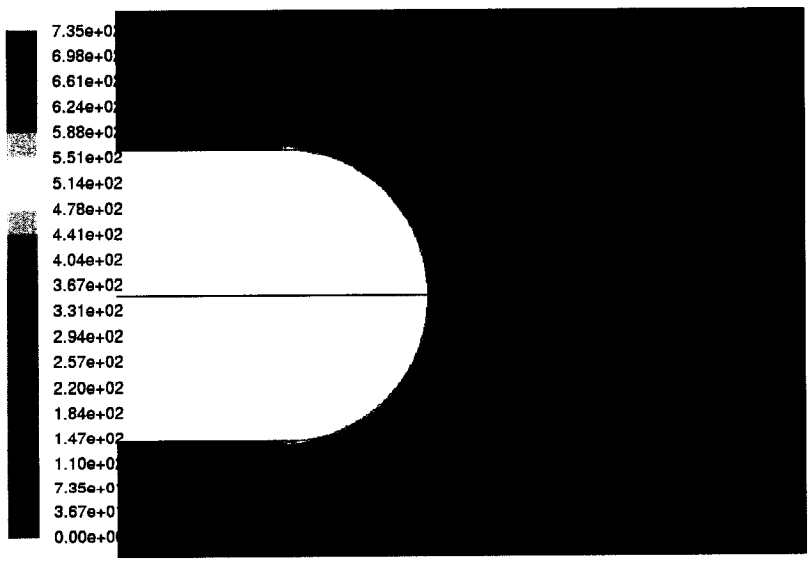

Figure 7.11 Carbon deposition rate for the HP-LCVD reactor

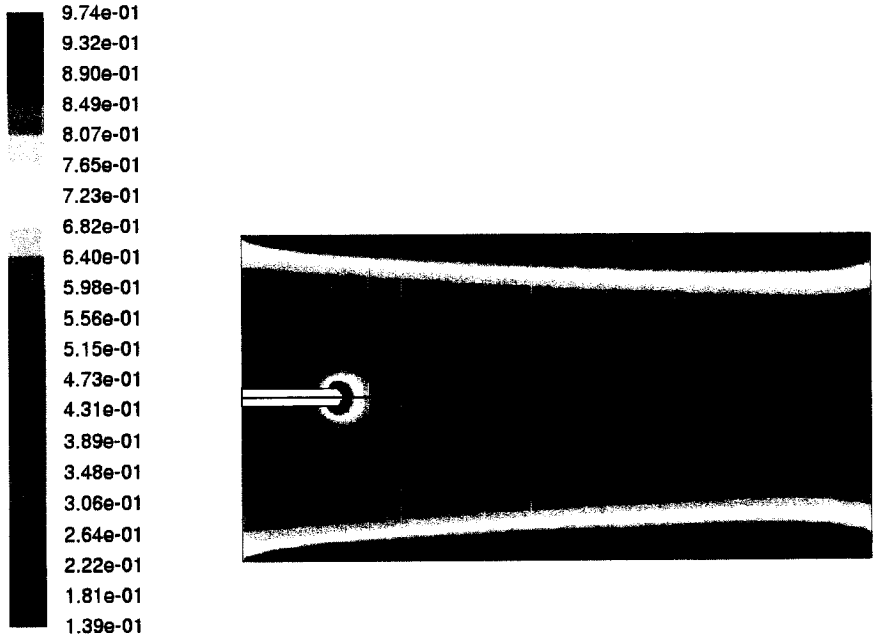

Figure 7.12 Map of HP-LCVD methane mole fraction in the reaction zone

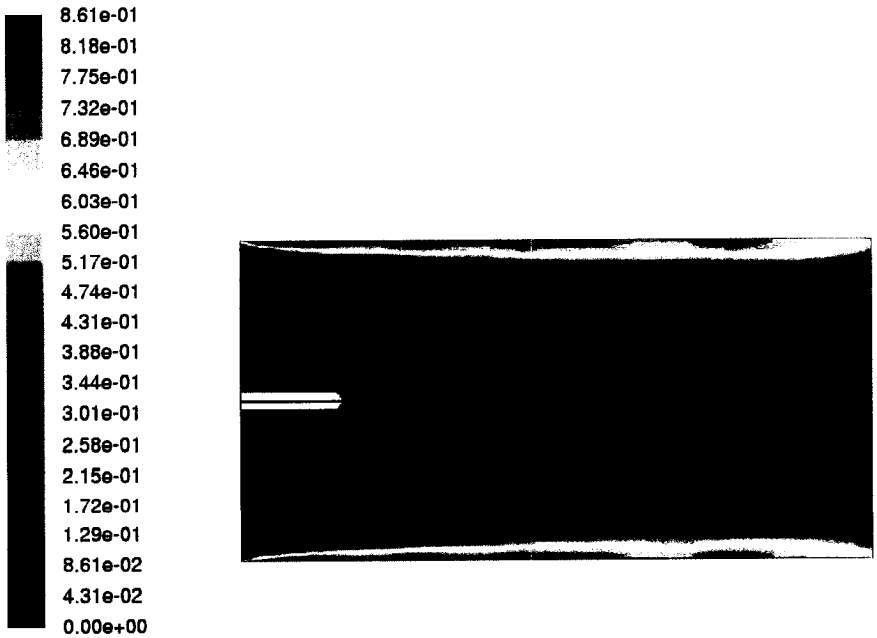

Figure 7.13 Map of HP-LCVD argon mole fraction in the reaction zone

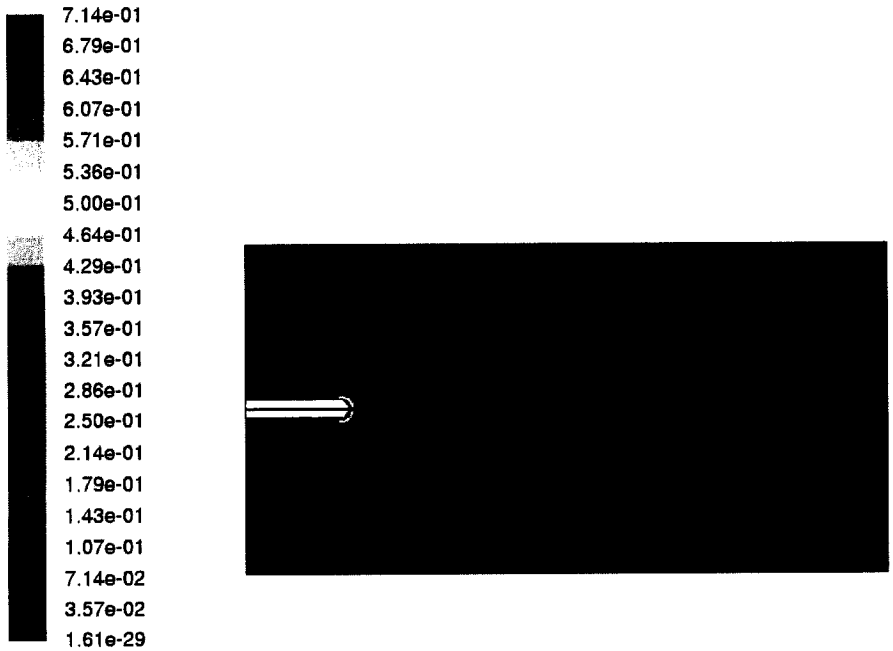

Figure 7.14 Map of HP-LCVD hydrogen mole fraction in the reaction zone

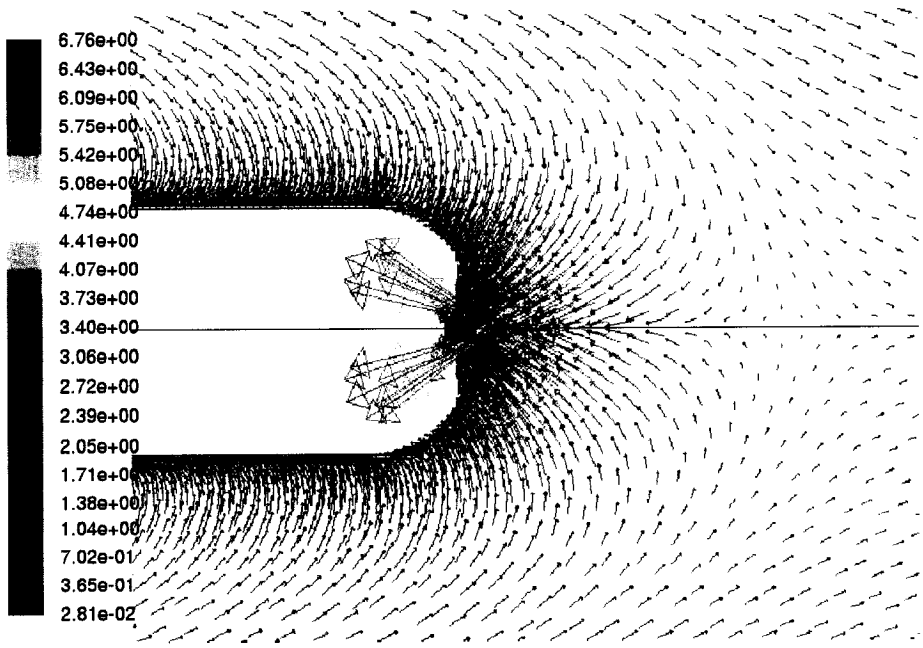

Figure 7.15 HP-LCVD Velocity vector in the reaction zone

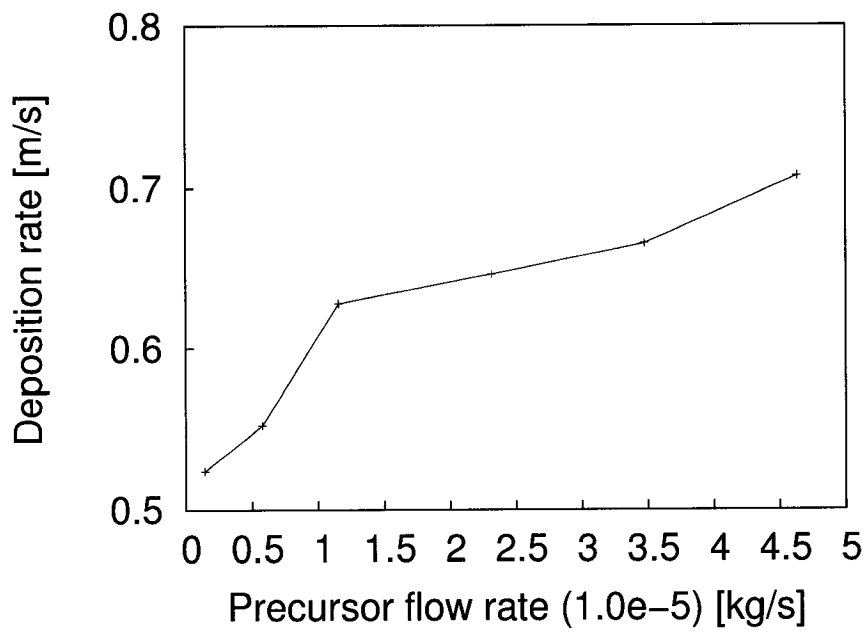

Figure 7.16 Carbon deposition rate versus methane flow rate

CHAPTER 8

CONCLUSIONS

8.1 Conclusions of the Current Research

LCVD is a new manufacturing process that holds great potential for the production of new materials, but the deposition process and its dependence on various operating conditions is still not very well understood. This is especially the case for reactor designs for the production of continuous fibers with forced convection, and extensions to high pressure.

The rationale for the comprehensive undertaking in the computer simulation of the LCVD fiber growth process carried out in this study aims at complementing the experimental development and building upon the acquired know-how at the FFL. Specifically, a computer model incorporating the various mass and energy exchange phenomena has been devised and implemented based on the commercial CFD software package FLUENT. While similar attempts have been reported in the literature, these were lacking in several aspects of the modelling methodology and do not address comprehensively the LCVD process. What is lacking is a reliable, validated simulation tool that can assist the scientist or engineer in the task or reactor design or analysis.

This research has attempted to achieve the reliability of the simulations by careful and systematic numerical experiments to assess such issues as grid adaptation, mesh independence, well-posed boundary conditions and solution convergence. These were carried out with actual geometries and realistic operating conditions.

Undoubtedly, the most important aspects of the present undertaking is the effort to validate the modeling methodology. The reviewed literature has shown that this crucial character-

istic is lacking in previously proposed models. The reasons are numerous and foremost is the complexity of the process and the coupling of the physical phenomena. In the absence of detailed measurements, this validation process can only be achieved indirectly and in global terms only. From existing measurements of the deposition rate, a comparison with the computed deposition rate could be used to validate the proposed physical and computational model. However, experimental studies rarely report operating conditions completely, nor in a form that can be used as numerical boundary condition. In addition, the experimental set up rarely matches the configuration for the present study, requiring to identify those which are the most similar, inferring such missing parameters as flow rates. For this purpose, the data of Maxwell & Boman (2006) have been found the most pertinent, those of Goduguchinta (2006) of course being designed with this process in mind were directly usable. This clearly points to the need in the LCVD community to address these issues.

Despite the uncertainty and inaccuracy resulting from this situation, it has been possible to show that results are in good agreement with available experimental data.

This confirms that the model and the simulation methodology are globally correct and yield convincing results, and that they can be used for the stated objectives:

- understanding and modeling the effects of the forced convection on the deposition processes.
- providing fundamental insights which then feed into virtual experiments and can be used to establish reactor design and process control guidelines.
- exploring configurations and/or operating conditions not readily reproducible in the laboratory.

In addition, this work not only provides insights into the LCVD process but also helps in establishing some chemical kinetics parameters through numerical modeling and analysis.

The modelling of the ambient LCVD process allowed to investigate separately the effects of the operating parameters such as the laser power, gas flow rates, and fiber tip positions. Several different combinations of precursor flow rate and carrier gas flow rate were tried and the virtual experiments exhibited the expected growth rate profiles. These results offer both scientific and engineering benefits. Obtaining a growth rate curve can be beneficial in knowing the maximum possible growth rate for a given process parameter set and positioning as well as maintaining the fiber growth front at points of known growth rates.

The simulation results of two forced convection with different gas-jet directions revealed that the gas-jet with the same direction of fiber growth contributed much more than other gas-jet directions to enhance cooling, increase growth rate and provides better mechanical support of the growing fiber.

Comparing the simulation results of open air reactor with those of HP-LCVD reactor, the models revealed that the growth rate can be improved significantly by increasing the reactor pressure. Although HP-LCVD kinetics parameters are not currently available for such configurations, it has been shown that the proposed modelling methodology can be made to work for such reactors, and how the parameters and the physical processes can be investigated in detail as a complement to experiments, or as guide to future reactor design

Even though we have to declare that the simulated results of HP-LCVD may not be reliable since the kinetics parameters were established using assumed growth rates, it can still yield qualitative information inside the HP-LCVD reactor. While incomplete due to the lack of experimental data, this HP-LCVD modelling nevertheless shows that computing flow, temperature, and species distributions and deposition rate in a virtual high pressure LCVD reactor is possible.

The LCVD process modelling proposed in this work can serve as a prototype fabrication tool for the production of a variety of fibers at high speed. Such prototypes can then be tested for their feasibility in terms of cost-effectiveness and efficiency. This approach based

on physical modelling and numerical simulation has the potential to significantly reduce the high cost and long cycle time necessary for the development of separate systems for individual fibers.

8.2 Contributions of This Research

The specific contributions of the current research are as follows:

1. Physical and mathematical modeling of the continuous fiber growth process to test virtually the hypothesis which is that a forced precursor jet along the fiber growth axis improves the growth rate. A quantitative understanding of the process is provided.

   Since such a numerical model of LCVD fiber growth has never been carried out previously, a successful outcome is that it is now possible to simulate the poorly understood LCVD phenomenon. The insight gained can be used as guidelines for reactor design and process control.

2. First detailed simulation of the process in the immediate vicinity of the moving fiber tip can provide the temperature and concentration distributions of the gas depending on the precursor gas flow rate, the pressure, and the other pertinent parameters. The model can also be used to investigate the temperature distribution of the fiber tip and the deposition rate.

3. First detailed demonstrated simulation of the process in high pressure LCVD.

4. Special methodologies were developed to address the disparity of scale of the quantities under study as well as moving boundaries. The approach taken in this research decomposes the problem into inter-depended regions. This allows to use different models where different phenomena dominate.

BIBLIOGRAPHY

Baehr, H. & Stephan, K. (2006). *Heat and Mass Transfer.* Springer Berlin Heidelberg New York.

Bird, R. & Stewart, W. (2002). *Transport Phenomena.* John Wilay and Sons, Inc.

Boman, M. (2001). *Thin Film Deposition Techniques.* A course offered at Louisiana Tech University.

Chen, Q. (2002). Modeling and experimental verification of growth of an axisymmetric cylindrical rod by three-dimensional laser-induced chemical vapor deposition. Ph.D. thesis, College of Engineering and science Louisiana Tech University.

Croteau, D. (2005). Simulation numerique du procédé de depot chimique en phase vapeur assiste par laser (lcvd) de fibre de carbone.

Dean, R. & Nordine, P. (1999). A novel method for fabricating 3-d helical thz antennas directly on semiconductor substrates. *Proceedings of SPIE: Proceedings of the 1999 TeraHertz Spectroscopy and Applications, Vol.3617, pp.67-77.*

Doppelbauer, J. & Bauerle, D. (1986). Kinetic studies of pyrolytic laser-induced chemical processes. *Laser Proceeding and Diagnostics (II), pp.53-56.*

Duty, C. (2001). Design, operation, and heat and mass transfer analysis of a gas-jet laser chemical vapor deposition system. Ph.D. thesis, Georgia Institute of Technology.

Duty, C. & Jean, D. (2001). Laser chemical vapour deposition: materials, modelling, and process control. *International Materials Reviews, Vol.46, No.6,pp. 271-287.*

Duty, C. & Johnson, R. (2003). Heat and mass-transer modeling of an angled gas-jet lcvd system. *Applied Physics A - Materials Science and Processing, Vol. 118, pp. 225-234.*

Fluent (2003). Fluent 6.1 user's guide. *FLUENT 6.1 user's guide, FLUENT Inc.*

Frischknecht, K. (1995). Laser assisted chemical vapor deposition of fibers. Ph.D. thesis, Clemson University.

Goduguchinta, R. (2004). High-performance fiber (hpf) by high-pressure laser chemical vapor deposition. *A report presented in partial fulfillment of requirements for the pre-doctoral exam in the Department of Mechanical Engineering, Ecole Polytechnique de Montreal.*

Goduguchinta, R. (2006). Axial convection enhanced laser cvd of carbon rods. Ph.D. thesis, Ecole Polytechnique de Montreal.

Hill, E. (1995). Finite element analysis of carbon rod growth by laser-induced chemical vapor deposition.

Jean, D. & Duty, C. (2002). Carbon fiber growth kinetics and thermodynamics using temperature controlled lcvd. *Carbon, Vol.40,pp.1435-1445.*

Johnson, R. (2005). Process development for the manufacture of an integrated dispenser cathode assembly using laser chemical vapor deposition. Ph.D. thesis, Georgia Institute of Technology.

Kajsa, B. (2001). Microfabrication of tungsten, molybdenum and tungsten carbide rods by laser-assisted cvd. Ph.D. thesis, ACTA UNIVERSITATIS UPSALIENSIS.

Kelly, B. (1969). *The thermal conductivity of graphite*, volume 5.

Kohler, W. & Wiegand, S. (editors) (2002). *Transport Phenomena*. Springer, Heidelberg.

Koutlas, G. & Vlachos, N. (2003). Numerical modeling of pyrolytic laser-induced chemical vapor deposition. *Journal of Applied Physics, Vol.93, No.5, pp.3049-3056.*

Lan, H. (2005). Integrated modeling and parallel computation of laser-induced axisymmetric rod growth. Ph.D. thesis, Louisiana Tech University.

Lan, H. & Nassar, R. (2003). Mathematical model for simulating axisymmetric rod growth with kinetically limited and mass transport limited rates. *Journal of Applied Physics, Proceesings of SPIE, Vol.4979, pp.549-560.*

Leyendecker, G. & Bauerle, D. (1993). Laser induced chemical vapor deposition of carbon. *Applied Physics, Vol.39,No.11, pp.921-923.*

Longtin, R. (2003). Etude des propriétés méchaniques des fibres de carbone déposées par lcvd.

Maxwell, J. (1996). Three-dimensional laser-induced pyrolysis: Modelling, growth rate control, and application to micro-scale prototyping. Ph.D. thesis, Rensselaer Polytechnic Institute.

Maxwell, J. & Boman, M. (1999). High-speed laser chemical vapor deposition of amorphous carbon fibers, stacked conductive coils, and folded helical springs. *SPIE, Vol.3874, pp.227-235.*

Maxwell, J. & Boman, M. (2005). Process-structure map for diamond-like carbon fibers from ethene at hyperbaric pressures. *Advanced Functional Materials, Vol.15, pp.1077-1087.*

Maxwell, J. & Boman, M. (2006). Hyperbaric laser chemical vapor deposition of carbon fibers from the 1-alkenes, 1-alkynes, and benzene. *J.AM.CHEM.SOC., pp.A-I.*

Maxwell, J. & Pegna, J. (1998). Method and apparatus for the freeform growth of threee-dimensional structure using pressurized flow and growth rate control. *USA patent, 5786023.*

Maxwell, J. & Pegna, J. (2004). A process structure map for diamond-like carbon fiber from 1-ethene at hyperbaric pressures. *Advanced Functional Materials, Vol.00, pp.00.*

Mazumder, J. & Kar, A. (1995). *Theory and Application of Laser Chemical Vapor Deposition.* Plunum Press, New York.

Nassar, R. & Dai, W. (2002). An axisymmetric numerical model for simulating kinetically-limited growth of a cylindrical rod and 3d laser-induced chemical vapor deposition. *Journal of Materials Science and Technology, Vol.18, No.2,pp.127-132.*

Nelson, L. & Richardson, N. (1972). Carbon fiber growth kinetics and thermodynamics using temperature controlled lcvd. *Materials Research Bulletin, Vol.7,No.9,pp.971-975.*

Oran, E. & Boris, J. (2001). *Numerical Simulation of Reactive Flow.* Cambridge University Press.

Patankar, S. (1980). *Numerical Heat Transfer and Fluid Flow.* New York:McGraw-Hill.

Perry, R. & Green, D. (1997). *Perry's Chemical Engineer's Hanndbook.* New York:McGraw-Hill, 7th edition.

Reid, R. (1977). *The properties of gases and Liquids.* McGRAW HILL BOOK COMPANY.

Saatdjian, E. (2000). *Transport Phenomena.* John Wilay and Sons, Inc.

Shaarawi, M. (2001). Laser chemical vapor deposition of millimeter scale three-dimensional shapes. Ph.D. thesis, The university of Texas at Austin.

Wallenberger, F. (1997). Inorganic fibres and microfabricated parts by laser assisted chemical vapour deposition (lcvd): Structures and properties. *Ceramics International, Vol.23, pp.119-126.*

Wallenberger, F. (2000). *Advanced Inorganic Fibers:Processes, Structures, Properties, Applications.* Bosten: Kluwer Academic Publishers.

Wallenberger, F. & Nordine, P. (1994). Inorganic fibers and microstructures directly from the vapor phase. *Composites Science and Technology, Vol.51, pp.193-212.*

Wanke, M. & Lehmann, O. (1997). Laser rapid prototyping of photonic band-gap microstructures. *Science, Vol.275, pp.1284-1286.*

Watt, W. & Perov, B. (1985). *Strong Fibres*, volume 1. Elsevier science publishers B.V.

Williams, K. (2000). Rapid prototyping of three-dimensional microstrucures using laser chemical vapor deposition.

Williams, K. & Maxwell, J. (1999). The laser microchemical lathe: Rapid freeform part fabrication from the vapor phase. *Solid Freeform Fabrication Symposium, pp.541-551.*

Wright, M. (2004). *An Introduction to Chemical Kinetics*. John Wiley and Sons, Ltd.

Yu, D. & Duncan, A. (1998). Investigation of induced thermal and fluid transport phenomena in laser assisted chemical vapor deposition. *Proceedings of ASME Heat Transfer Division, Vol.4, pp.183-191.*

Zhang, Y. (2003). Quasi-steady state natural convection in laser chemical vapor deposition with a moving laser beam. *Journal of Heat Transfer, Vol.125, pp.429-437.*

Zhang, Y. (2004). Effect of natural convection on laser chemical vapor deposition with a stationary laser beam. *International Journal of Heat and Fluid Flow, Vol.25, pp.683-691.*

Zheng, P. (2003). Modeling of the inverse heat-conduction problem with application to laser chemical vapor deposition and bio-heat transfer. Ph.D. thesis, College of Engineering and science Louisiana Tech University.